SIRIUS-M: A Symmetric Illumination, Inertially Confined Direct Drive Materials Test Facility

B. Badger, S.I. Abdel-Khalik, H.M. Attaya, R.L. Engelstad, G.L. Kulcinski, J.H. Liang, E.G. Lovell, G.A. Moses, Z. Musicki, R.R. Peterson, M.E. Sawan, I.N. Sviatoslavsky, L.J. Wittenberg, C. Verdon, R. McCrory, P. McKenty, S. Skupsky

October 1986

UWFDM-711

FUSION TECHNOLOGY INSTITUTE

UNIVERSITY OF WISCONSIN

MADISON WISCONSIN

SIRIUS-M: A Symmetric Illumination, Inertially Confined Direct Drive Materials Test Facility

B. Badger, S.I. Abdel-Khalik, H.M. Attaya, R.L. Engelstad, G.L. Kulcinski, J.H. Liang, E.G. Lovell, G.A. Moses, Z. Musicki, R.R. Peterson, M.E. Sawan, I.N. Sviatoslavsky, L.J. Wittenberg, C. Verdon, R. McCrory, P. McKenty, S. Skupsky

Fusion Technology Institute
University of Wisconsin
1500 Engineering Drive
Madison, WI 53706

http://fti.neep.wisc.edu

October 1986

UWFDM-711

DOE/DP10529-1

SIRIUS-M: A SYMMETRIC ILLUMINATION, INERTIALLY CONFINED DIRECT DRIVE MATERIALS TEST FACILITY

B. Badger, S.I. Abdel-Khalik, H.M. Attaya, R.L. Engelstad,
G.L. Kulcinski, J.H. Liang, E.G. Lovell, G.A. Moses, Z. Musicki,
R.R. Peterson, M.E. Sawan, I.N. Sviatoslavsky, L.J. Wittenberg

Fusion Technology Institute
University of Wisconsin

C. Verdon, R. McCrory, P. McKenty, S. Skupsky

Laboratory for Laser Energetics
University of Rochester

October 1986

UWFDM-711

Table ES-1 lists the main design and performance parameters for SIRIUS-M. The capital and operating costs are given in Table ES-2. Figure ES-1 identifies the major items contributing to the capital cost of SIRIUS-M; the laser equipment and target factory represent nearly half the total cost. The cost of tritium is nearly 50% of the annual operating costs ($74 M/y).

Figure ES-2 is a cross section of the 2 m radius SIRIUS-M cavity. It is designed to achieve a neutron wall loading of 2 MW/m^2. In order to achieve such a wall loading at a reasonable repetition rate (10 Hz) and target yield (13.4 MJ), it is necessary to protect the first wall by placing 1 torr of xenon in the cavity. Gas protection is based on the principle that the soft x-rays and ionic debris produced by the explosions will be stopped in the gas which reradiates that energy to the wall over a relatively "long" period of time ($\sim 10^4$ s) and thus limit the wall surface temperature rise and evaporation. Actively-cooled, graphite-faced tiles are used to cover the SIRIUS-M cavity as shown in Fig. ES-3.

Detailed analyses of the thermal response of the SIRIUS-M cavity indicate that the minimum cavity radius, i.e. the maximum neutron wall loading, will be limited by the amount of reflected laser light from the target. For 10% reflected light (100 kJ) with 50% tile surface reflectivity, the maximum compressive stress at the tile surface will be about 88% of its compressive strength. If the amount of reflected light can be reduced to the point where cavity size would be limited by the reradiated x-ray and ionic debris energy, the corresponding neutron wall loading could be increased by nearly 80% (3.6 MW/m^2). The economic impact of such a change in target performance was quantified and found to be significant.[2] Compared to the reference design, the total lifetime cost can be reduced by ~ 21% if the fusion power and cumu-

Table ES-1. Design and Performance Parameters for SIRIUS-M

	Value	Unit
Fusion power	134	MW
Tritium consumption rate	3.4	kg/CY
Target yield	13.4	MJ
Target gain	13.4	---
Repetition rate	10	Hz
Laser energy (KrF)	1	MJ
Number of laser beams	32	---
Neutron wall loading	2	MW/m^2
Chamber inner radius	2	m
Cavity gas	xenon	---
Gas pressure	1	torr
Xenon inventory	800	liters (STP)
Number of tiles	20	---
Tile area	2.5	m^2/tile
Face material	graphite	---
Tile thickness	1.0	cm
Back material	PCA	---
Coolant	water	---
Module diameter	1.14	m
Module depth	0.20	m
Capsule diameter	5	cm
Capsule length	20	cm
Capsule volume	0.39	liters
Number of capsules	434	---
Active test volume	171	liters
Maximum dpa/FPY (Fe)	24	dpa/FPY
Maximum appm He/FPY (Fe)	145	appm/FPY
Total dpa-ℓ per FPY	2840	dpa-ℓ/FPY

Table ES-2. Capital and Operating Costs for SIRIUS-M

Capital Costs:	
Bare direct cost	$452 M
Total direct cost (incl. contingency)	$519 M
Total overnight cost (incl. indirect costs)	$855 M
Total capital cost (1986 $) (incl. time-related costs)	$1016 M
Total capital cost (current $)	$1281 M
Operating Costs:	
O & M	$25 M/y
Tritium fuel	$36 M/y
Electricity	$13 M/y
Total annual costs (1986 $)	$74 M/y

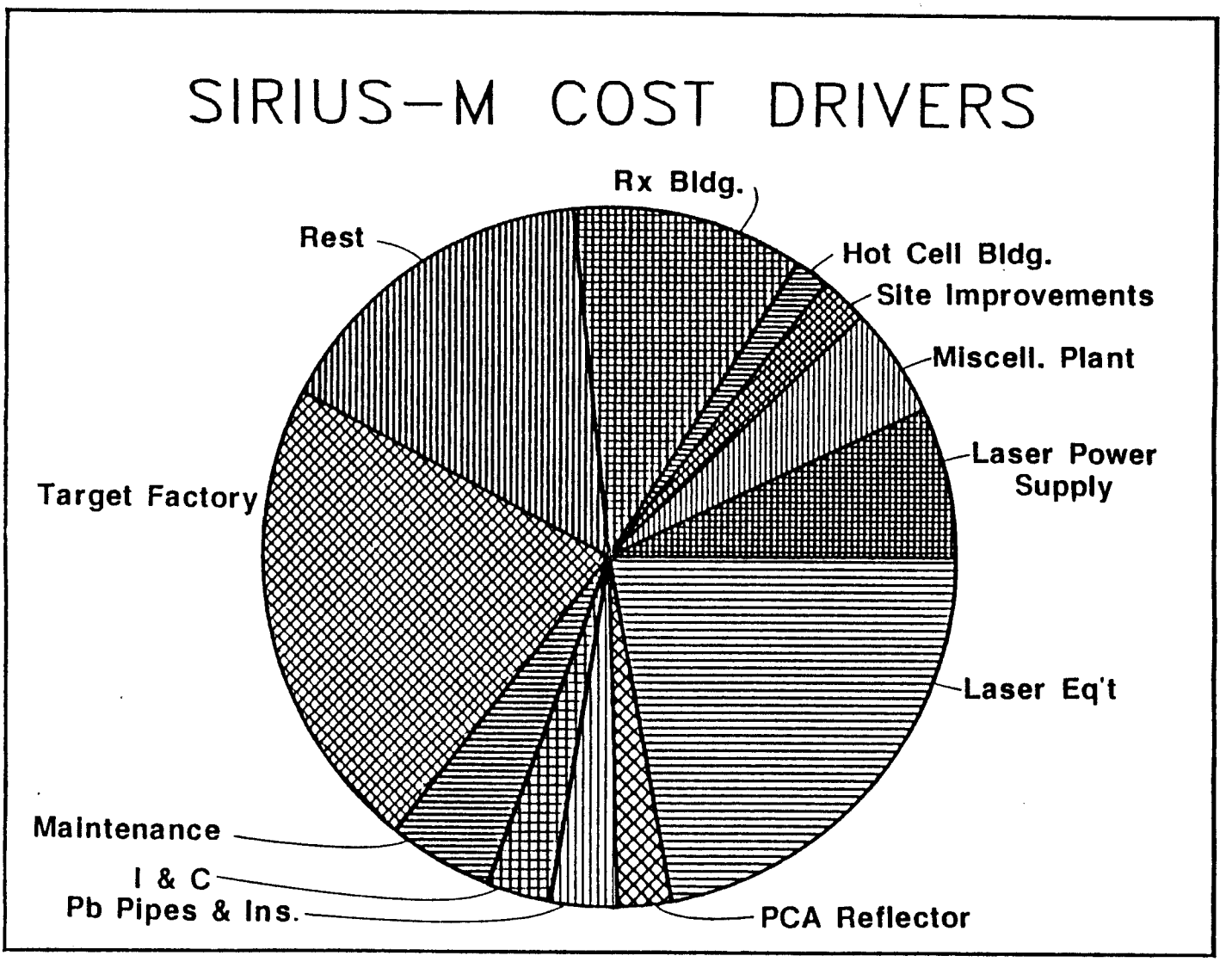

Fig. ES-1. SIRIUS-M cost drivers.

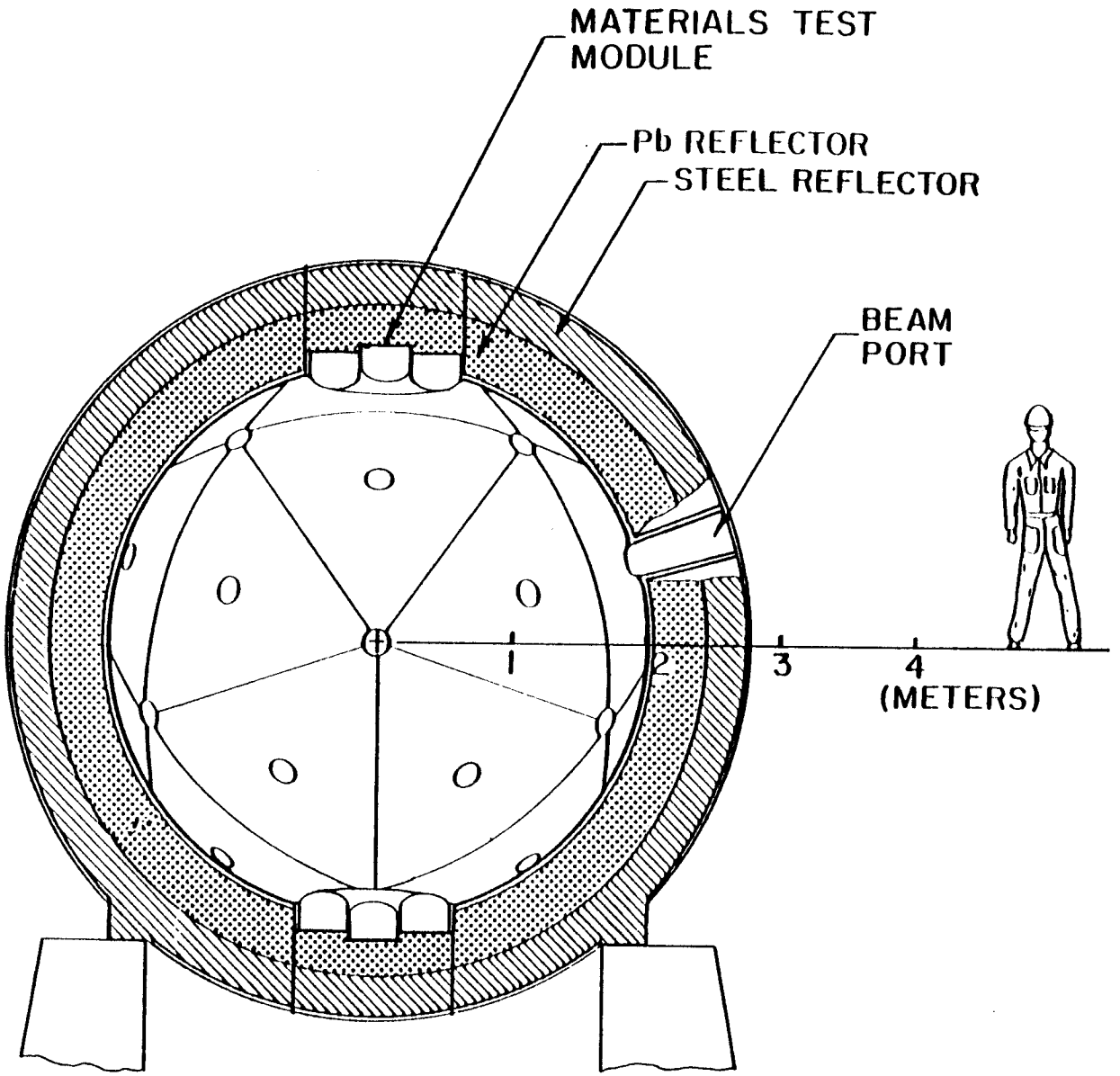

Fig. ES-2. Cross section of SIRIUS-M chamber.

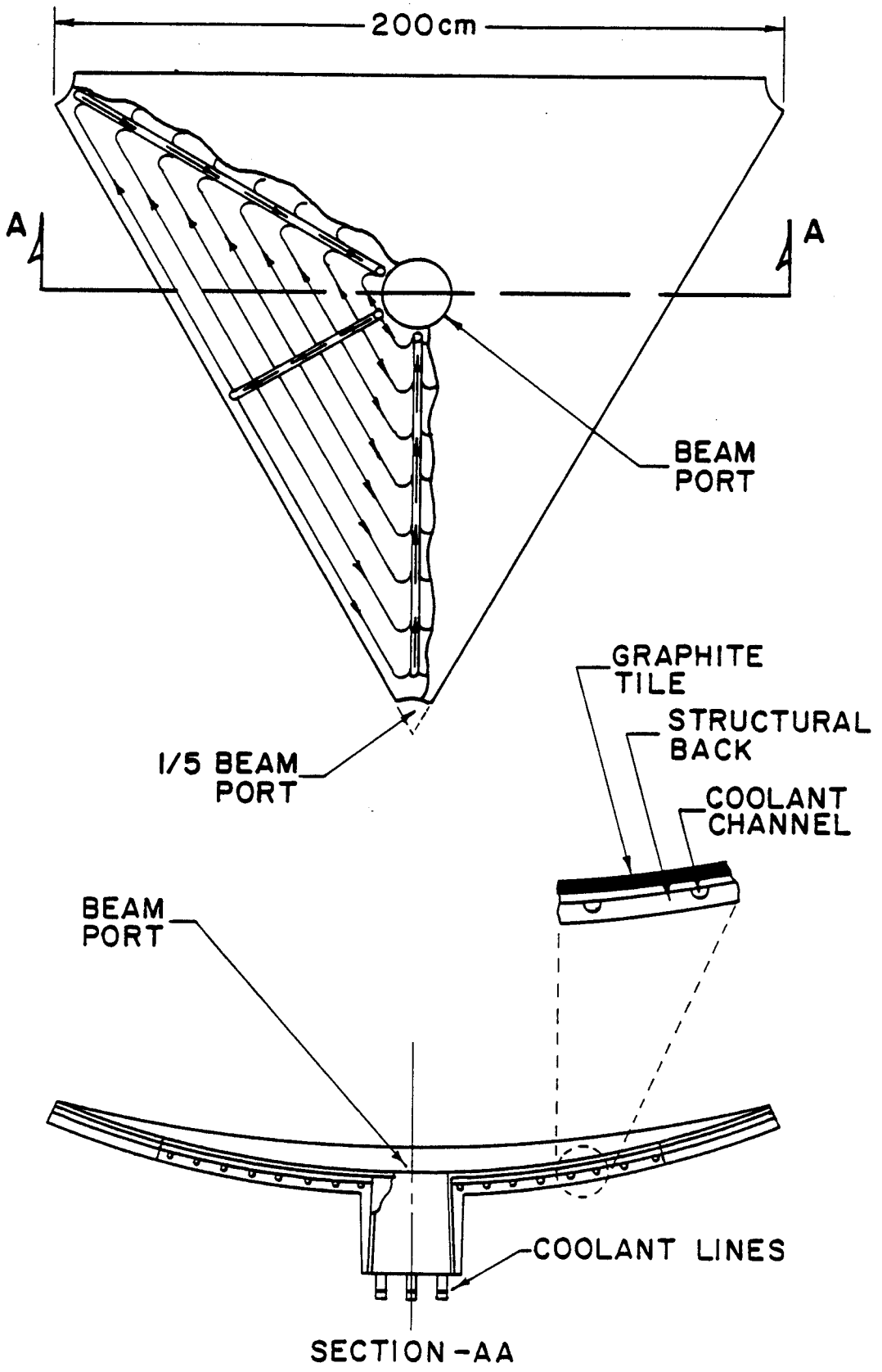

Fig. ES-3. Actively cooled graphite-faced tile.

lative performance are to be kept the same. The cost per dpa-ℓ can be reduced by nearly 44% without significant change in the total lifetime cost if the fusion power and operational time are to be kept the same.

Two circular test modules are used in SIRIUS-M. Each module has a front surface area of 1 m^2 and fits between three beam ports. No significant radial and azimuthal damage variation in the module results from these penetrations. The peak dpa rate is 24 dpa/FPY yielding a peak accumulated damage of 120 dpa at the end of life of the SIRIUS-M facility. A total volume integrated damage figure of merit of 2,840 dpa-ℓ per full power year can be achieved in SIRIUS-M which is considerably higher than that for other test facilities.[1] A detailed materials test matrix has been developed.[3] It identifies the types of alloys and number of specimens to be tested at various temperatures, stresses, chemical environments and neutron fluences (Chapter 3).

A scoping study has been conducted to identify the unique ICF blanket testing requirements. Most of these problems can be tested within the materials test module. Two unique problems requiring separate testing arrangements have been identified. The first deals with pulsed heating of liquid coolants/breeders and the resulting impulse pressures within the blanket structure. A model has been developed to estimate the magnitude of such stresses. Appropriate instruments to be placed within the lead shield zone of SIRIUS-M have been identified in order to be able to validate the model. The second unique problem deals with the effect of pulsed heating on the corrosion rates of structural materials. A blanket test module and test matrix have been designed to obtain the necessary data (Chapter 4).

Considerable effort has been devoted to the design of the shield and building for SIRIUS-M. The design criteria include: dose rate less than

2.5 mR/hr outside the building during operation; minimum neutron streaming to the laser building through the optical window during operation; acceptable damage levels to optical windows and final mirrors; and near-surface burial waste disposal rating. Various design options have been examined. Figure ES-4 shows a schematic of the selected design for the SIRIUS-M reactor building. This design meets the above criteria; its success, however, depends on the viability of the beam crossover shielding concept.

Single-shell target design calculations have been performed by LLE.[4] Using the higher flux limit for heat transport presently supported by theory and experiment, it was found that the SIRIUS-M target can have a gain of about 7 times higher than previously estimated. The amount of reflected laser light from these targets has also been reduced by about 30%.

The work performed so far has shown that an ICF materials test facility, such as SIRIUS-M, which uses symmetrically-illuminated targets can provide the necessary critical data and technology base for an ICF demonstration facility. However, several critical issues remain to be solved before a viable, complete, self-consistent design can be done. These include: the effect of tritium breeding and self-sufficiency on the design and economics of SIRIUS-M; impact of enhanced target performance on cavity design; and analysis of the beam crossover shielding concept. Resolution of the latter issue is fundamental to the proper design and operation of such a facility.

Fig. ES-4

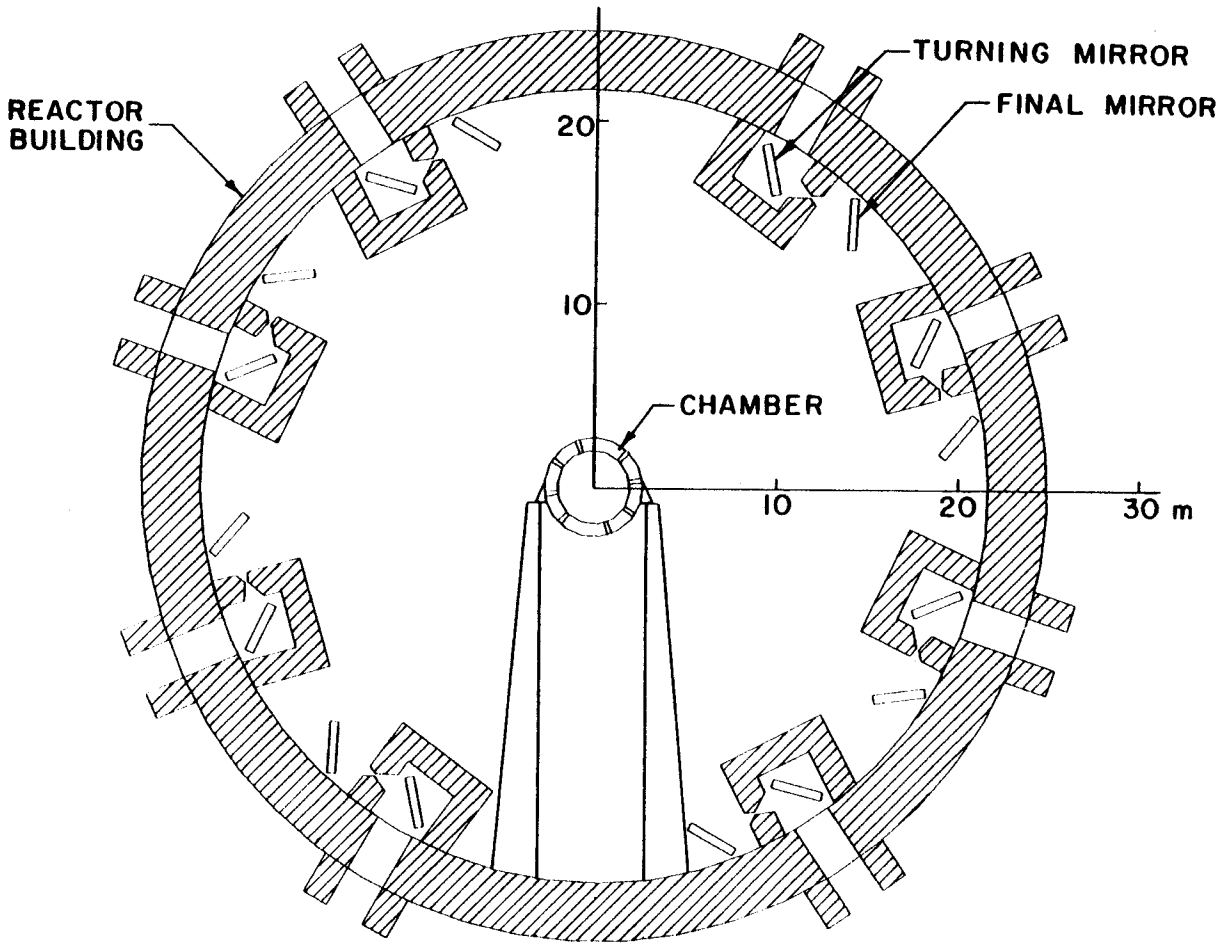

Fig. ES-4. SIRIUS-M reactor building.

References for Executive Summary

1. B. Badger et al., "SIRIUS-M: A Symmetric Illumination, Inertially Confined Direct Drive Materials Test Facility," University of Wisconsin Fusion Technology Institute Report UWFDM-651 (September 1985).

2. Fusion Technology Institute, the University of Wisconsin, "A Scoping Study of SIRIUS-M, A Symmetric Illumination, Inertially Confined Direct Drive Materials Test Facility," presented at DOE Review Meeting (September 1986).

3. M.E. Sawan and G.L. Kulcinski, "Materials Testing in the ICF Test Facility SIRIUS-M," J. Nuclear Materials 0, 00 (1986), Second Int. Conf. on Fusion Materials, Chicago, IL (April 1986).

4. C. Vernon, R. McCrory, P. McKenty and S. Skupsky, "Target Design Considerations for SIRIUS-M," University of Rochester, Laboratory for Laser Energetics (July 1986).

1. INTRODUCTION

The need to test structural materials under realistic fusion reactor conditions has been discussed in both the magnetic confinement fusion (MCF) and inertial confinement fusion (ICF) communities for over a decade. Irradiating small size materials samples in a neutron flux can be accomplished in fission reactors or small DT neutron source facilities. However, the restricted temperature range and small individual test volumes, along with serious neutron energy spectral differences, make complete testing of materials in these facilities impossible. The MCF program has taken the lead in attempting to solve this problem by sponsoring several test reactor studies such as FERF,[1] TETR,[2] INTOR,[3] TASKA,[4] TASKA-M,[5] TDF[6] and FEF.[7] Most of these studies have concentrated on providing a nuclear and thermal environment which would closely simulate that to be expected in the first demonstration reactor or the first commercial magnetic fusion reactor.

In contrast to the MCF technology program, the efforts of the ICF technology program have been on conceptual design of commercial power plants and there has been a curious lack of near term test facility designs. The singular exception is a brief scoping study of a device called LA FERF[8] in 1975 at LLNL. It is commonly assumed by the ICF community that the MCF materials program will provide the data needed for designing inertial confinement reactors. However, the large differences between the damage conditions in ICF and MCF environments arising from geometrical, spectral, and temporal effects make it necessary to develop a dedicated ICF materials test facility. To this end, beginning in 1985, the Fusion Technology Institute of the University of Wisconsin (FTI) and the University of Rochester's Laboratory for Laser Energetics (LLE), in cooperation with the Naval Research Laboratory (NRL),

initiated a study of the critical issues related to the design of an ICF materials test facility, SIRIUS-M. The facility uses symmetrically-illuminated targets and is designed to duplicate the time-dependent radiation damage structure unique to ICF systems, in order to provide the technology base necessary for an ICF demonstration facility. The results obtained during the first year of the study (1985) are given in Ref. 9. This report summarizes the results obtained by the FTI and LLE team related to the SIRIUS-M design effort during 1986.

In order to simplify the design of this first-of-a-kind facility and reduce its capital cost, its "mission" has been limited to materials testing; tritium breeding and high-temperature recovery of thermonuclear energy have not been included. During the first year of the study (1985), attention was focused on several areas unique to an ICF materials test facility including: test module design and damage rates estimation; cavity design and first wall protection; target design; placement and damage to the final mirrors.[9]

The work performed during the second year (1986) builds on the knowledge gained in these areas. Efforts have been devoted to resolving the critical issues identified in the first year so that a complete, self-consistent design could be initiated. These included: a cost estimate, cavity design optimization, stress analysis, materials testing schedule, identification and testing of unique ICF blanket problems, shield design and radioactivity.

The remainder of this report is organized as follows. Chapter 2 deals with cavity design optimization. An overall description of the cavity and first wall is given in Section 2.1. The reference cavity design which is limited by the amount of reflected light from the target is described in Section 2.2. Analyses performed to determine the optimum cavity design based

on thermal response to the target debris are described in Section 2.3. The economic impact of reduced cavity size is discussed in Section 2.4.

Chapter 3 describes the detailed materials test matrix developed for the ten-year operational period for SIRIUS-M. It identifies the types of alloys, and number of specimens to be tested at various temperatures, stresses, chemical environments and neutron fluences.

Unique testing problems associated with ICF blankets are discussed in Chapter 4. Stress analysis problems associated with isochoric heating of liquid coolants/breeders are presented in Section 4.2. A blanket test module aimed at determining the effect of pulsed heating on the corrosion rates of structural materials is described in Section 4.3.

Shield and building design for SIRIUS-M are described in Chapter 5. The design goals and methods used in the neutronic analyses are given in Section 5.1. Results comparing various design options are given in Section 5.2; the final building and shield design selected is also described. Analysis of the radioactivity produced and waste disposal rating of activated components are given in Section 5.6.

The costing model developed for SIRIUS-M is described in Chapter 6. Estimates of the initial costs of various systems and subsystems as well as the operational costs of the facility are given. Various sensitivity studies are also included.

Target design optimizations performed by LLE are presented in Chapter 7. These indicate that the SIRIUS-M target can have a gain of about 7 times higher than previously estimated while the amount of reflected light is reduced by about 30%.

Conclusions and recommendations are given in Chapter 8.

References for Chapter 1

1. T.M. Batzer et al., "Conceptual Design of a Mirror Reactor for a Fusion Engineering Research Facility (FERF)," UCRL-51617, Aug. 1974.

2. B. Badger et al., "TETR - A Tokamak Engineering Test Reactor to Qualify Materials and Blanket Components for Early DT Fusion Power Reactors," University of Wisconsin Fusion Technology Institute Report UWFDM-191 (1977).

3. "INTOR - International Tokamak Fusion Reactor, Phase I Report," International Atomic Energy Agency, Vienna, 1982.

4. B. Badger et al., "TASKA - A Tandem Mirror Fusion Engineering Test Facility," KfK-3311/2, UWFDM-500, June 1982.

5. B. Badger et al., "TASKA-M, A Materials Test Reactor for the 1990's," KfK-3680, UWFDM-600, 1983.

6. J. Doggett et al., "A Fusion Technology Demonstration Facility (TDF)," UCRL-90824, 1984.

7. T. Kawabe, to be published.

8. J. Hovingh, "Analysis of a Laser-Initiated, Inertially-Confined Reactor for a Fusion Engineering Research Facility (LA FERF)," UCRL-76517, May 1975.

9. B. Badger et al., "SIRIUS-M: A Symmetric Illumination, Inertially Confined, Direct Drive Materials Test Facility," University of Wisconsin Fusion Technology Institute Report UWFDM-651 (Sept. 1985).

2. CAVITY DESIGN OPTIMIZATION

There are several variations in the target chamber design that can affect the economic operation of the plant. It is our current belief that laser driver light reflected from the target sets the minimum first surface radius at 2 m. However, this is based on the poorly understood reflection fractions of intense laser light from ablating and imploding targets and reflection coefficients for neutron irradiated graphite. If nature is kind, reflected laser light might be less important than energy coming from the target burn and the target chamber radius may be as small as 1.5 m. This can increase the neutron wall loading and make the plant more economically attractive.

In this chapter we describe investigations into the two situations mentioned above: the reflected light limit and the target debris limit. However, we begin with a general description of the target chamber and first wall design. We then discuss the limits on the wall radius for the two situations. The target debris limit is found to be sensitive to the target design, so we have studied this limit for three target designs. We conclude with an economic comparison of the options.

2.1 Cavity Design Optimization

2.1.1 Cavity and First Wall Description

The cavity in the SIRIUS-M materials test reactor is spherical, having an inner radius of 2 m and an outer radius of 2.7 m. The radial build in the cavity consists of a first wall made of actively cooled graphite tiles, followed by a 40 cm thick lead reflector and finally by a 30 cm thick steel reflector.

The target within the cavity is illuminated with 32 laser beams, equidistantly distributed around the sphere. Beam distribution is based on a

twenty-sided icosahedron, where the sides are equilateral triangles superimposed on a spherical surface. The thirty-two equidistant points come from the centers of each triangle (20) plus the points at which the vertices of the triangles converge (12). Figure 2-1 is a cross section through the center of the cavity intersecting one of the beam ports. The figure shows the first wall consisting of triangular graphite tiles, followed by the lead and steel reflector zones. A 1.8 m man is shown to provide a perspective on size. The cavity is contained within an evacuated building and the laser light from the final mirror to the cavity travels through vacuum without the benefit of beam tubes.

The cavity will have two material test modules, one at the top and the other on the bottom as shown in Fig. 2-1. A blanket test module (not shown in Fig. 2-1) will also be incorporated into the cavity. These modules are described in Chapters 3 and 4.

The first wall is protected with twenty water cooled graphite faced tiles shaped as equilateral triangles conforming to a spherical surface. Each tile has a 20 cm diameter beam tube in its center and consists of a 316 stainless steel base structure of 2 cm nominal thickness which has cooling channels machined into it as shown in Fig. 2-2. The base structure has a collar in the center which is the primary support for the tile and which has cooling line fittings built into it. A 1 cm thick graphite surface is brazed onto the front surface of the base structure and extends into the support collar to form the protective surface for the beam tube.

Each tile is supported only by the central collar and is therefore unrestrained at any other point. This is done to prevent the buildup of thermal stresses. The outer side of the collar will have a reverse conical configu-

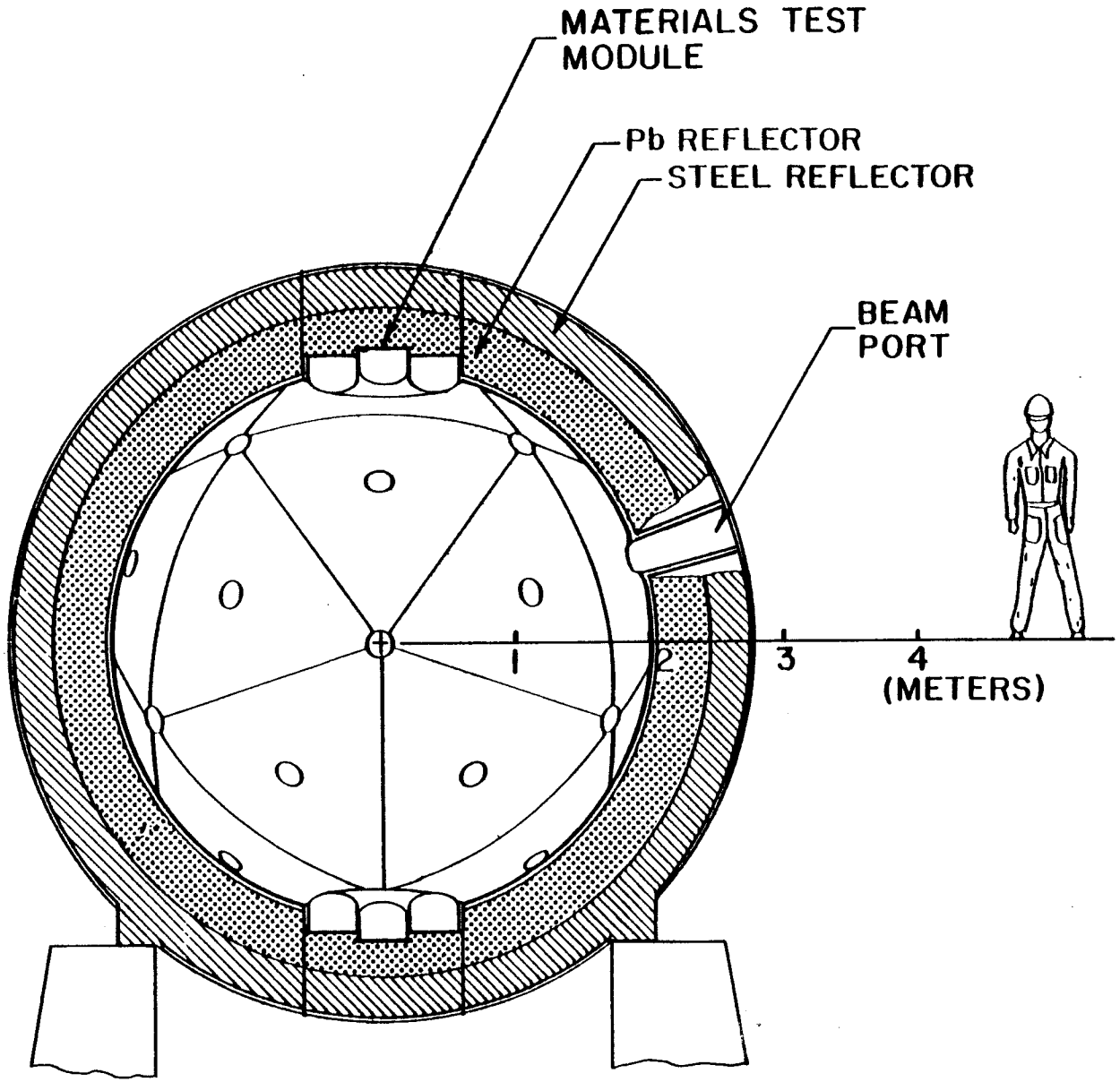

Fig. 2-1. Cross section of SIRIUS-M chamber.

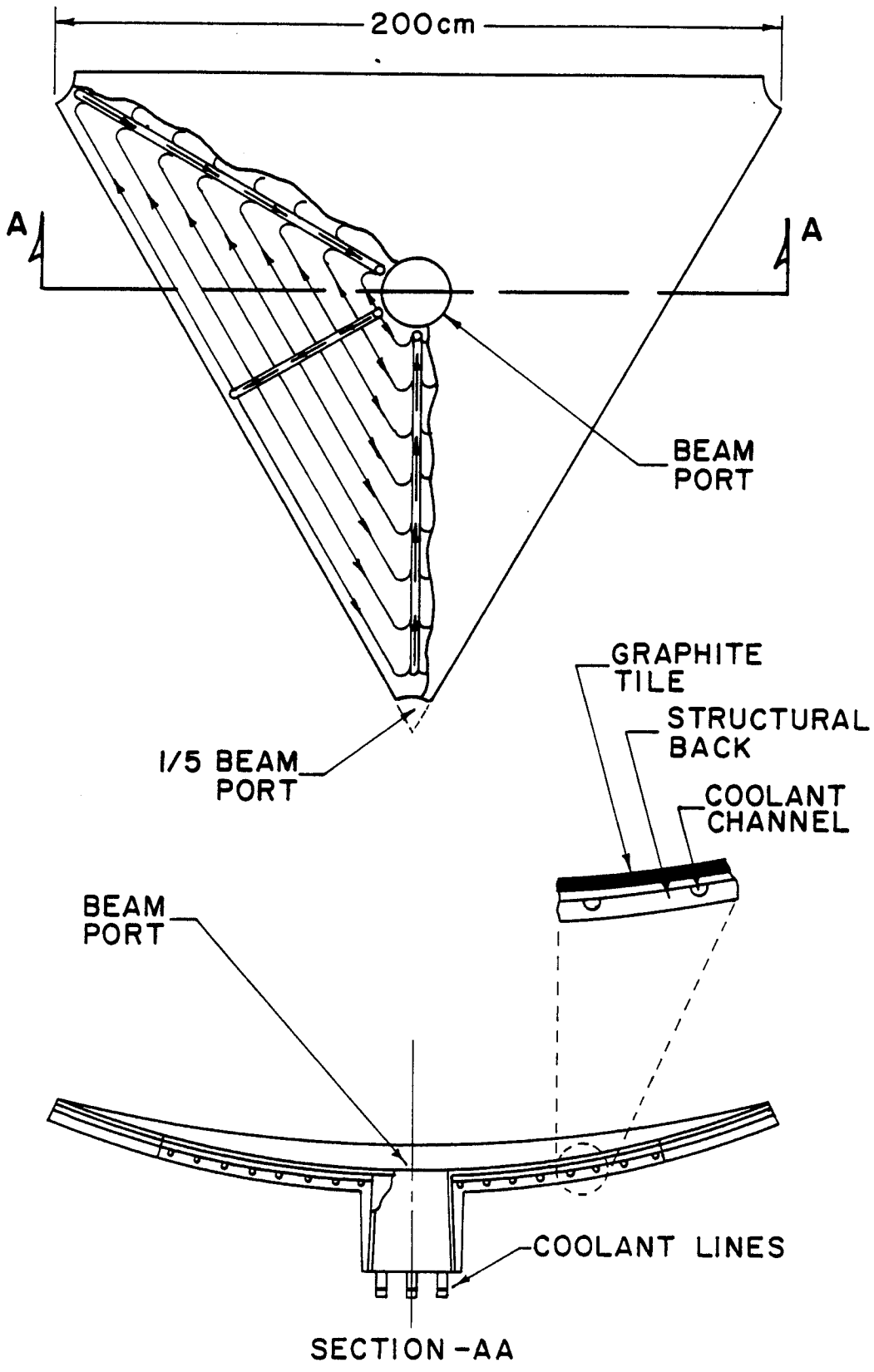

Fig. 2-2. Actively cooled graphite-faced tile.

ration from the beam tube to which it is attached, thus making insertion from inside the cavity possible. A locking mechanism is provided on the collar to anchor the tile to the beam port along with guide slots for proper orientation of the tile within the cavity. Clearly, some of the tiles will have to be modified to accommodate the materials and the blanket test modules.

The Pb reflector zone is 40 cm thick and follows immediately behind the protective tiles. It consists of two concentric spherical shells made of 316 stainless steel, with the outer and inner shells connected by the beam tubes. The function of this zone is to absorb most of the nuclear heating and it can either be self-cooled or actively cooled. In a self-cooled design, the molten lead is pumped out to a heat exchanger and then returned to the cavity. In an actively cooled design, the lead remains static and is cooled with water or helium gas. Since the nuclear heating in SIRIUS-M is nominal, the design of the Pb reflector is not critical.

The primary support structure for the cavity is the 30 cm thick stainless steel reflector zone. The function of this zone is to absorb or reflect neutrons and γ's which leak through the lead zone. Since water cooling is used for the first wall tiles, it would make sense to use water cooling for the steel reflector also. The scope of the study does not provide for a detailed design of the cavity and for this reason we have not determined a procedure for fabricating the various structures. In principle, it would be possible to combine the Pb and the steel reflectors into a single structure, thus simplifying the overall design.

The reactor cavity is contained within an evacuated spherical building which has no beam tubes between the final mirror and the cavity. Thus the cavity is supported within the center of the building on elevated columns.

One major advantage of this scheme is that the cavity support can be decoupled from the final mirror support, eliminating the possibility of transmitting vibration. Additionally, the accurate location of the cavity is not necessary as long as the location of the target within the cavity is consistent with the point at which the laser beams converge.

2.1.2 Cavity Maintenance

Most of the components of the reactor cavity will be designed to last the lifetime of the reactor. The components which will most likely require maintenance are the first wall tiles. Maintenance and replacement of the graphite faced tiles will require access to the inside of the reactor cavity. The 1.14 m diameter penetrations for the material test modules can serve as the access ports for insertion of a remote control special purpose machine which can service the tiles. Some modification of one of the materials test module penetrations will be needed to accommodate the insertion of first wall tiles which are ~ 2 m at their widest dimension.

Provision must also be made for servicing coolant lines at the back of the cavity. A special purpose remote maintenance machine designed to maneuver around the cavity will be needed for this purpose.

2.2 Reference Design - Reflected Light Limit

The major design goal of SIRIUS-M is to achieve the highest neutron wall loading. This is required for SIRIUS-M as a material test facility to accomplish the facility mission in the shortest possible time. For fixed target yield, the highest neutron wall loading is determined by the minimum cavity radius that would preserve the integrity of the first wall under the operating conditions.

It was shown[1,2] that the viability of the SIRIUS-M graphite first wall design depends critically on the laser light reflected from the target and the graphite reflectivity. For these reasons the laser absorption in the target should be maximized (see Chapter 7). In the base line design of SIRIUS-M, we assumed that 10% of the laser light (0.1 MJ) would be reflected from the target to the first wall, and the reflectivity of the graphite was assumed to be 50%.

The targets used in SIRIUS-M have a yield of 13.4 MJ, of which 0.8 MJ are carried by the x-rays, 2.6 MJ are carried by 10 ns, and the remainder by the neutrons. The x-ray, ion and neutron spectra for these targets are shown in Fig. 2-3. The 1 torr xenon gas used in the cavity absorbs most of the x-ray and ion energies and reradiates these energies as heat flux. The reradiated heat flux is spread over a long enough time to reduce the surface temperature rise considerably. The reflected laser light is, however, deposited over an extremely short time and is, therefore, more limiting.

It was found, based on the results of the parametric study conducted[1] to determine the minimum cavity radius (base-case), that for 2 m cavity radius, the maximum surface temperature is 1666 K, and the maximum thermal stress is only 12% lower than the compressive strength of the graphite at the peak surface temperature. The surface evaporation rate for this case is negligible. Figure 2-4 shows the incident power on the first wall (a) and the resulting temperature rise (b). The first three peaks in Fig. 2-4b are due to the leaked x-rays and the multiple reflections of the laser in the cavity; the next peak is due to the leaked carbon ions, and the last one is due to the reradiated heat flux from the Xe gas. Note that the multiple laser reflections are not shown in Fig. 2-4a, only the original laser pulse is shown.

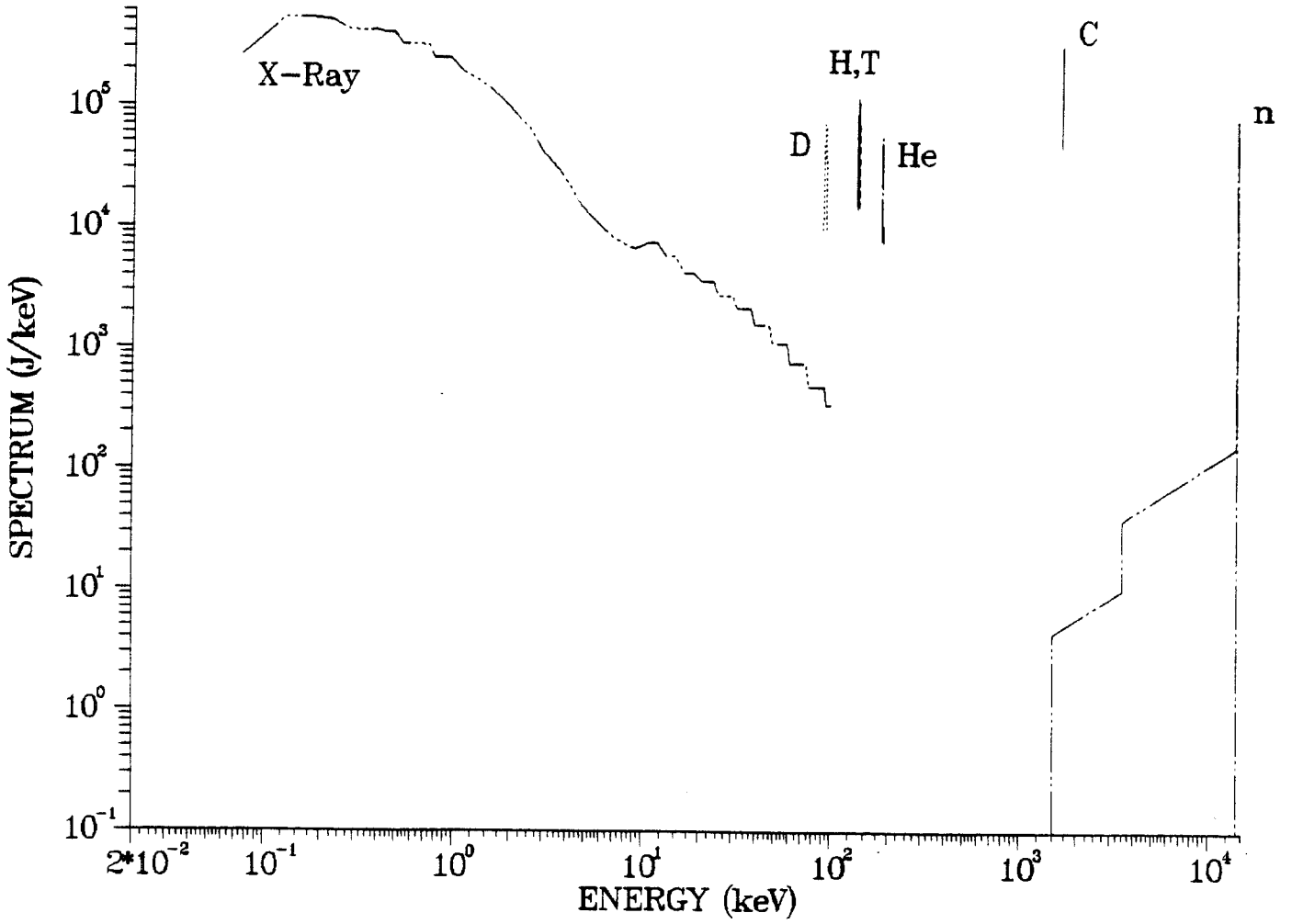

Fig. 2-3. X-ray, ion and neutron spectra for the SIRIUS-M target.

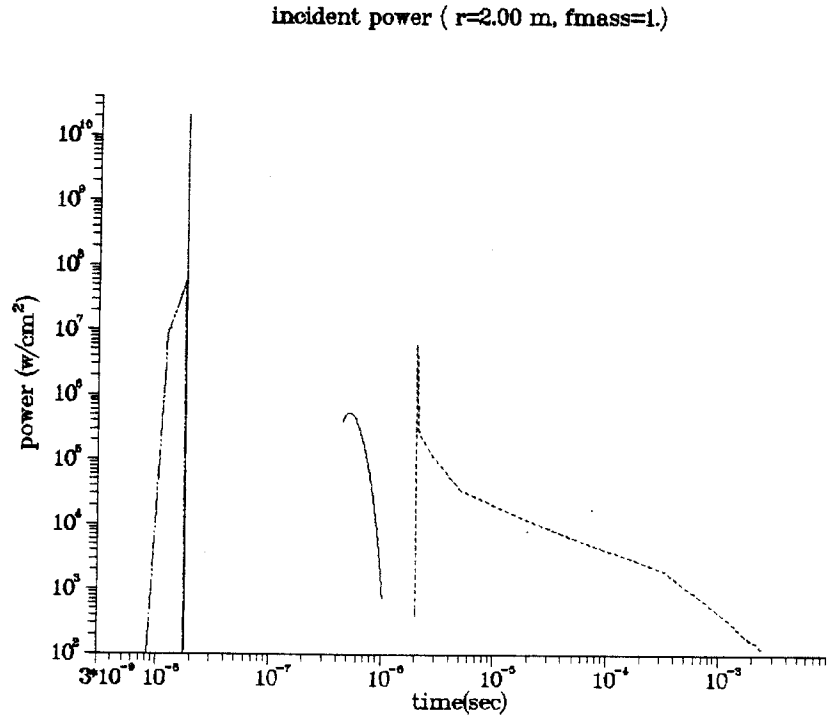

a)

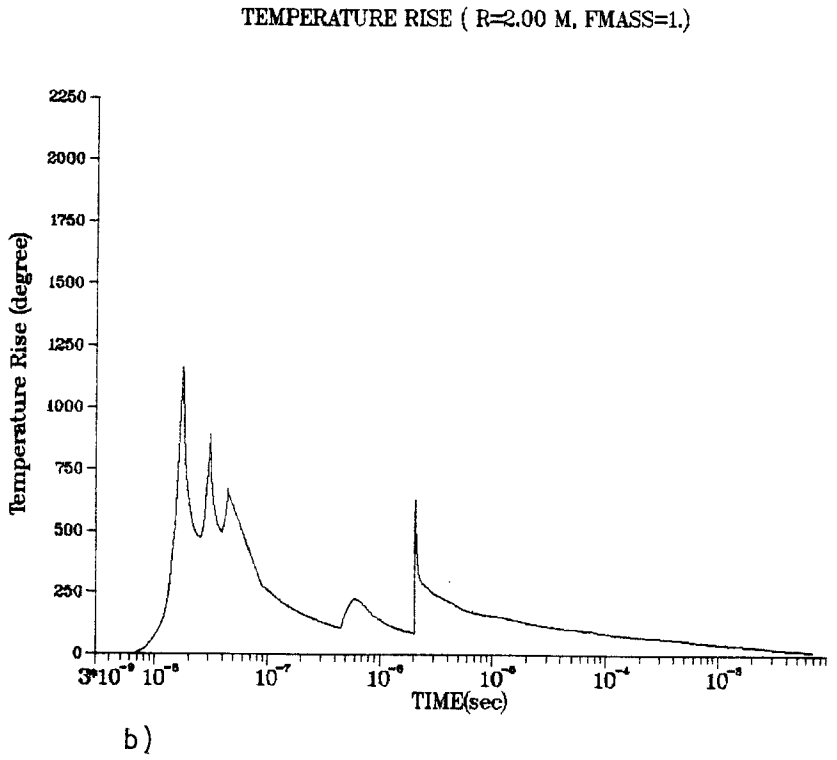

b)

Fig. 2-4. Incident power and temperature rise for the base case.

2.3 Optimal Design - Target Debris Limit

In the event that the laser light reflected from the target is less than expected, the minimum target chamber radius is set by the range of target debris ions in the target chamber gas. We have based the design on the requirement that the all target debris ions be stopped within the target chamber gas. Small changes in the design of the target can lead to significant differences in the energies and therefore ranges, of the debris ions. Therefore, we have designed target chambers and analyzed the behavior of chamber gases for three possible debris ion spectra. We have done ion stopping, fireball simulations, and wall heat transfer and vaporization calculations for these three designs.

The three targets considered are all based on the target design done by the University of Rochester.[1] All three designs yield 13.4 MJ for an input energy of 1 MJ. The three targets vary only in the different thicknesses of the plastic ablator. The product of the number of debris ions and their energies remains equal to the amount of energy deposited in the ablator by the target explosion. Therefore, an increase in the ablator mass leads to a decrease in energy per ion. The three target designs are the base case described in previous work,[1] a case with a 40% more massive ablator, and one with 2.1 times the ablator mass. The ion energies and numbers are shown in Table 2-1 for the three targets.

Ion stopping calculations have been done for the three targets, where the stopping medium is xenon gas at density that sustains a 1 torr pressure at 300 K. The details of these calculations are given elsewhere[1] and are not discussed here. The results are given in Fig. 2-5, where the energy density is shown plotted against distance into the gas for the three targets. Some-

Table 2-1. Energies and Number of Particles of Ion Debris for Different Cases

	Case 1*		Case 2		Case 3	
Ion	Energy[A]	Number of Particles	Energy	Number of Particles	Energy	Number of Particles
H	137.5	1.31 +19[B]	103.35	1.87 +19	68.9	2.8 +19
D	92.5	1.21 +19	93.9	1.3 +19	93.9	1.3 +19
T	139.0	1.21 +19	140.8	1.3 +19	140.8	1.3 +19
He	185.0	4.67 +18	187.7	5.0 +18	187.7	5.0 +18
C	1649.0	6.54 +18	1237.5	9.33 +18	825.0	1.4 +19

*Base Case. A. The unit is keV. B. Read as 1.4×10^{19}.

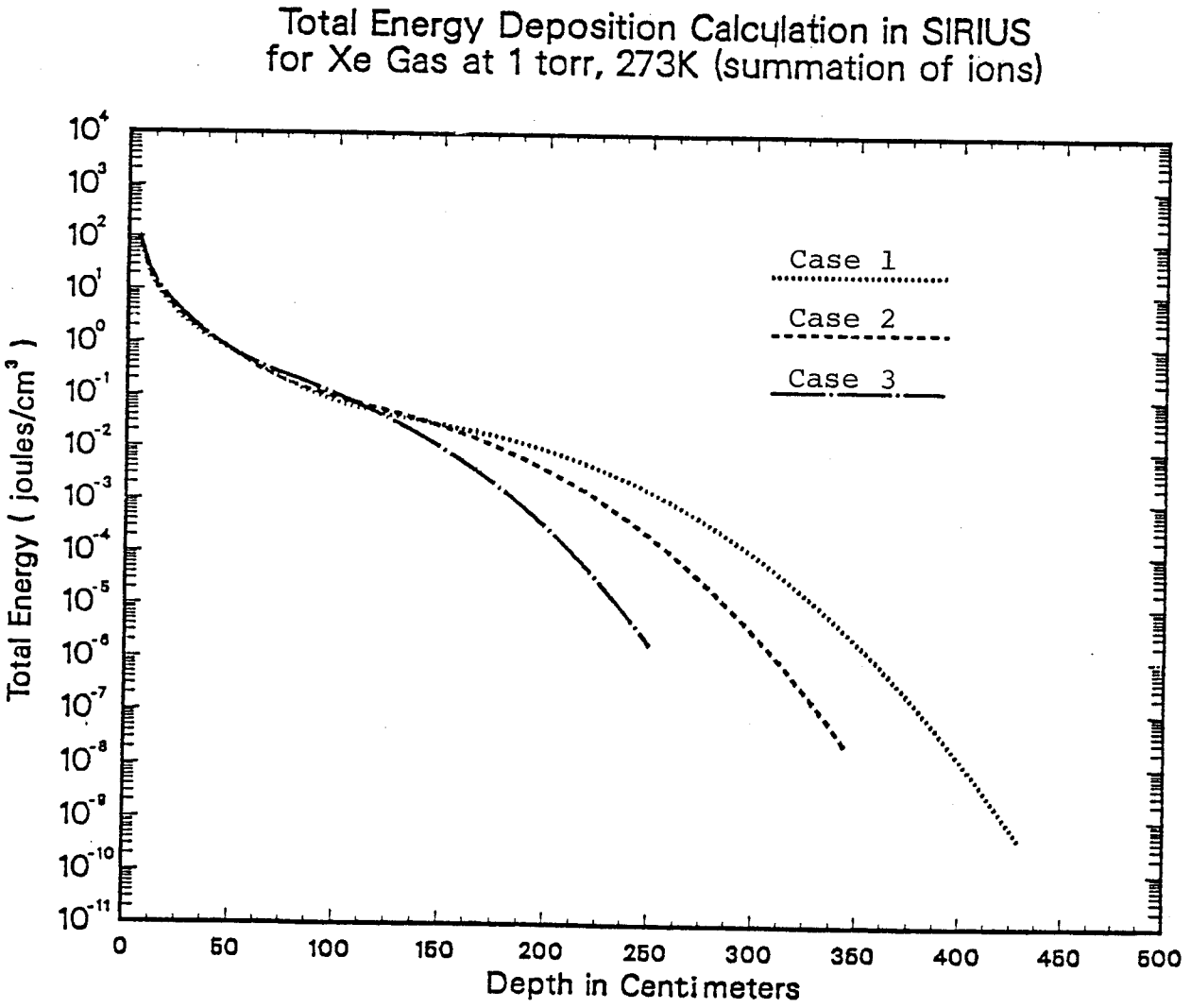

Fig. 2-5. Energy deposition profiles for three target debris spectra in 1 torr xenon.

what arbitrarily, 10^{-2} J/cm^2 was chosen as the acceptable energy density at which the target chamber wall may be placed. Therefore, the first wall may be at 2.0 m, 1.75 m, or 1.5 m, depending on the target.

Wherever the first wall is positioned, the thermal and mechanical forces on it must not be excessive. CONRAD,[3] a radiation-hydrodynamics computer code, has been used to simulate the formation of a blast wave from the energy density profiles shown in Fig. 2-5. In addition to the heating of the gas by ions, x-ray deposition is considered. The blast wave applies a pressure pulse and a heat flux onto the wall of the target chamber. The pressure pulse is low in amplitude and is of little importance. The heat flux is significant and is shown for the three cases in Fig. 2-6. These heat fluxes lead to temperature rises and thermal stresses that have been calculated in the first surface, which we assume is made of graphite. The heat fluxes on the surface and temperature rises are shown for cases 2 and 3 in Figs. 2-7 and 2-8. In addition to the reradiated heat of Fig. 2-6, the laser and ion contributions are included. The heat flux from the carbon ions, which occurs at about 10^{-6} s, decreases for these two cases from the base case. The calculated thermal stresses are shown in Fig. 2-9, plotted against the wall radius. The compressive strength of a graphite sphere is also shown to be above the calculated stresses, which are compressive, so that all three target-wall radius combinations lead to viable target chamber designs.

2.4 Economic Impact of Cavity Size

Several scenarios have been analyzed in order to quantify the economic impact of the cavity size and its operating parameters. The reflected light limited design of the 2 m cavity is the base case. Cases I-IV deal with various operating scenarios for the 1.5 m cavity (target debris limited design).

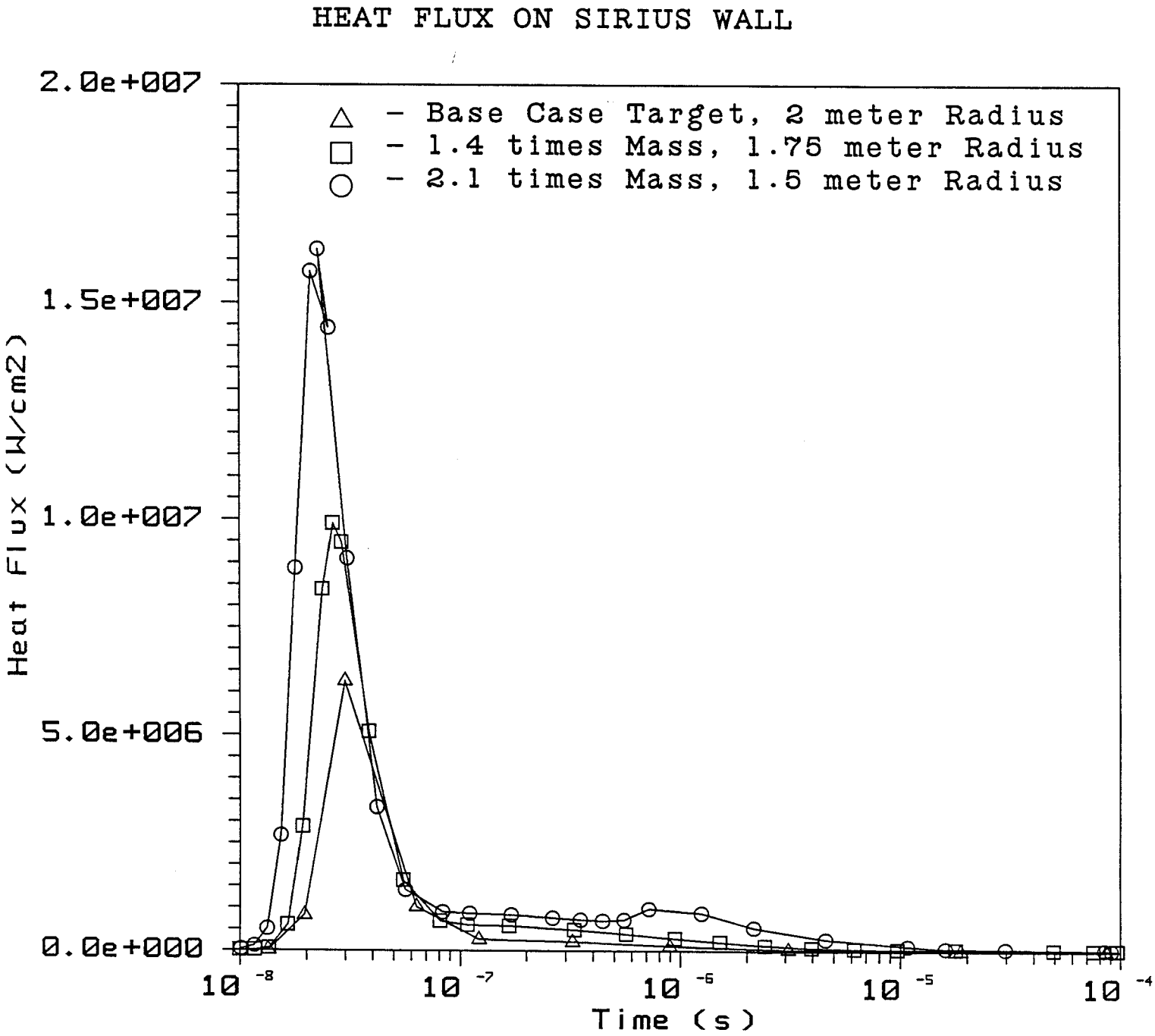

Fig. 2-6. Heat fluxes on SIRIUS first walls for three target-wall radius combinations.

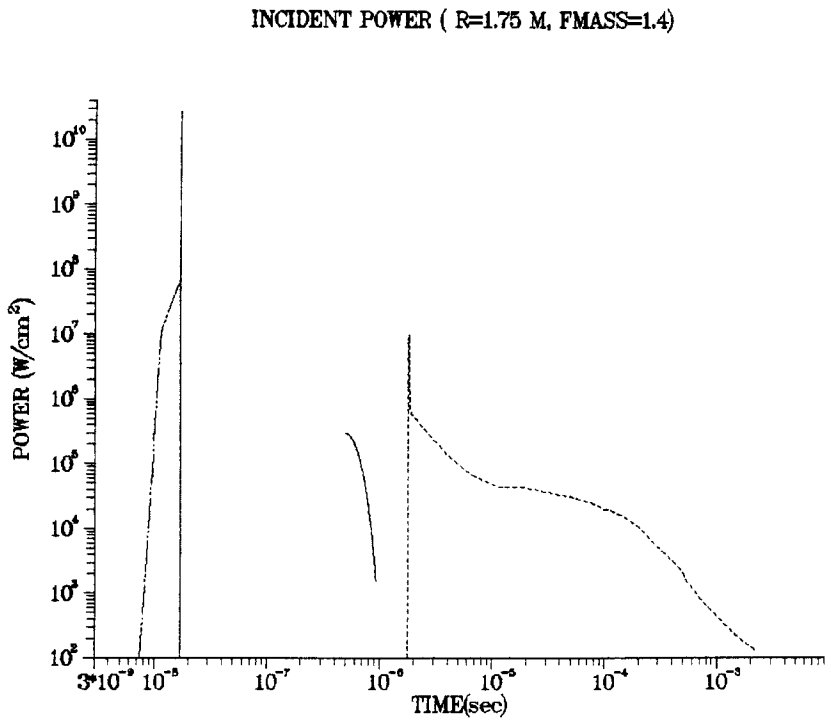

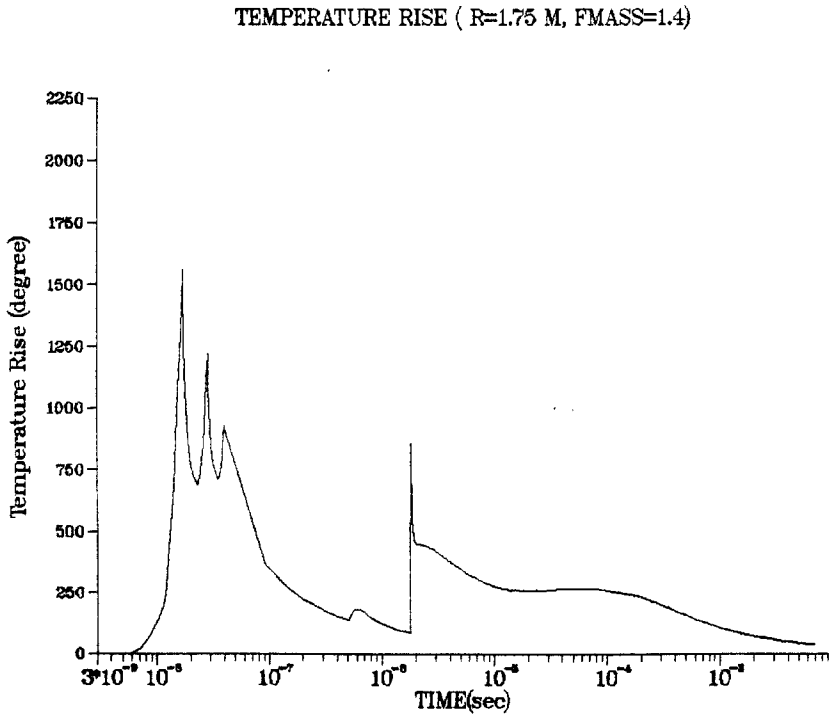

Fig. 2-7. Heat flux and surface temperature rise for SIRIUS first wall for case 2 target design.

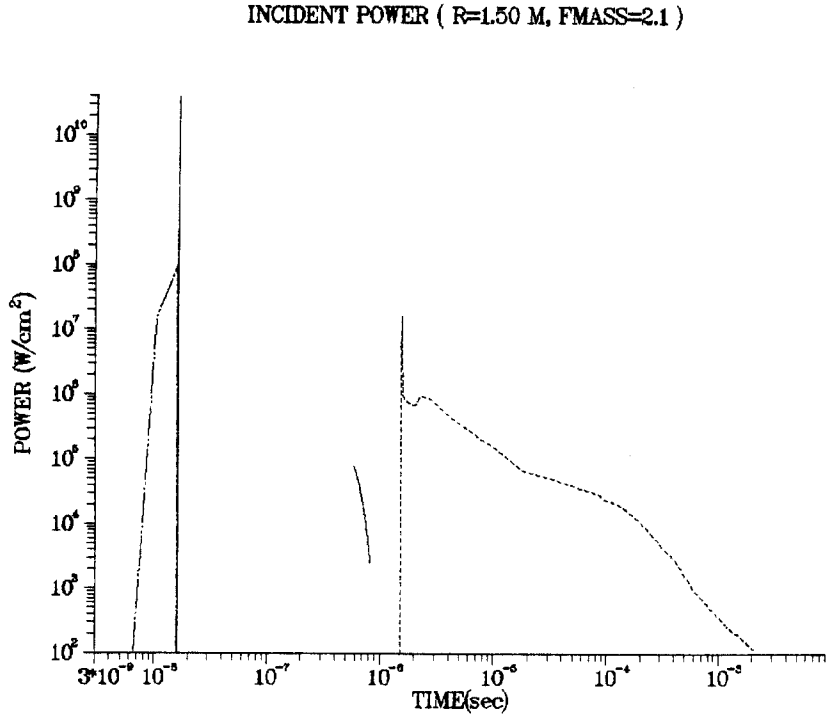

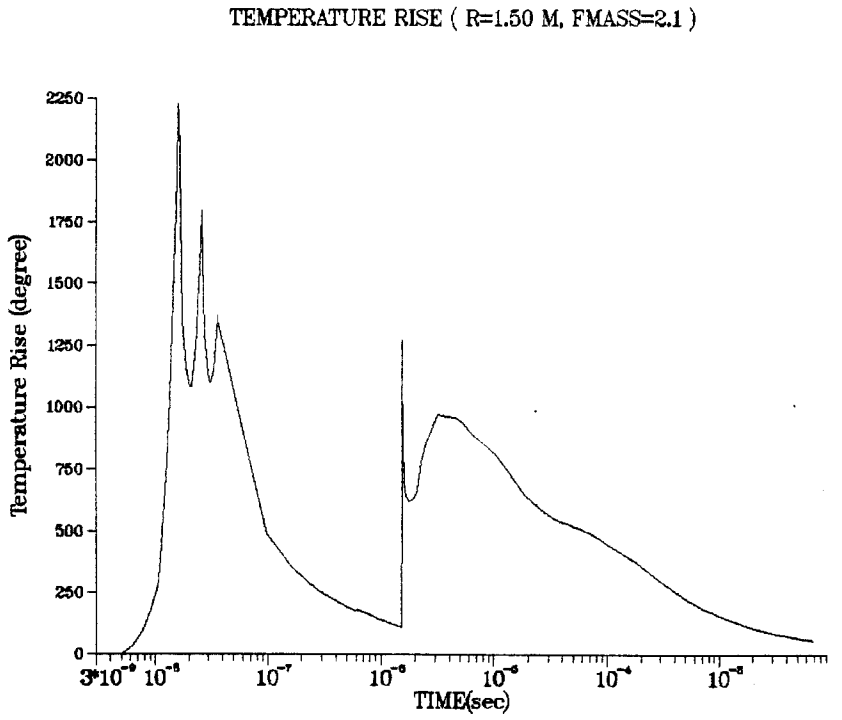

Fig. 2-8. Heat flux and surface temperature rise for SIRIUS first wall for case 3 target design.

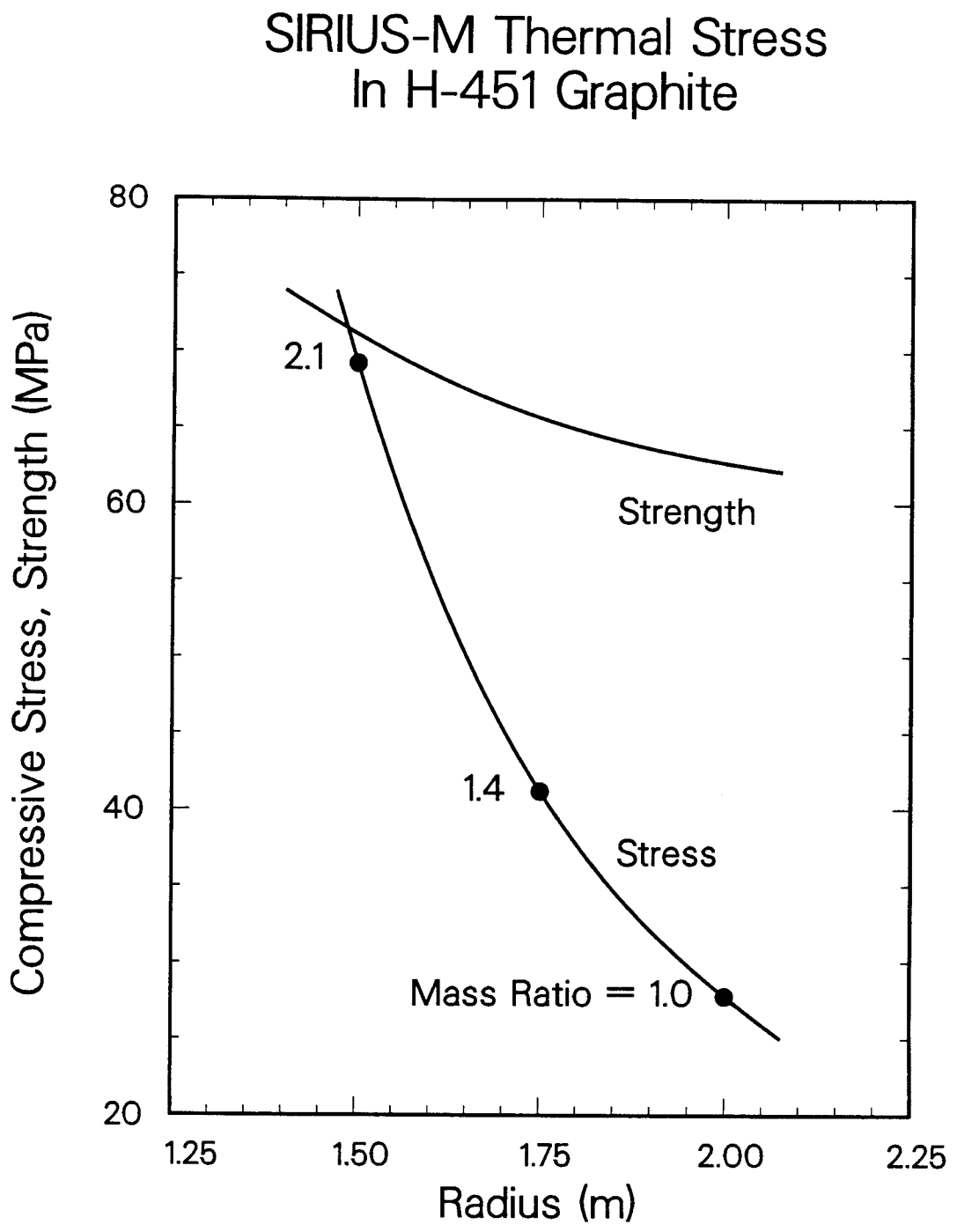

Fig. 2-9. Thermal stresses in SIRIUS first walls versus first wall radius. The target design is changing as the wall radius changes. The compressive strength on graphite is also shown.

Case I conserves the fusion power of the device and its cumulative performance (defined as the amount of damage, in dpa-ℓ, in the engineering test modules). This is accomplished by decreasing the total operating time from 10 years to 5.6 years. Case II keeps the wall loading and the cumulative performance constant (compared to the base case). Therefore the rep-rate is decreased to 5.6 Hz (from 10 Hz) in order to meet this criterion. Case III is for constant fusion power and total operating time of the device. This means that the cumulative performance significantly exceeds that of the base case. Case IV preserves the fusion power, cumulative performance and operating time. This is accomplished via lower availability of the facility (28% vs. 50% for the base case).

All the cases assume a target yield of 13.4 MJ. Cases I, III and IV have a significantly higher wall loading (3.6 MW/m^2) than the 2.0 MW/m^2 assumed in the base case and case II.

The economic impact of various options is based on the cost per dpa-ℓ. This figure is arrived at by dividing the total lifetime cost of the facility option by its cumulative performance in dpa-ℓ. The total lifetime cost is defined to be the sum of the total operating cost and the total overnight cost. The total operating cost is simply the product of the annual operating cost (involving the cost of fuel, electricity and operations and maintenance) and the total postulated number of years of operation. The total overnight cost is the sum of the total direct cost and total indirect cost of the facility, but doesn't include the interest and escalation during construction, if money is borrowed and invested over time.

Table 2-2 presents the pertinent operating parameters and the resulting cost figures for the various alternatives discussed above. Figure 2-10 shows

Table 2-2. Comparison in Design and Economic Parameters of the Reflected Light Limited and Target Debris Limited Options

	Base Case	Case I	Case II	Case III	Case IV
Wall loading (MW/m^2)	2.0	3.6	2.0	3.6	3.6
Target yield (MJ)	13.4	13.4	13.4	13.4	13.4
Rep rate (Hz)	10	10	5.6	10	10
Operation time (y)	10	5.6	10	10	10
Cumulative performance (dpa-ℓ)	14,200	14,200	14,200	25,245	14,200
Availability (%)	50	50	50	50	28
Total direct cost ($M)	519	510	490	510	510
Total overnight cost ($M)	855	841	807	841	841
Annual operating cost ($M/y)	74	74	52	74	52
Total lifetime cost ($M)	1595	1255	1323	1581	1357
Performance cost ($k/dpa-ℓ)	112	88	93	63	96

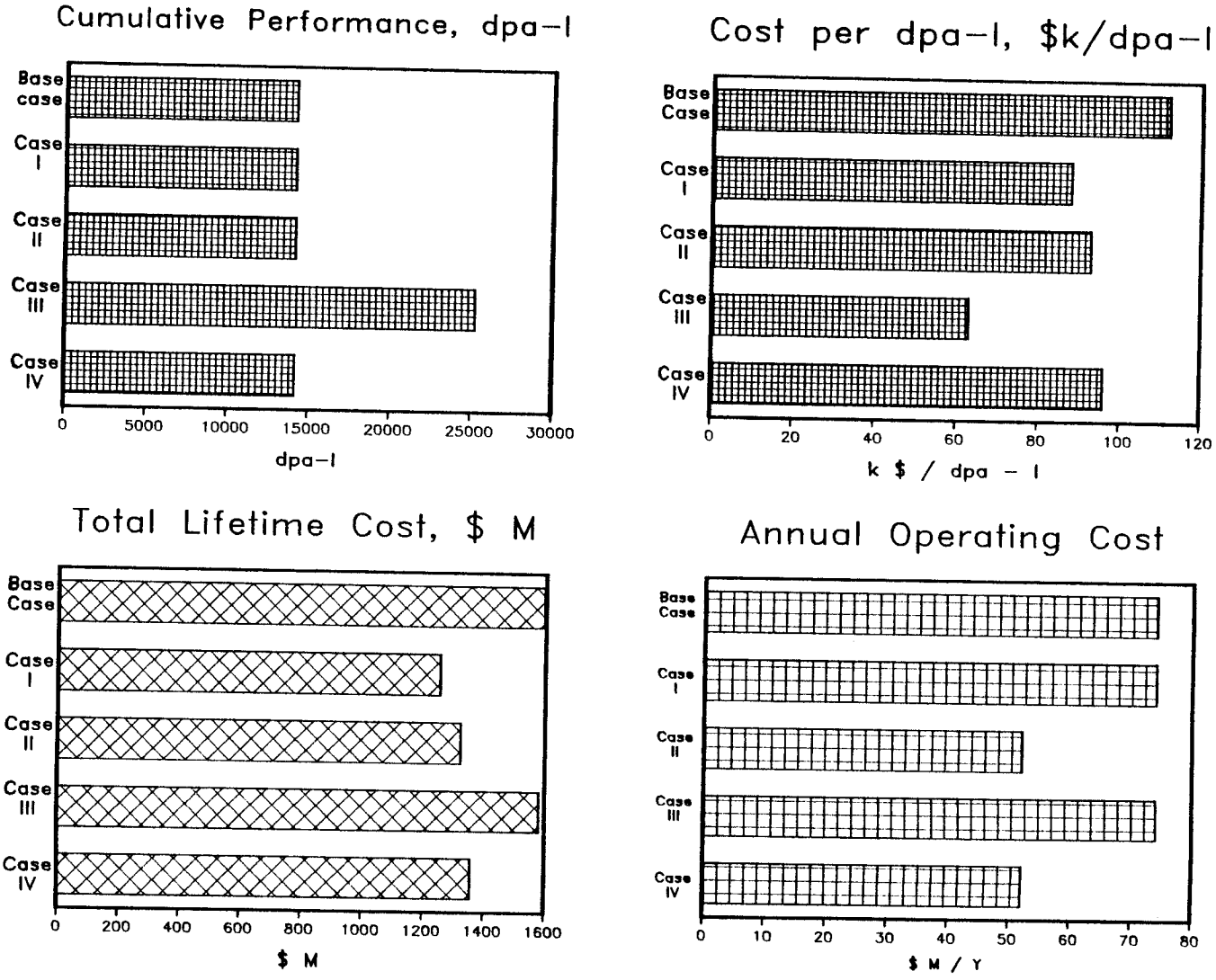

Fig. 2-10. Comparison in performance and economic impact of various design options.

the comparison in cumulative performance and certain economic parameters for these options. It is obvious that case III has, by far, the lowest economic impact (in $k/dpa-ℓ) due to the high cumulative performance, but its lifetime cost is the highest of all the target debris limited design options considered, and the wall loading is higher than that allowed by the present design.

References for Chapter 2

1. B. Badger et al., "SIRIUS-M: A Symmetric Illumination, Inertially Confined Direct Drive Materials Test Facility," University of Wisconsin Fusion Technology Institute Report UWFDM-651 (Sept. 1985).

2. H. Attaya et al., "Graphite First Wall Thermal Performance in ICF Reactors," J. Nucl. Mat. (1986) (in print).

3. R.R. Peterson, "CONRAD - A Combined Hydrodynamics-Condensation/Vaporization Computer Code," University of Wisconsin Fusion Technology Institute Report UWFDM-670 (April 1986).

3. MATERIALS TEST PLAN

3.1 Introduction

A test matrix has been devised that will provide data for an ICF Demonstration reactor on a timely basis. The data needs can be divided into three areas.

A. Scoping Studies for Structural Alloys

This is applied to the top four structural candidates which will be selected by the materials community and which are most likely to be the primary structural alloy. The selection of the four alloys will be made on the basis of data from:

a. fission reactor irradiations,

b. unirradiated properties,

c. any high energy neutron data which would be available from solid, liquid or plasma targets (including a magnetic fusion test facility).

Scoping studies will be conducted to narrow down to a primary and backup alloy which can be subjected to even more rigorous testing during the qualification stage.

B. Qualification Studies for Structural Alloys

These tests will concentrate on the two alloys (a primary and a backup) which appear to be the leaders at the beginning of the studies outlined in Section 3.1.1 above. However, after the data from irradiation to 25% of the goal fluence has been analyzed, a reranking of the alloys could be made and the choice of the top two alloys selected for qualification would be verified or one would start qualification studies on the "new" leaders. These subsequent tests would concentrate on a finer temperature

mesh and include larger test specimens. They would also investigate further minor impurity or metallurgical influences.

C. Nonstructural Materials Tests

In this category we include accelerated testing (to a few dpa) of laser mirror coatings, mirror structural and shielding components. Medium to long term tests (60 to 120 peak dpa) would also be conducted on neutron multipliers such as Be. Finally, longer term (up to the peak 120 dpa) tests of tiles and solid breeder materials could be conducted at temperatures much higher than expected in the structural components.

It will be shown below that it is possible to perform all the tests that are needed for the ICF Demo in the two SIRIUS-M test modules, each of which contains 217 capsules.

3.2 Scoping Studies for Structural Alloys

3.2.1 Explanation of Number of Specimens Required

The information needed to make the final capsule allocations is listed below.

- Number of Alloys Considered

At the present time we feel that there are three leading candidates for the ICF Demo structure and that one should leave room for at least one, high performance, refractory alloy. Current data from the materials community would center on the following for the prime candidates:

HT-9 Ferritic Steel

2-1/4 Cr-1 Mo Ferritic Steel

316 Steel with Ti Modifications

The high performance alloy could be a V-Ti alloy or a Mo-Re alloy.

- Number of Materials Variations

This category covers three areas: weldments, heat to heat impurity variations, and deliberate thermal mechanical treatments (e.g. cold working followed by specific tempering treatments). It is obvious that the welds are critical to the containment of the vacuum or coolants and designers have learned about the importance of such manufacturing influences from the LMFBR program.

- Duplicates

In any testing program, one has to expect equipment failures or human mistakes. Therefore, it is important to have duplicates of every specimen to insure that the continuity of the data is maintained. Many programs in the past have opted for more than one duplicate but we will use a single duplicate here until a more detailed analysis is made.

- Temperature Variations

It is important to not only test the materials over the anticipated operating temperature range, but also at off-normal conditions above and below the design temperatures. The choice of the actual test temperatures is usually a compromise between the need for a finer temperature mesh and the constraint of limited test space.

For SIRIUS-M we choose four test temperatures for the scoping studies and then designate another four temperatures, more closely spaced, for the qualification tests. For the steels, we choose 300, 400, 500 and 600°C for the scoping tests and 375, 425, 475 and 525°C for the qualification tests. The refractory metals will generally have a higher scoping temperature test range, e.g., 500, 600, 700, 800°C.

- Fluence Variation

The main idea in SIRIUS-M is to get data quickly, spaced at reasonable damage levels, and up to no less than 1/3 of the anticipated commercial operating fluence. Past experience indicates that extrapolations of more than a factor of three are very risky and some scientists would prefer to cut this to less than a factor of two. Since we anticipate a commercial reactor to require a first wall lifetime of > 200 dpa, this suggests that one should have scoping and qualification data in hand up to 70 dpa or more at the end of SIRIUS-M operation.

A possible operating scenario for the scoping studies would utilize four distinct capsule groupings for each temperature, labeled A, B, C and D for illustration here, and these capsules will be replaced on the following schedule.

Group A Remove first capsule at 2% of goal fluence and reinsert an identical capsule which will itself be removed at the 77% level to yield data corresponding to 75%.

Group B Remove first capsule after 5% of the goal fluence level and reinsert another capsule to be removed at the 30% level to yield data at 25% of the SIRIUS-M lifetime fluence.

Group C Remove first capsule after 15% of the SIRIUS-M life is achieved and reinsert another capsule to be removed after the 65% level is reached. This latter capsule will yield data at the 50% level.

Group D Leave the original capsule in for the full lifetime (100% damage level).

- Post Irradiation Tests

Very often a sample irradiated at a given temperature and stress level will be tested at different conditions after it has been removed from the reactor. For example, different tensile specimens, all irradiated at 600°C, may be tested at 600, 700 and 800°C to ascertain helium embrittlement possibilities. Likewise, post-irradiation tests may be conducted at a variety of strain rates to simulate off-normal transients. Fatigue samples may be tested at different strain levels or stress levels to fully measure fatigue life. To accommodate the above, and other experimental contributions, one may have to include samples for several post irradiation conditions.

3.2.2 Size of Test Specimens Required

There have been nine types of test specimens identified for SIRIUS-M testing. These specimens are similar in some cases to those used in TASKA-M, a tandem mirror, magnetic confinement fusion device designed for materials testing.[1] The dimensions of the specimens are given in Table 3-1 and they are graphically depicted in Fig. 3-1. The volume of each specimen is quoted as the "smooth" volume, i.e. as if an envelope was stretched over the maximum dimensions. The individual specimen volume varies by a factor of 1000 ranging from 0.014 cm^3 for microscopy specimens to 13.5 cm^3 for crack growth specimens.

3.2.3 Number of Specimens Required

Table 3-2 summarizes the number of specimens required for a complete understanding of the irradiation response for each of the four alloys. The total number of specimens for each alloy is 5600 and these specimens occupy 8229 cm^3 of volume. However, the test capsules must also contain coolants,

Table 3-1. Dimensions of Structural Alloy Test Specimens for SIRIUS-M

Description	Diameter cm	Thickness cm	Max. Width cm	Length cm	Vol. cm^3 (a)
Tensile - Surveillance	1.25	-	-	4.8	5.89
Tensile - Flat	-	0.075	0.5	4.5	0.17
Tensile - Round	0.64	-	-	4.8	1.54
Fatigue - High Cycle	0.6	-	-	3.0	1.07
Fatigue - Low Cycle	0.6	-	-	2.7	0.86
Fatigue - Crack growth	-	0.6	2.5	9.0	13.5
Fracture Toughness					
- Charpy	-	0.5	1.0	5.5	2.75
- Compact Tension (Surveillance)	-	1.27	3.04	3.18	12.3
- Compact Tension	-	0.5	2.1	2.2	2.31
Swelling/Microstructure	0.3	0.02	-	-	0.014
Creep Rupture	0.5	-	-	2.5	0.49

a) "Smooth" volume, outside envelope.

Table 3-2. Materials Test Matrix for Each Structural Alloy Tested in SIRIUS-M Scoping Studies

Test Types	Mat. Var.	Dupl.	Temp.	Fluence	Post-Irr. Test	Total # - Initial Load[a]	Initial Specimen Vol.-cm^3	Total #- Lifetime	Total Specimen Vol.-cm^3
Tensile									
Round	2	2	4	7	4[b]	256	394	448	690
Fatigue									
High Cycle	2	2	4	7	4[c]	256	274	448	479
Low Cycle	2	2	4	7	4[c]	256	220	448	385
Crack growth	2	2	4	7	2	128	1728	224	3024
Fracture Toughness									
Charpy	2	2	4	7	6[d]	384	1056	672	1848
Compact Tension	2	2	4	7	6[d]	384	887	672	1552
Swelling	8[e]	5	4	7	2	1280	18	2240	31
Creep/Rupture	8[f]	2	4	7	-	256	125	448	220
						3200	4702	5600	8229

(a) Initial load, replacement capsules reinserted after initial capsule removed.
(b) 2 rates, 2 temperature
(c) 2 stress levels, 2 strain levels
(d) 6 different temperature to determine DBTT
(e) 4 different heats/impurity levels x 2 weld variations
(f) 4 stress levels x 2 weld variations

TENSILE SPECIMEN
SURVEILLANCE TENSILE (ST)

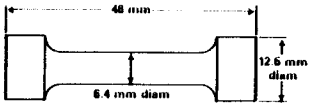

TENSILE SPECIMEN
FLAT TENSILE (FT)

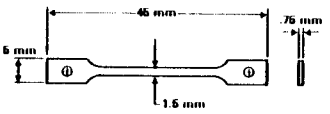

FRACTURE TOUGHNESS
COMPACT TENSION LARGE (CTL)

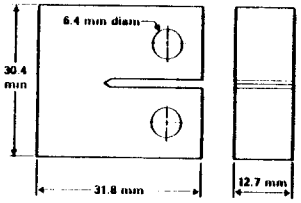

FRACTURE TOUGHNESS
COMPACT TENSION (CT)

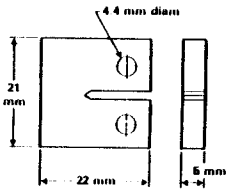

TENSILE SPECIMEN
ROUND TENSILE (RT)

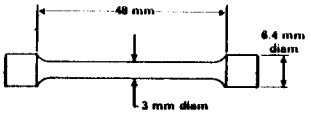

FRACTURE TOUGHNESS
CHARPY SPECIMEN (CH)

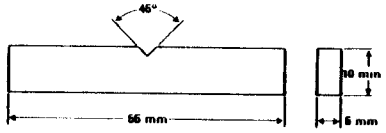

FATIGUE-CRACK GROWTH RATE SPECIMEN

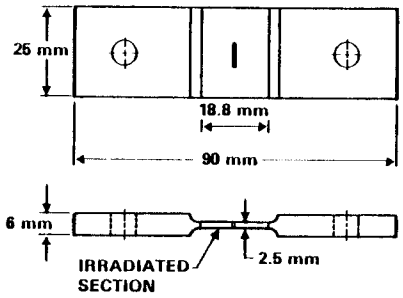

FULL SCALE

CONSTANT-AMPLITUDE LOAD-CONTROLLED HIGH-CYCLE FATIGUE SPECIMEN (HC)

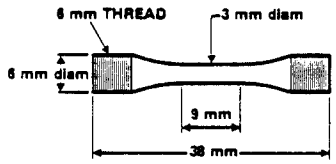

PRESSURIZED TUBE-CREEP SPECIMEN (C)

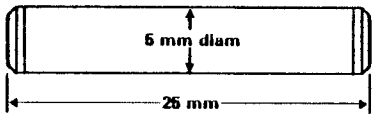

CONSTANT-AMPLITUDE STRAIN-CONSTROLLED LOW-CYCLE FATIGUE SPECIMEN (LC)

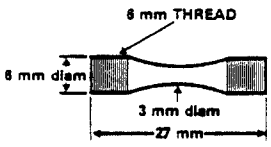

SWELLING AND MICROSTRUCTURAL SPECIMEN (TEM)

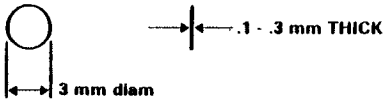

Fig. 3-1. Structural materials test specimens specified in the SIRIUS-M test matrix.

temperature control modifications, instrumentation, and diagnostics. Typically, the test specimens only occupy 1/3 to 1/2 of the space available. For this study we will assume 40% which means each 5 cm diameter by 20 cm long capsule (393 cm^3) contains ~ 157 cm^3 of specimens. One can see that roughly 32 capsules are initially needed for each alloy and there are 56 capsules needed for each alloy for all the fluences and temperatures.

Table 3-3 summarizes the total initial loading of capsules for the scoping studies and Table 3-4 lists the number of specimens available at each dpa/temperature test matrix position. It is expected that each set of test specimens will be immersed in a coolant contained in a can of the same material, i.e. HT-9 samples in a HT-9 can filled with NaK or other suitable heat transfer medium. Ferritic, austenitic and refractory alloys will not be mixed.

3.3 Material Qualification Tests

It is anticipated that after the data from the 25% of goal fluence specimens are analyzed, a reevaluation of the rank ordering will be made establishing the most likely primary and backup alloy for the ICF Demo. At that point larger surveillance samples and a finer temperature mesh will be used to provide a stronger case for the designers. Table 3-5 gives the modified test matrix for the materials qualification studies while Tables 3-6 and 3-7 summarize the number of capsules and specimens discharged at each temperature and fluence mesh point. An initial load of 112 capsules is required and eventually another 84 replacement capsules are required.

3.4 Special Materials Tests

These test capsules contain non-first wall and blanket structural samples, some of which do not require high fluences and others which would require lifetime fluence values. The short term tests include coatings for

Table 3-3. Summary of Capsules Needed for Each Alloy in the Scoping Studies

Damage Level % of Goal dpa	300°C(d)	400°C(d)	500°C(d)	600°C(d)	
2(a)	2	2	2	2	32 Initial Capsules
5(b)	2	2	2	2	
15(c)	2	2	2	2	
100	2	2	2	2	
25(b)	2	2	2	2	24 Replacement Capsules
50(c)	2	2	2	2	
75(a)	2	2	2	2	

Total - 56 Capsules

(a) After 2% capsule is discharged it is replaced with a 75% capsule.
(b) After 5% capsule is discharged it is replaced with a 25% capsule.
(c) After 15% capsule is discharged it is replaced with a 50% capsule.
(d) These temperatures become 500, 600, 700 and 800°C for the refractory alloy.

Table 3-4. Summary of Samples Available from Each Materials Scoping Studies dpa/Temperature Test Matrix Position in SIRIUS-M

	# of Samples at each Damage Level and Temperature[a]	Volume of Sample at each Damage Level and Temp. - cm^3
Tensile - Round	16	25
Fatigue		
High Cycle	16	17
Low Cycle	16	14
Crack growth	8	108
Fracture Toughness		
Charpy	24	66
Compact Tension	24	55
Swelling	80	1.1
Creep/Rupture	16	7.8
TOTAL	200	294[b]

(a) % of goal dpa = 2, 5, 15, 25, 50, 75, and 100
temperature = 300, 400, 500, 600°C for steels
temperature = 500, 600, 700 800°C for refractory metal

(b) total volume 294 cm^3, requires 2 capsules using approximately 40% of its volume for test specimens and 60% for coolant, structure, gas gaps, etc.

Table 3-5. Materials Test Matrix for Each Structural Alloy in SIRIUS-M Qualification Studies

Test Types	Mat. Var.	Dupl.	Temp.	Fluence	Post-Irr. Test	Total # - Initial Load[a]	Initial Spec. Vol. cm^3	Total #-Lifetime	Total Spec. Vol. cm^3
Tensile									
Surveillance	4	2	4	7	4	512	3,016	896	5,278
Fatigue									
High Cycle	4	4	4	7	4	1024	1,096	1,792	1,917
Low Cycle	4	4	4	7	4	1024	881	1,792	1,541
Crack growth	4	2	4	7	2	256	3,456	576	7,776
Fracture Toughness									
Charpy	4	4	4	7	6	1536	4,224	3,456	9,504
Compact Tension	2	2	4	7	6	384	4,723	864	10,627
Swelling	16	4	4	7	2	2048	29	4,608	65
Creep/Rupture	16	2	4	7	-	512	251	1,152	565
						7296	17,676	15,136	37,273

Table 3-6. Summary of Capsules Needed for Each Alloy in the Materials Qualification Studies

% of Goal Fluence	375°C[a]	425°C[a]	475°C[a]	525°C[a]	
2[b]	7	7	7	7	Initially
5[c]	7	7	7	7	112
15[d]	7	7	7	7	Capsules
100	7	7	7	7	
25[c]	7	7	7	7	84
50[d]	7	7	7	7	Replacement
75[b]	7	7	7	7	Capsules

Total - 196 Capsules

(a) These temperatures become 550, 650, 750 and 850°C for the refractory alloy.
(b) After 2% capsule is discharged, it is replaced with a 75% capsule.
(c) After 5% capsule is discharged, it is replaced with a 25% capsule.
(d) After 15% capsule is discharged, it is replaced with a 50% capsule.

Table 3-7. Summary of Samples Available from Each Materials Qualification Studies Temperature and Fluence Mesh Point in SIRIUS-M

	# of Samples at each Damage Level and Temperature[a]	Volume of Samples at each Damage Level and Temp. - cm^3 [b]
Tensile - Surveillance	16	94
Fatigue		
High Cycle	64	68
Low Cycle	64	55
Crack growth	16	216
Fracture Toughness		
Charpy	96	264
Compact Tension	24	295
Swelling	128	2
Creep/Rupture	32	16
TOTAL	440	1010

(a) % of goal damage = 2, 5, 15, 25, 50, 75, and 100
temperature = 300, 400, 500, 600°C for steels
temperature = 500, 600, 700 800°C for refractory metal

(b) total volume 1010 cm^3, requires 7 capsules at approximately 40% test specimens and 60% coolant, structure, gas gaps, etc.

laser optics, mirror support alloys, and shield materials such as B_4C, W, etc. Long level tests would include Be or other neutron multipliers as well as tiles/coatings to face the target and ceramic breeder materials.

The volume of each specimen is given below in cm^3.

Tiles - 0.5

Laser Coatings - 0.1

Solid Breeders - 1

Be - 1

Shield Materials - 1

Mirror Support

- Tensile - 1.54
- Fatigue - 1.07
- Crack growth - 13.5
- Microstructure - 0.014

Table 3-8 gives the test matrix for the special materials along with the number and volume of test specimens while Table 3-9 summarizes the total number of capsules needed. It can be seen that 8 capsules are needed for short term tests and 12 capsules are needed for reincapsulation studies. The reincapsulation probably can be included in the quick turnaround, central parts of the test modules, each of which contains 24 capsules.

3.5 Total Number of Test Capsules Required

Table 3-10 summarizes the total test matrix requirements. It can be seen that the initial load requires 372 capsules out of 434 available positions leaving 62 "open" capsules. These capsules could be used to map the neutron flux or be fitted with neutron multipliers such as Pb, Be or even U. This space can also be utilized for advanced material development. The materials test schedule in SIRIUS-M is shown in Fig. 3-2.

Table 3-8. Materials Test Matrix for Nonstructural Materials in SIRIUS-M

Test Types	Mat. Var.	Dupl.	Temp.	Fluence	Post-Irr. Test	Total #	Total Vol. cm^3
Tiles	6(a)	2	3(b)	5(c)	6(d)	1080	540
Laser Coatings	6(e)	2	2(f)	2(g)	2	96	10
Solid Breeder	6(h)	2	3	7	2(j)	504	504
Be	2	2	3	7	2(k)	168	168
Shield Material	4(l)	2	2	2(g)	2	64	64
Mirror Support							
Tensile	2(m)	2	2(f)	2(g)	2	32	49
Fatigue	2(m)	2	2(f)	2(g)	2	32	37
Crack growth	2(m)	2	2(f)	2(g)	2	32	432
Microstructure	2(m)	2	2(f)	2(g)	2	32	1

(a) C, SiC, and a ceramic to be specified x 2 fabrication procedures
(b) 1000, 1200, 1400°C
(c) 10, 25, 50, 75, 100 % of goal fluence
(d) Thermoconductivity, tensile (2 strain rates), fatigue (3 conditions)
(e) 3 different coatings x 2 process variables
(f) RT, 100°C
(g) 1 and 2% of goal fluence
(h) Li_2O, $LiAlO_3$, $LiSiO_3$ x 2 process variables
(j) Thermal conductivity, T_2 content
(k) Dimensions, thermal conductivity
(l) W and B_4C x 2 process variables
(m) 2 alloys

Table 3-9. Summary of Test Capsules for Nonstructural Materials

Test Types	# of Temp.	Capsules at Each Temp.	Initial Total Capsules
Long term			
Tiles	3	2	6(a)
Solid Breeder	3	1	3(d)
Be	3	1	3(d)
Short term			8(c)
Shield Material	2	(b)	(b)
Laser Coating	2	(b)	(b)
Mirror Support			
Tensile	2	(b)	(b)
Fatigue	2	(b)	(b)
Microstructure	2	(b)	(b)
Crack growth	2	(b)	(b)
			18

(a) Samples will be removed at 10, 25, 50, 75 and 100% of goal fluence and the capsule reinserted.
(b) Included in 8 test capsules for shield, coating, and support materials.
(c) First 4 capsules removed at 1 dpa and second 4 capsules removed at 2 dpa.
(d) Samples removed at 2, 5, 15, 25, 50, 75 and 100% of goal fluence and capsule reinserted.

Table 3-10. Total Test Capsule Requirements for SIRIUS-M

Test Type	Load Initially	Replacement Capsules	Total Capsules
Scoping			
HT-9	32	24	56
2 1/4 Cr-1 Mo	32	24	56
316 + Ti	32	24	56
Refractory Alloy	32	24	56
Qualification			
Primary	112	84	196
Backup	112	84	196
Special Materials			
Short Term	8	0	8
Reincapsulation	12	0	12
	372	364	636

Total Capsule Positions Available 2 x 217 = 434

2 x 24 = 48 quick change capsules, 2 x 193 = 386 long term capsules

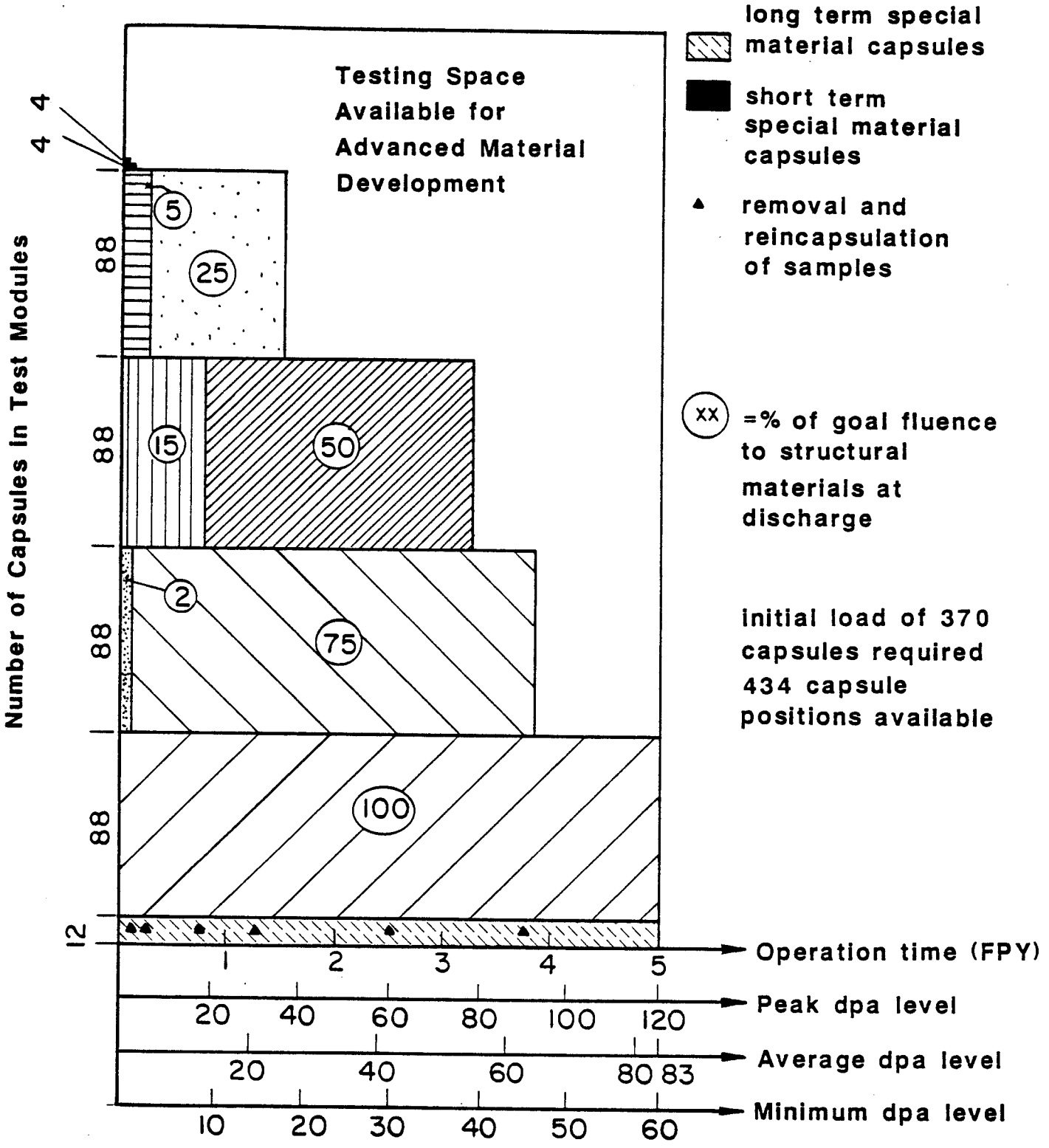

Fig. 3-2. Materials testing schedule in SIRIUS-M.

References for Chapter 3

1. B. Badger et al., "TASKA-M, A Low Cost, Near Term Tandem Mirror Device for Fusion Technology Testing," University of Wisconsin Fusion Technology Institute Report UWFDM-600. Also, Kernforschungszentrum Karlsruhe Report KfK-3680 (1984).

4. BLANKET TESTING REQUIREMENTS

4.1 Unique ICF Blanket Problems

A scoping study has been conducted to identify the unique ICF blanket testing requirements. With the exception of two, most of the problems can be tested within the materials test module. The two unique problems have to do with isochoric heating in reactor coolant/breeder materials, particularly liquid metals. The first problem is discussed in Section 4.2 and has to do with the stresses and their effect on blanket structures, resulting from impulse pressures due to isochoric heating. The second problem deals with the effect of pulsed heating on the corrosion rates of structural materials. A test module design for determining this effect is described in Section 4.3.

Table 4-1 summarizes the unique blanket testing requirements for ICF reactors. We have broken the problem into four distinct areas, self-cooled and He-cooled liquid breeders, He-cooled solid breeders, water cooled solid breeders and hybrid blankets. The table classifies the test duration as short or long, and indicates the location where the test will be carried out. The only short term tests have to do with determining the magnitude of isochoric heating in liquid metals and water and model validation as well as verification of the solution for these cases. These tests will be performed in instrumented zones of the Pb reflector and water cooled elements. Corrosion rate dependence on the state of stress due to isochoric heating is a long term test which will be performed in a special blanket test module.

All the other tests have to do with breeder/multiplier material integrity, T_2 removal issues, transient effects on T_2 diffusion and effectiveness of T_2 diffusion barriers. These are all long term tests and will be carried out in the materials test modules.

Table 4-1. Unique Blanket Testing Requirements

Unique ICF Blanket Problem	Test Duration	LOCATION: Instrumented Zone of Pb Reflector	LOCATION: Materials Test Module	LOCATION: Blanket Test Module
1 Self-Cooled & He-Cooled Liquid Breeders				
• Pulsed Heating				
- Model Validation	Short	X		
- Efficacy of Solution	Short	X		
• Corrosion Rate Dependence on State of Stress				
- Pulsed Heating Effect	Long			X
2 He-Cooled Solid Breeders				
• Breeder/Multiplier Integrity				
- Effect on T_2 Removal Capability	Long		X	
- Impact of Transient Effects on T_2 Diffusion	Long		X	
3 Water Cooled Solid Breeders				
• Breeder/Multiplier Integrity	Long		X	
• Effect of Pulsed Heating				
- T_2 Diffusion into Coolant	Long		X	
- Effectiveness of Diffusion Barriers	Long		X	
• Pulsed Heating of H_2O	Short	X		
4 Hybrids				
• Integrity of T_2 Breeder, Fissile Material and Multiplier	Long		X	

4.2 Mechanical Response from Isochoric Heating

Energy deposition in the liquid metal blanket of SIRIUS-M will produce temperature and pressure gradients. Pressure waves may develop and travel through the blanket, dynamically loading structural walls and components. Load magnitudes and blanket mechanical response have been determined in order to assess structural integrity.

The model consists of liquid metal contained between two thin concentric spherical shells representing the structural walls. The initial pressure distribution from the practically instantaneous temperature change is approximated as

$$p(r) = [\beta b Y / c_p \rho \lambda \pi (r_o + r_i)^2] \exp [-(r - r_i)/\lambda]$$

where β = adiabatic bulk modulus

b = volumetric thermal expansion coefficient

Y = neutron yield

c_p = heat capacity

ρ = liquid density

λ = e-folding distance

r_o, r_i, r = outer, inner and generic radii

Pressure and fluid velocity histories can be obtained from linear wave theory. Generally the amplitude of the pressure wave increases directly with blanket thickness, but at a diminishing rate. Increases in blanket thickness will also result in a lower mean pressure rise since there is more material to absorb energy.

For structural loading purposes, the impulsive pressure is required and obtained by integrating the pressure exerted on the inner shell during the compressive phase of the pulse. Results are shown in Fig. 4-1 for a 2 m radius shell, as a function of blanket thickness, with comparisons made between lithium, lead and $Li_{17}Pb_{83}$. For SIRIUS-M, a 40 cm thick lead blanket is used.

The mechanical response of the inner shell of the blanket is assumed to be a completely symmetric elastic displacement mode. A thin spherical shell has a single natural frequency for symmetric motion. A thick shell has multiple frequencies but for a moderate thickness, the fundamental frequency is much lower than any others and the contribution to stress and strain from the higher modes is negligible. The spherical shell frequency depends upon the elastic modulus, density, Poisson's ratio and radius but is independent of thickness. Under uniform impulsive pressure, the maximum dynamic circumferential normal stress is independent of chamber radius. Peak values are represented in Fig. 4-2 for various wall thicknesses; damping and inertia effects of the liquid metal were not included but would result in lower stresses. It is also assumed that such damping would preclude the necessity of considering sequential impulse effects. Generally, maximum dynamic stresses in the blanket shell appear quite low. For example, the undamped maximum for a 1 cm thick shell is less than 30 MPa, a value below endurance limits for structural steels.

Since tubular components are also proposed for the blanket test module, maximum dynamic stress from impulsive pressure was also determined and is shown parametrically in Fig. 4-2. Again, these stresses are radius-independent. As a first approximation, if it is assumed that the impulsive

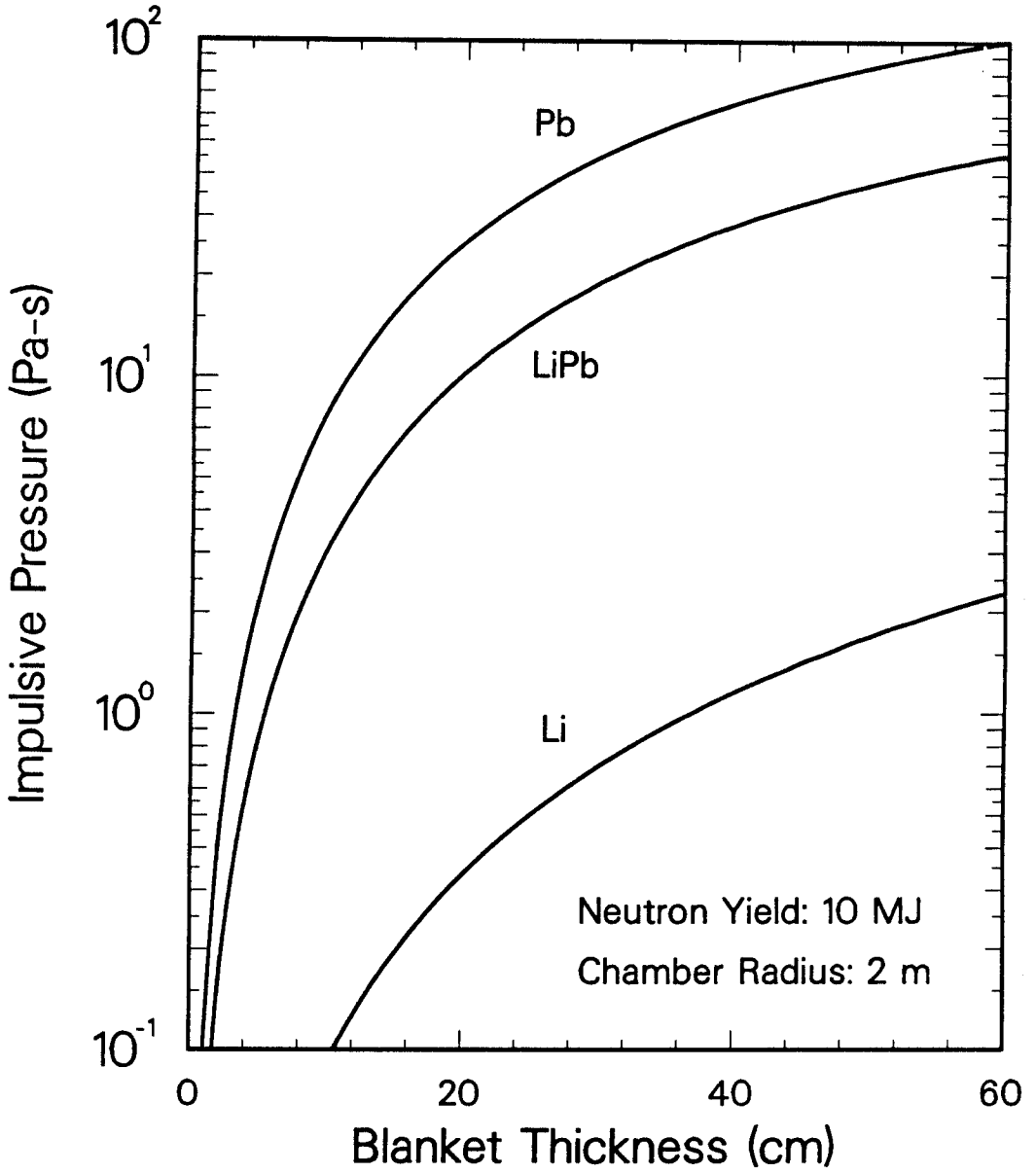

Fig. 4-1. Mechanical impulse from isochoric heating of SIRIUS-M blanket.

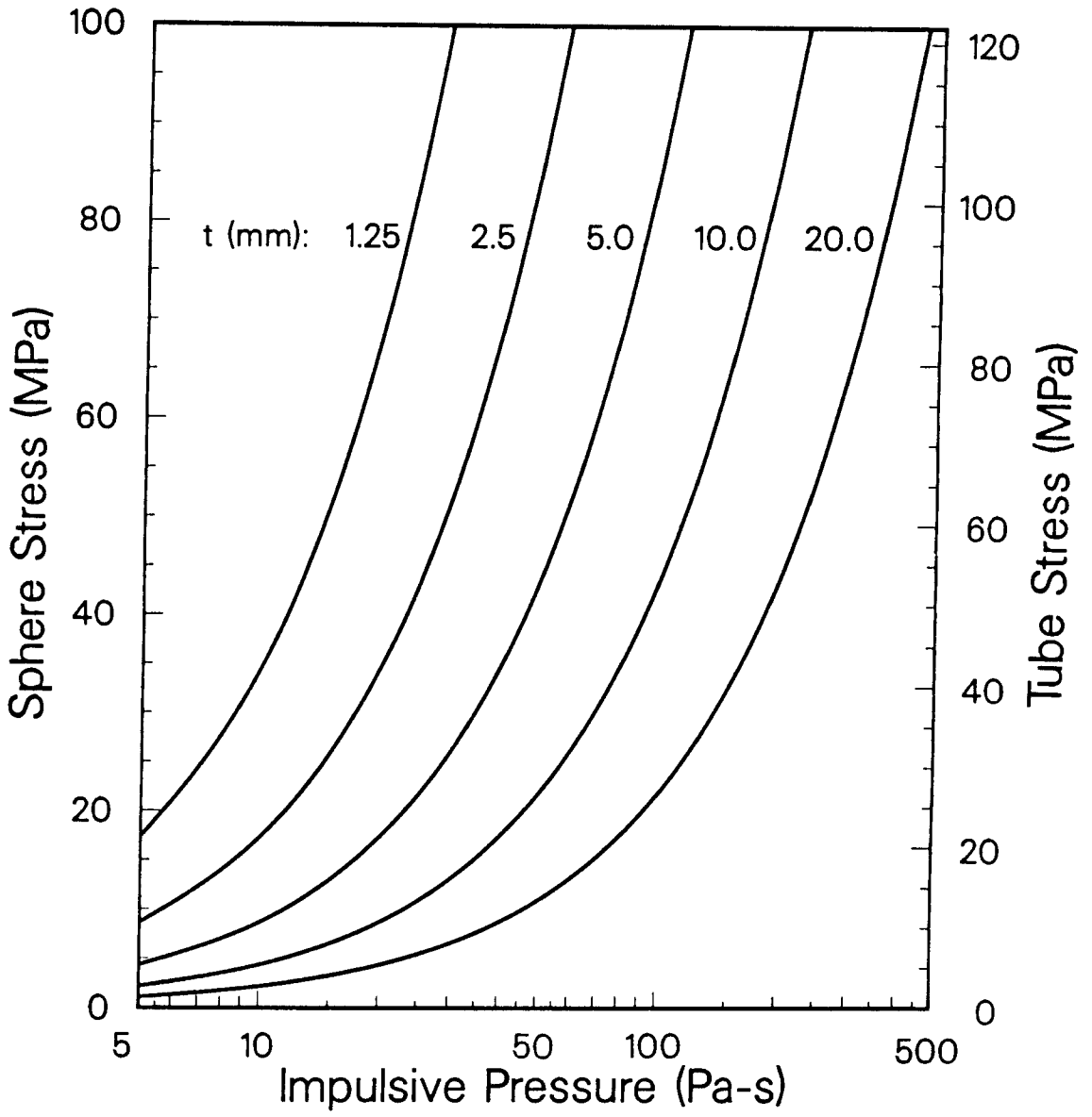

Fig. 4-2. Maximum impulsive stress in steel tubes and spherical shells.

pressure on tubular members is no greater than that on the blanket shell, it can be seen that corresponding maximum stresses will also be low for practical tube wall thicknesses.

4.3 Blanket Test Module Design and Testing Schedule

Although the problem of liquid metal corrosion of structural materials has been investigated extensively for magnetic confinement fusion, there has never been a test which also incorporates pulsed heating inherent in ICF reactors. The instantaneous release of neutrons in an ICF reactor causes rapid expansion of liquids, which if confined within structures such as pipes, produce shock loading and resulting cyclic stresses. Although it is not immediately obvious, such a state of cyclic stress can have deleterious effects on the corrosion rate of structural materials. The intent of this experiment will be to investigate these effects and compare them with test results obtained under identical conditions of temperature and flow, but without shock loading.

In any corrosion experiment the parameters which are carefully controlled are the material composition, temperature, velocity and duration of test. Ideally, the test zone can be disassembled periodically, the corrosion rate determined as a function of distance down the pipe, and then reassembled in the exact configuration for further testing over predetermined periods of time. In this way the corrosion rate is determined as a function of temperature, velocity, location in the loop and time. To conduct such an experiment in SIRIUS-M would have been difficult because of geometric considerations. A compromise test arrangement has been scoped out which will yield the needed information in a simpler and more expeditious way.

The blanket test module consists of seven coiled tubes grouped in a circular array as shown in Fig. 4-3. The coiled tubes will be immersed in lead, and in this respect will be a part of the Pb reflector zone. Each tube will have liquid metal (LiPb or Li) flowing through it at the same condition of temperature, pressure and velocity. Nuclear heating in each coil turn will vary as a function of the radial distance from the first wall. Thus the pulsed loading and consequent stresses will vary in the same way. The tubes will be instrumented to provide the condition of stress in each turn.

The idea of the experiment is to remove tubes from the array at predetermined times and replace them with identical tubes in order not to disturb the experimental conditions. Once a tube is removed, it will be cut up, the segments weighed, probed for surface characterization and finally tested for mechanical properties. Typically, initial corrosion rates are high, tending to saturate as the surface conditions and materials become modified by dissolution. It is therefore important to determine early corrosion rates and the onset of saturation. The frequency of tube replacement will have to be consistent with these considerations.

For this experiment to be meaningful, it will be necessary to conduct a control experiment under the same conditions of temperature, pressure and velocity but without isochoric heating. This means an identical set of tubes will be tested outside the reactor with the nuclear heating simulated by electric heaters. Comparing the corrosion rates from the two experiments will determine the effect of shock loading due to isochoric heating.

Figure 4-4 gives a typical schedule of tube replacement for determining corrosion as a function of time. The first four tubes will be taken out at two week intervals, and the last three, at one month intervals. The replace-

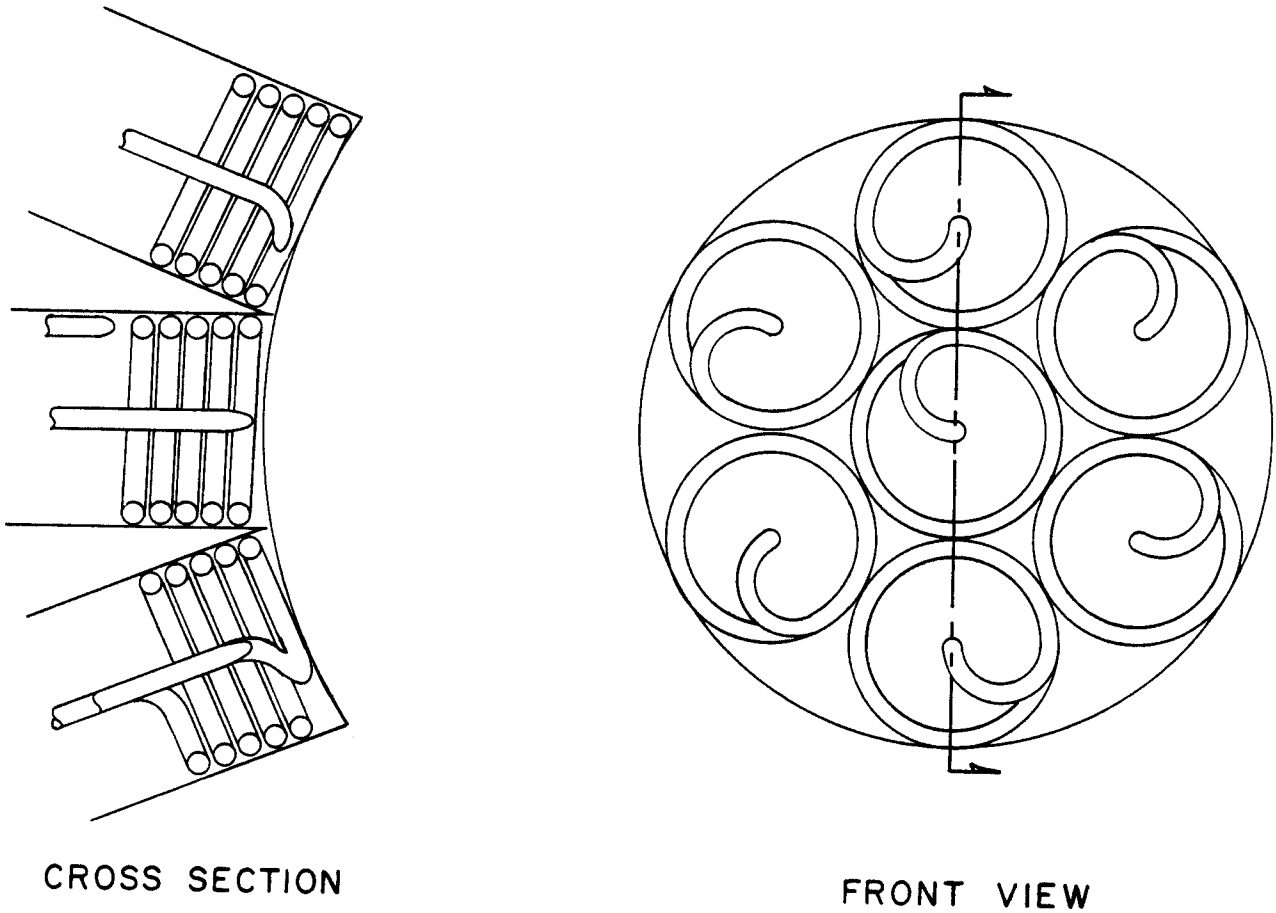

Fig. 4-3. Blanket test module.

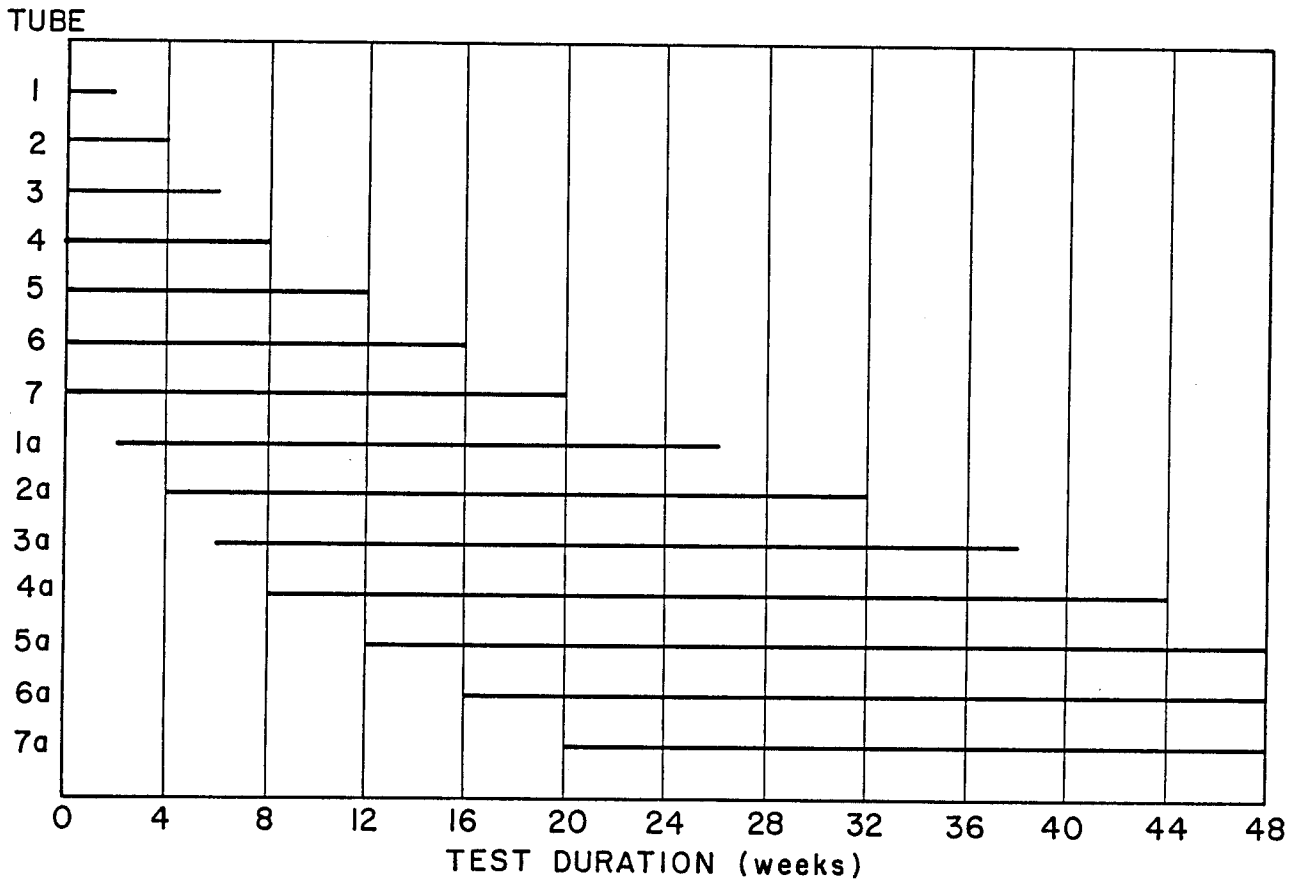

Fig. 4-4. Typical tube replacement schedule for testing a combination of materials in the blanket test module.

ment tubes 1a-7a will represent corrosion testing from 6-9 months. One calendar year of operation will be needed for each material combination at a typical operating temperature.

5. SHIELD AND BUILDING DESIGN

5.1 Design Goals

A major goal of the shield and building design is to reduce the biological dose rate outside the building to values below 2.5 mrem/hr during operation. This ensures that reactor personnel will not receive more than 1.25 rem per quarter in the restricted zone outside the reactor. The shield design is aimed also at minimizing nuclear heating and radiation damage to the final mirrors which impacts the replacement frequency during the reactor lifetime of 5 FPY. It is felt that a limit of no more than 2-3 x 10^{10} rads to the laser mirror coating is desirable based on experimental studies of ion irradiated coatings (D. Pertzborn, University of Wisconsin, unpublished results).

Radiation streaming through the laser beam ducts to the laser building could damage vital components and may lead to uncontrollable serious operational and safety problems. The neutron leakage after two beam reflections in SOLASE resulted in a large flux of the order of 10^{10} n/cm^{2}s.[1] A major requirement for the shield and building design of SIRIUS-M is to minimize radiation streaming into the laser building. This will consequently result in minimizing the damage to the optical windows.

For hands-on maintenance of the reactor chamber to be possible, the dose rate should not exceed 2.5 mrem/hr one day after shutdown at the back of the chamber. Earlier work in the magnetic fusion reactor studies[2] indicates that activation of the shield and outlying components will be low enough to yield a dose rate of 2.5 mrem/hr one day after shutdown if the neutron flux at the back of the shield is kept at a level of ~ 2 x 10^6 n/cm^{2}s during operation. The flux distribution will be calculated in the different shield design options to assess the feasibility of hands-on maintenance. Activation of

the reactor chamber components and last mirrors will result also in high level waste. The waste disposal rating for the activated components will be determined and the feasibility of near-surface burial will be assessed.

5.2 Design Options

Three-dimensional neutronics calculations have been performed for eight shield and building design options. The geometrical configurations used in options I-IV are shown in Fig. 5-1. In these four designs, a 3 m thick concrete biological shield surrounds the reactor chamber. This shield acts as the building wall in option I with concrete shield surrounding the laser beam ducts and last mirrors. Due to the reflection of direct source neutrons incident on the final mirror, a relatively thick penetration shield ($\tilde{>}$ 3 m) is needed to reduce the dose rate outside the building to an acceptable level. The smallest distance between beam centerlines at the back of the bulk shield (at radius of 5.7 m) is only 3.7 m implying that the penetration shields for the adjacent beam ducts will overlap and a large amount of concrete will be needed for the 32 laser beam penetrations. This motivated considering options II, III and IV, where a single 1 m thick concrete wall is used at a radius of 15 m and acts as the building wall. In this case, there is no need for shielding the 10 m long beam ducts. In option II, vacuum is maintained in all the space between the chamber bulk shield and the outer reactor building. In option III, a 1 cm thick A16061 pipe surrounds the laser beam. In option IV, the space between the chamber bulk shield and building wall is filled with borated water to absorb the neutrons reflected from the final mirror and surrounding shield.

Radiation streaming from the reactor cavity into the final mirrors compartment necessitates surrounding these mirrors by a relatively thick concrete

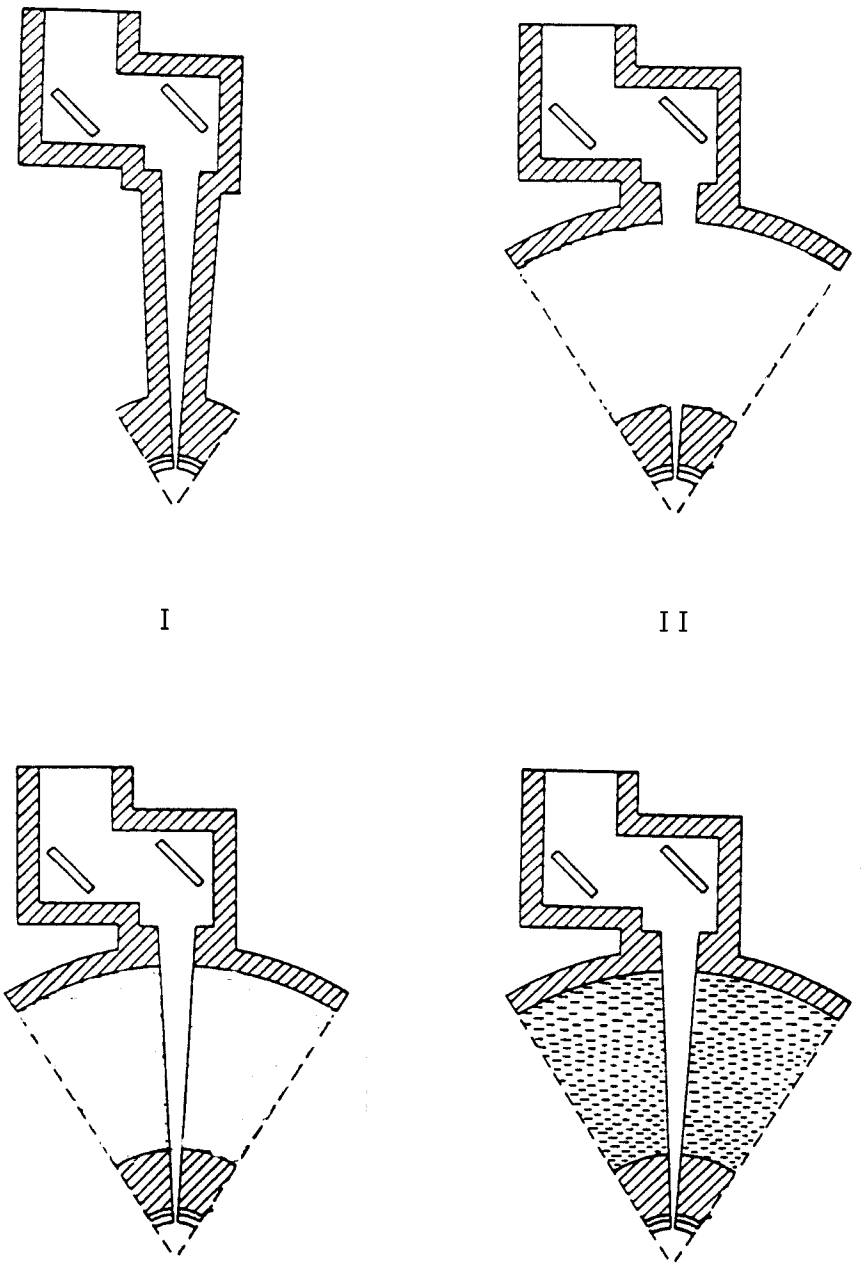

Fig. 5-1. Geometrical configuration for design options I-IV.

shield (~ 3 m) to reduce the dose rate to acceptable levels. The final mirrors enclosures for the 32 beams will, therefore, overlap leading to an effective 10 m thick building wall with beam ducts and last mirrors embedded in it.

Since a concrete shield with a thickness of at least 3 m is required behind the final mirror to attenuate the neutrons streaming directly from the target, locating the building wall behind the final mirrors is considered in options V-VIII as shown in Fig. 5-2. In this case no concrete bulk shield surrounds the reactor chamber. In option V no shield is used to enclose the final mirrors. In option VI, only the turning mirror is surrounded by concrete shield with a large opening allowing beam transport between the two last mirrors. In option VII, both last mirrors are surrounded by concrete shield with an opening that allows the transport of the beam from the final focusing mirror to the target. In option VIII, the turning mirror is surrounded by concrete shield with a 10 cm diameter opening midway between the two last mirrors. In this design the beam point crossover proposed by Ragheb et al.[1] for reducing streaming to the laser building is adopted. This approach was found to reduce the streaming by ~ 3 orders of magnitude in SENRI-I.[3] Possible filling gas breakdown due to high light intensity at the crossover region is a concern in this design.

The impact of these geometrical variations on streaming into the laser building will be assessed. In all eight options considered here, the beam ducts are lined with 1 cm thick layers of boral. Boral lining was found to reduce the streaming in SOLASE by an order of magnitude.[1]

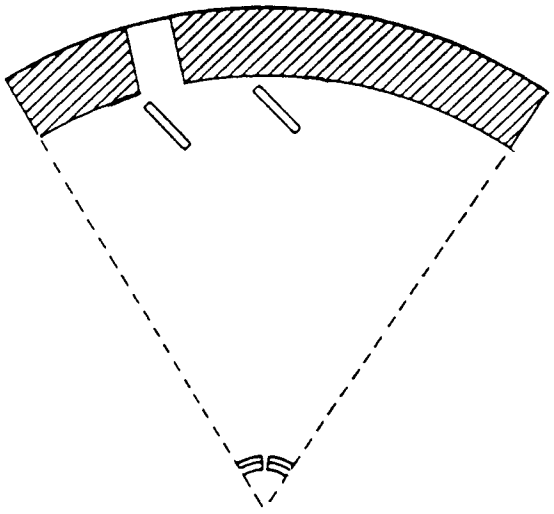

V

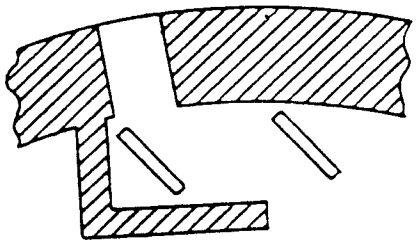

VI

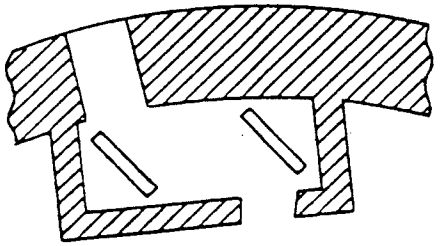

VII

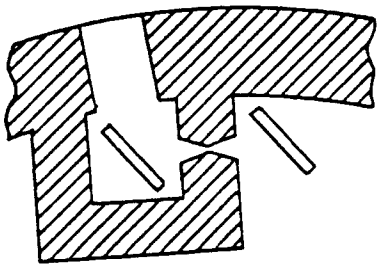

VIII

Fig. 5-2. Geometrical configuration for design options V-VIII.

5.3 Neutronics Calculational Method

Three-dimensional neutronics calculations have been performed for the different shield and building design options using the continuous energy coupled neutron-gamma Monte Carlo code MCNP[4] with ENDF/B-V[5] cross section data. Each calculation used 20,000 histories and took ~ 2 hours of the CRAY XMP CPU time. Several variance reduction techniques were utilized to improve the accuracy of the calculation. These included angular source biasing and geometry splitting with Russian Roulette.

Only one of the 32 beam penetrations was modeled with the associated final mirrors and shield. A reflecting conical boundary with a conical half angle of 31.7° was used. A point neutron source was used at the origin emitting neutrons isotropically within the solid angle subtended by the conical section of the geometry modeled here. For a target yield of 13.4 MJ and a repetition rate of 10 Hz the target emits 5×10^{19} neutrons per second. Hence, a neutron source strength of 3.73×10^{18} n/s was used in the calculations. The energy spectrum of neutrons emitted from the SIRIUS-M target was used to represent the energy spectrum of the source. There are 78% of these neutrons at 14.1 MeV, 21% in the range 3.5-14.1 MeV and 1% in the range 1.5-3.5 MeV.

The laser beam radius is constrained by damage thresholds to at least 1 m. For f/10 final optics, this implies that the final mirrors should be located at a distance of 20 m from the target. The beam focusing on the target has a conical half angle of 2.86°. The inner surface of the beam duct in this region was considered to have a conical shape with a conical half angle of 3.14° that allows for 10% clearance between the beam and duct wall. The two last mirrors were taken to be 5 m apart and are surrounded by intersecting

cylindrical shield segments with inner radii of 1.8 m. A mirror design similar to that used in SOLASE[1] is adopted in this work. The mirror consists of two front and rear plates cooled by water circulating through square grooves and connected by a honeycomb structure. The front and rear plates were considered to be 2 cm thick with 25% water cooling. The total mirror thickness is 44 cm and the radius is 150 cm. The aluminum alloy Al6061 was used as mirror structural material. The mass density used for the aluminum honeycomb structure is 0.0833 g/cm^3.

The reactor cavity with a radius of 2 m is surrounded by a 0.4 m thick lead reflector zone consisting of 90% molten lead and 10% PCA structure that is required to enhance the testing capability of the materials test module. The lead reflector is followed by a 0.3 m thick steel reflector consisting of 90% PCA and 10% water coolant. The concrete shield was considered to consist of 87% concrete (2.321 g/cm^3 density),[6] 8% carbon steel (C-1020) reinforcement and 5% water coolant. 1 cm thick boral[7] sheets were used as beam duct liners. The boral density was taken to be 2.53 g/cm^3 with 20 wt.% B_4C and 80 wt.% Al. The borated water used in design option IV was considered to contain 5 wt.% boric acid.

The results of the three-dimensional Monte Carlo calculations included the neutron and gamma flux in the different zones. The zones were divided into several segments with the volume averaged flux calculated at each segment. The energy spectrum of the neutrons was used to perform activation calculations for the reactor chamber and the last mirrors. Nuclear heating resulting from both neutrons and gamma photons was calculated in the different zones using the appropriate kerma factors for the constituent elements. The atomic displacement damage in the aluminum structure of the last mirrors was

determined using the appropriate dpa cross sections. Radiation streaming to the laser building was quantified by locating a trapping surface at the laser inlet to the final mirrors compartment. Particles crossing this surface were counted according to energy bins and used to determine the absorbed dose rate in the SiO_2 laser window.

The neutron and gamma energy spectra calculated in the different zones were coupled with the flux-to-dose conversion factors[8] to determine the biological dose rate during reactor operation. A 10 cm thick void zone was used at the outer surface of the shield to determine the dose outside the reactor building. In options I-IV a 1 m thick concrete shield was used around the beam duct and the calculated dose rate was coupled with the results from one-dimensional calculations to estimate the required shield thickness. The variation of dose rate with shield thickness was determined using the deterministic discrete ordinates code ONEDANT.[9] In options V-VIII, the 3.2 m thick building wall was divided into four zones and extensive particle splitting was utilized to improve the accuracy of the calculated dose at the outer surface.

5.4 Discussion of Neutronics Results

5.4.1 Biological Dose Rate

The one-dimensional chamber calculations were used to determine the dose rate variation with shield thickness. The calculations were performed with the graphite tile, lead reflector, and steel reflector surrounded by the biological shield. The results are shown in Fig. 5-3 for the concrete shield and normalized to 5×10^{19} neutrons emitted per second from the target. The results indicate that a shield thickness of 2.9 m will be adequate to reduce the dose rate to 2.5 mrem/hr if no penetrations exist. The beam penetrations result in much higher dose levels in regions adjacent to them. However, the

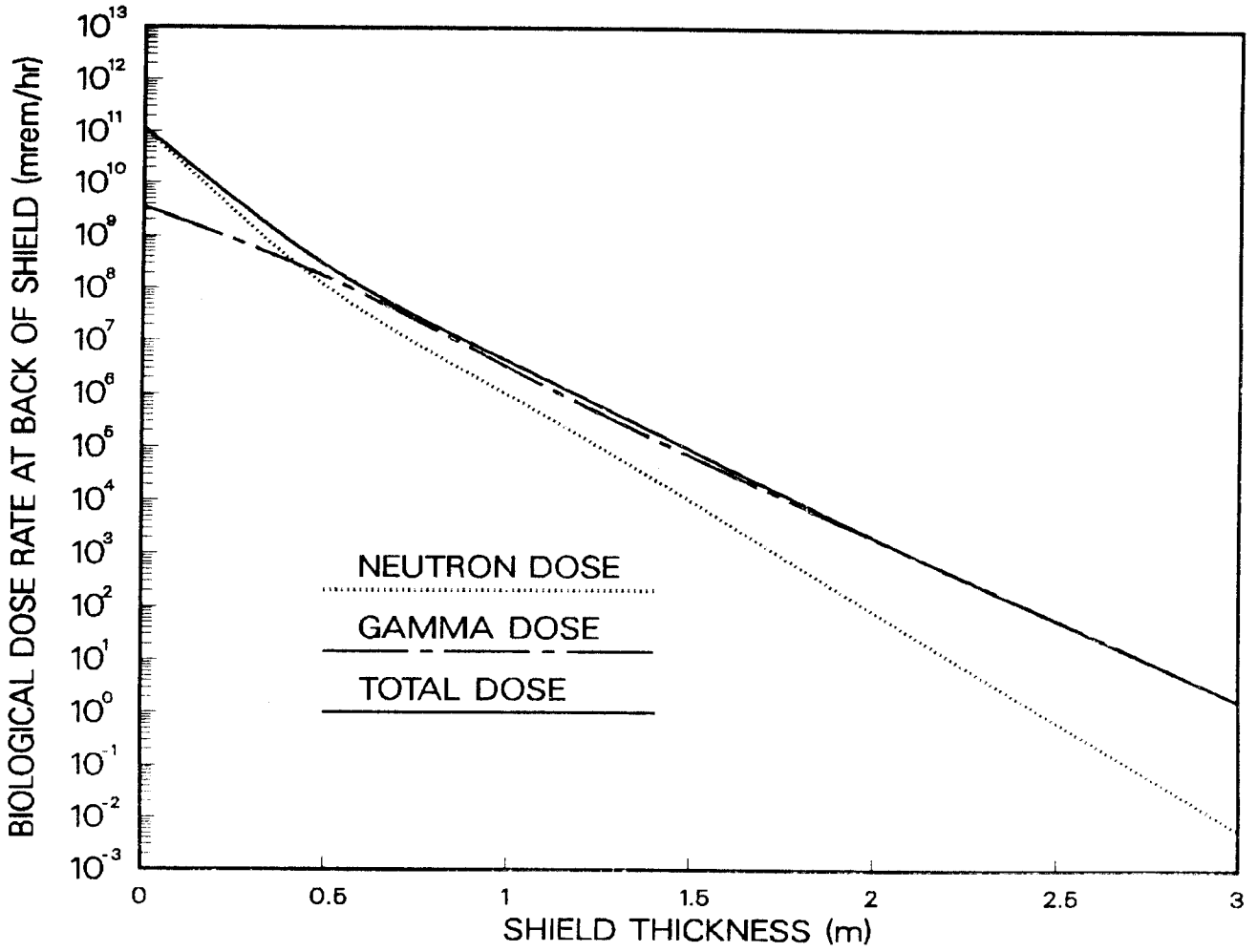

Fig. 5-3. Variation of biological dose with thickness of concrete shield.

one-dimensional results are useful in determining the dose attenuation in the shield. The results indicate that the dose is attenuated by an order of magnitude in 32 cm of the concrete shield. Similar calculations were performed for the borated water shield which was found to attenuate the dose by an order of magnitude in a thickness of 84 cm.

Table 5-1 gives the biological dose rate calculated in the different zones around the beam duct for options I-IV. The fractional standard deviation varied from ~ 0.03 at the boral liner to ~ 0.5 at the back of the shield. It is clear that design option I results in higher doses than the other options. This is due to the fact that the neutrons reflected from the final mirrors compartment towards the chamber will have a larger chance of being reflected back into the mirror region by the concrete wall of the beam duct. In options II, III and IV, the neutrons reflected towards the chamber have a smaller chance of reentering the final mirrors compartment due to dispersion in the large space between the chamber and building wall or absorption in the borated water. No significant difference is observed between doses calculated in options II, III and IV.

The dose attenuation parameters for concrete shield were used with the results of Table 5-1 to estimate the shield thickness required to get 2.5 mrem/hr dose rate at the back of the shield in options II, III and IV. Shield thicknesses of 3, 3.2 and 2.8 m are required for the duct zones between final focusing mirror and chamber, between two mirrors, and between laser window and turning mirror, respectively. About 0.1 m thicker shield is needed in option I. These large shielding thicknesses required around the last mirrors imply that each set of the last mirrors has to be enclosed in a cylindrical shield with height of ~ 15 m and outer radius of ~ 5 m. These concrete

Table 5-1. Biological Dose Rate (mrem/hr) Distribution in Design Options I, II, III and IV

Region	Option I	Option II	Option III	Option IV
Beam Duct Between Final Focusing Mirror and Chamber				
Boral liner	2.15 +10[a]	9.12 +9	9.22 +9	8.95 +9
Concrete shield	2.04 +9	8.67 +8	8.76 +8	8.52 +8
Outer surface of shield	7.42 +5	3.58 +5	3.34 +5	2.34 +5
Duct Between Turning and Final Focusing Mirrors				
Boral liner	3.14 +10	1.57 +10	1.77 +10	1.82 +10
Concrete shield	4.12 +9	2.62 +9	2.73 +9	2.72 +9
Outer surface of shield	3.34 +7	1.82 +7	2.71 +7	1.92 +7
Duct Between Turning Mirror and Laser Window				
Boral liner	1.21 +9	6.35 +8	6.43 +8	7.13 +8
Concrete shield	1.25 +8	7.42 +7	7.65 +7	6.57 +7
Outer surface of shield	1.64 +6	7.63 +5	6.96 +5	7.44 +5

(a) Reads 2.15×10^{10}

shields for the 32 beam penetrations cover ~ 95% of the spherical surface area at 20 m radius leading to an effective 10 m thick building wall with beam ducts and last mirrors embedded in it. This lead to considering the option of moving the building wall behind the final mirrors. In this case only a 3.2 m thick concrete wall is needed. Different options for enclosing the last mirrors lead to design options V-VIII.

Table 5-2 gives the biological dose rate in the four 0.8 m thick segments of the building wall for options V-VIII. The innermost segment of the shield is designated segment 1. The dose values represent an average over the whole segment volume including parts close to the laser beam penetration. The large dose rate in the beam penetration can, therefore, significantly impact the average dose values in the shield. The dose rates in the beam penetration and laser window are also given in Table 5-2. The fractional standard deviation varies from ~ 0.03 at the inner segment of shield to ~ 0.8 at the laser window. The dose rates in the beam duct and laser window are the smallest in option VIII due to the reduced streaming through the 10 cm diameter orifice at the beam crossover point. These doses are the highest in option V due to the lack of shielding by the mirror concrete enclosure. The large dose rate in shield regions adjacent to the beam penetration influences the average dose rate in the shield segments yielding large values in the back segments of the shield. The dose rate drops rapidly as one moves away from the beam penetration. This effect is less pronounced for option VIII with minimal streaming and for the innermost segment of the shield where the dose rate in the penetration is comparable to the average in the shield. Using the average dose rate in the innermost segment of the shield together with the dose attenuation parameters for the shield we estimated the dose rate at the back of the build-

Table 5-2. Biological Dose Rate (mrem/hr) Distribution in Design Options V, VI, VII and VIII

Region	Option V	Option VI	Option VII	Option VIII
Concrete Building Wall				
Segment 1	1.76×10^9	1.1×10^9	8.7×10^8	1.23×10^9
Segment 2	7.11×10^6	2.8×10^6	1.0×10^6	6.12×10^6
Segment 3	8.87×10^5	1.49×10^5	1.8×10^5	3.32×10^3
Segment 4	4.52×10^5	1.03×10^4	5×10^4	---(a)
Beam Duct	9.4×10^9	3.05×10^9	2.4×10^9	1.0×10^6
Laser Window	1.36×10^9	2.72×10^8	9.2×10^7	3.8×10^4(b)

(a) No tracks entered this segment

(b) Scaled from value for option VII.

ing wall to be 1.19, 0.74, 0.59, and 0.83 mrem/hr, for options V, VI, VII, and VIII, respectively, at locations not in the vicinity of the laser window. The beam duct going from the laser window to the laser building should be surrounded by concrete shield to reduce the dose rate below 2.5 mrem/hr. We estimated the duct shield thickness needed at the laser window to be 2.8, 2.6, 2.4, and 1.3 m, for Options V, VI, VII, and VIII, respectively. A smaller thickness can be used as one moves away from the reactor building. It is clear that design option VIII yields an acceptable dose level outside the reactor building with the least amount of shield.

The neutron flux in the different zones was used to estimate the dose after shutdown by observing that a neutron flux of $\sim 2 \times 10^6$ n/cm^{2}s at the back of the shield in magnetic fusion reactors[2] yields a dose of $\sim$ 2.5 mrem/hr one day after shutdown from activation of the shield and outlying components. The neutron flux in different reactor zones is given in Table 5-3. The statistical uncertainty is in the range 1-5%. These flux levels are excessive and do not allow hands-on maintenance inside the building. The dose rate one day after shutdown inside the building is estimated to vary from $\sim 10^8$ mrem/hr at the outer surface of the chamber to $\sim 10^5$ mrem/hr at the inner surface of the building wall in options V-VIII. All remote maintenance is, therefore, required. Although an average flux in the chamber shield of $\sim 6 \times 10^{11}$ n/cm^{2}s in option I implies a flux of $\sim 10^4$ n/cm^2 at the back of the shield with possible hands-on maintenance, this is not feasible due to the overlapping duct shields ($\sim$ 3 m thick) leaving no space for maintenance. Chamber hands-on maintenance will be difficult in options II, III and IV since the average neutron flux in the zone between the chamber and building

Table 5-3. Neutron Flux (n/cm^2s) in Different Zones

Zone	Options							
	I	II	III	IV	V	VI	VII	VIII
Steel reflector in chamber	1.90 +14[a]	1.91 +14	1.89 +14	1.90 +14	1.93 +14	1.93 +14	1.93 +14	1.93 +14
Bulk shield around chamber	5.82 +11	6.53 +11	5.94 +11	5.89 +11	NA	NA	NA	NA
Innermost segment of building wall	NA	5.85 +9	2.96 +9	2.66 +8	7.42 +10	5.19 +10	4.72 +10	5.42 +10
Front of final focusing mirror	1.12 +12	1.10 +12	1.08 +12	1.09 +12	1.90 +12	1.57 +12	1.26 +12	1.57 +12

[a] Reads 1.90×10^{14}

wall is ~ 10^7 n/cm^{2}s. Hands-on maintenance for the final mirrors is not possible in all cases.

5.4.2 Radiation Damage to Last Mirrors

The peak radiation damage to the mirror structural material is given in Table 5-4 for the final focusing and turning mirrors in the eight design options considered. The damage is given in terms of the dpa rate in aluminum. The peak nuclear heating is also given in terms of the absorbed dose rate. The results in Table 5-4 represent average values over the 2 cm thick front plate of the mirror. The statistical uncertainty in the results ranges from 2% in the final focusing mirror to 18% in the turning mirror. The results for design options I-IV are nearly identical with the damage in the turning mirror being about two orders of magnitude less than in the final focusing mirror. The difference in radiation damage levels in the last four design options is related to the way these mirrors are enclosed. The final focusing and turning mirrors suffer the largest damage in option V where no shield encloses the last mirrors and neutrons streaming from all 32 beam penetrations in the chamber can contribute to mirror damage. The damage in the turning mirror is extremely low in option VIII since it is almost fully enclosed by the shield.

Based on the information in Table 5-4, our initial prediction is that the final focusing mirror will have to be replaced once or twice during a calendar year operation. On the other hand, the final turning mirror should last the entire SIRIUS-M lifetime.

5.4.3 Radiation Streaming to the Laser Building

For each neutron emitted from the target, 7.5 x 10^{-4} neutrons stream directly through each beam penetration in the chamber towards the final focusing mirror. Some of these neutrons will end up streaming to the laser building

Table 5-4. Peak Radiation Effects in Last Mirrors

Option	Final Focusing Mirror		Turning Mirror	
	Al dpa/FPY	Rad/FPY	Al dpa/FPY	Rad/FPY
I	0.0762	6.12×10^{10}	0.0011	9.72×10^{8}
II	0.0741	6.03×10^{10}	0.0010	9.85×10^{8}
III	0.0725	5.90×10^{10}	0.0009	7.88×10^{8}
IV	0.0729	5.93×10^{10}	0.0011	7.58×10^{8}
V	0.0980	8.52×10^{10}	0.0035	4.80×10^{9}
VI	0.0967	8.17×10^{10}	0.0008	1.33×10^{9}
VII	0.0777	6.32×10^{10}	0.0011	9.11×10^{8}
VIII	0.0779	6.55×10^{10}	2.5×10^{-9}	1.17×10^{7}

Table 5-5. Neutron Streaming to Laser Building and Absorbed Dose in Laser Window

Option	Neutrons Streaming per cm^2 of Laser Window for One Source Neutron	Dose Rate in SiO_2 Laser Window (rad/FPY)
I	3.65×10^{-11}	7.22×10^{7}
II	4.01×10^{-11}	7.93×10^{7}
III	3.98×10^{-11}	7.87×10^{7}
IV	3.55×10^{-11}	7.02×10^{7}
V	7.37×10^{-10}	1.33×10^{9}
VI	4.56×10^{-11}	8.13×10^{7}
VII	5.53×10^{-11}	1.02×10^{8}
VIII	2.50×10^{-14}	4.61×10^{4}

and producing damage in the laser window and some will be reflected back towards the chamber. While the beam ducts are nearly decoupled as far as streaming is concerned in options I and IV, neutrons reflected back to the chamber from the different beam ducts can contribute to streaming from other beam penetrations in the other design options. The number of neutrons streaming to the laser building per unit area of the laser window is shown in Table 5-5 for each source neutron. The estimated values for the dose rate in the SiO_2 laser window are also included. The dose was calculated from the neutron fluence assuming a conversion factor of 1 rad per 10^9 n/cm^2. The fractional standard deviation ranges from 0.15 to 0.35. In option VIII no tracks crossed the laser window and the streaming value was estimated by scaling the value for option VII down by the ratio of the number of neutrons entering the mirror compartment. For each source neutron, 7.7×10^{-4} neutrons entered the mirror compartment through the beam penetration and 2.9×10^{-6} neutrons entered through the compartment wall in option VII. In option VIII, 3.5×10^{-7} neutrons entered through the orifice and 5×10^{-10} neutrons entered through the wall. The negligible amount entering through the wall implies that this contribution can still be negligible while reducing the thickness of the concrete wall enclosing the turning mirror in option VIII to $\sim$ 1.5 m.

It is clear that design option V results in the largest streaming and damage to laser window due to lack of shielding by the mirror concrete enclosure. About three orders of magnitude reduction in streaming is obtained by adopting design option VIII. In this case the flux at the laser window is 1.5×10^6 n/cm^{2}s. At that neutron flux the total number of neutrons per cm^2 for the 5 FPY's is 2.4×10^{14} (0.24 Mrad). This exposure level is so low that the density decrease will be negligible ($<<$ 0.01%) and very little optical

degradation is expected. Therefore, we expect the final optical window to last for the full reactor lifetime. Our results indicated a factor of 20 reduction in streaming due to the beam duct bend at the turning mirror. Therefore, if the beam point crossover option is not optically feasible, at least two additional bends will be required before the laser window in order to maintain the same level of damage. While this is feasible, the economic impact remains to be calculated.

5.5 Building Description

The containment building for the SIRIUS-M test reactor is spherical with a minor radius of 21.6 m and a wall thickness of 3.2 m. This configuration was adopted over more conventional structures after considerable investigation and debate.

In an attempt to select the most suitable configuration for the containment building we considered conventional building structures such as square, rectangular, and cylindrical with a dome roof as well as unconventional such as spherical and icosahedron shaped. In the final analysis the decision was based on four aspects:

1 - Support of the final and turning mirrors.

2 - Integration with 32 incoming laser beams.

3 - Vacuum and pressure containment.

4 - Construction difficulty.

Of these four, the first is by far the most important. Support and alignment of the final optics is crucial in ICF reactors and especially so with symmetric illumination. Only in the case of a spherical building are the final and turning mirrors supported at a uniformly short distance from the wall, insuring a solid base as an anchor. A spherical building is also the

most conducive from the standpoint of integrating the large number of beams needed for symmetric illumination. Since all the beams intersect the building wall at right angles, the shield housing of the turning mirror and the support alignment system for both turning and final mirrors will be standard. This results in considerable design simplification as well as a saving in cost. Although a spherical building is best capable of supporting a vacuum or an overpressure, this issue is not crucial, since other building configurations can be designed to do the same. Finally, it is the construction difficulty which made the selection of a spherical building somewhat uncertain. We feel, however, that with modern techniques for making reinforced concrete structures, this is not an insurmountable job.

Figure 5-4 shows a cross section of the reactor building in a plane which intersects eight of the 32 beams. The cavity is shown supported on columns in the center of the building. Note that there are no beam tubes between the cavity and the final mirror. Instead the building is evacuated and has the same xenon atmosphere at the inside of the cavity. At a pressure of one torr, the steady state vacuum system needed to maintain the desired gas turnover in the cavity is quite nominal. A question still remains whether gas breakdown at the focal point between the final and turning mirrors will render this scheme of neutron shielding impractical. Differential pumping within the beam line to reduce the pressure in the aperture is possible but will require further investigation.

Finally, in order to give a perspective on the size of the SIRIUS-M building, we have included Fig. 5-5. This figure compares the SIRIUS-M building with that of the French Super Phenix breeder reactor which is presently in operation. Although the Super Phenix building is of a conventional cylindri-

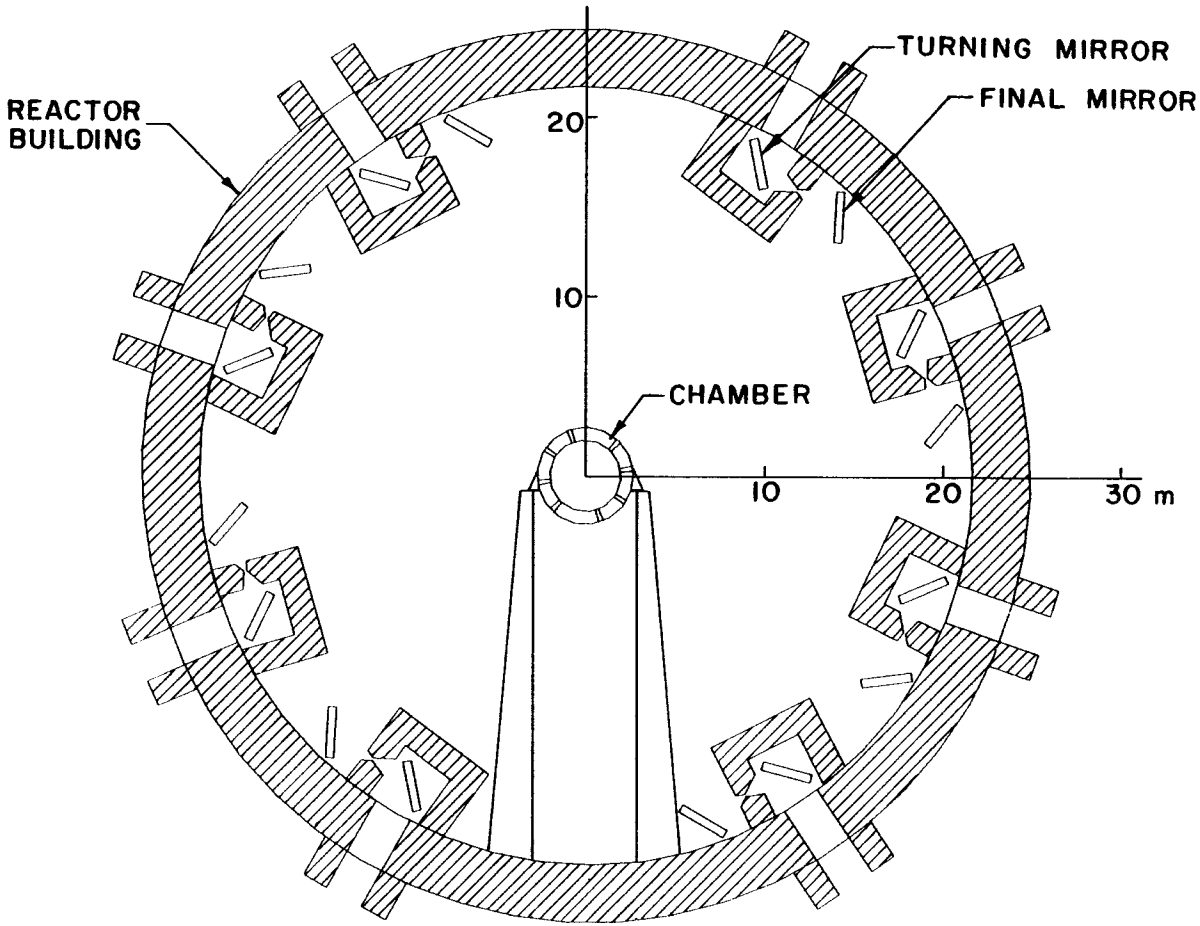

Fig. 5-4. SIRIUS-M reactor building.

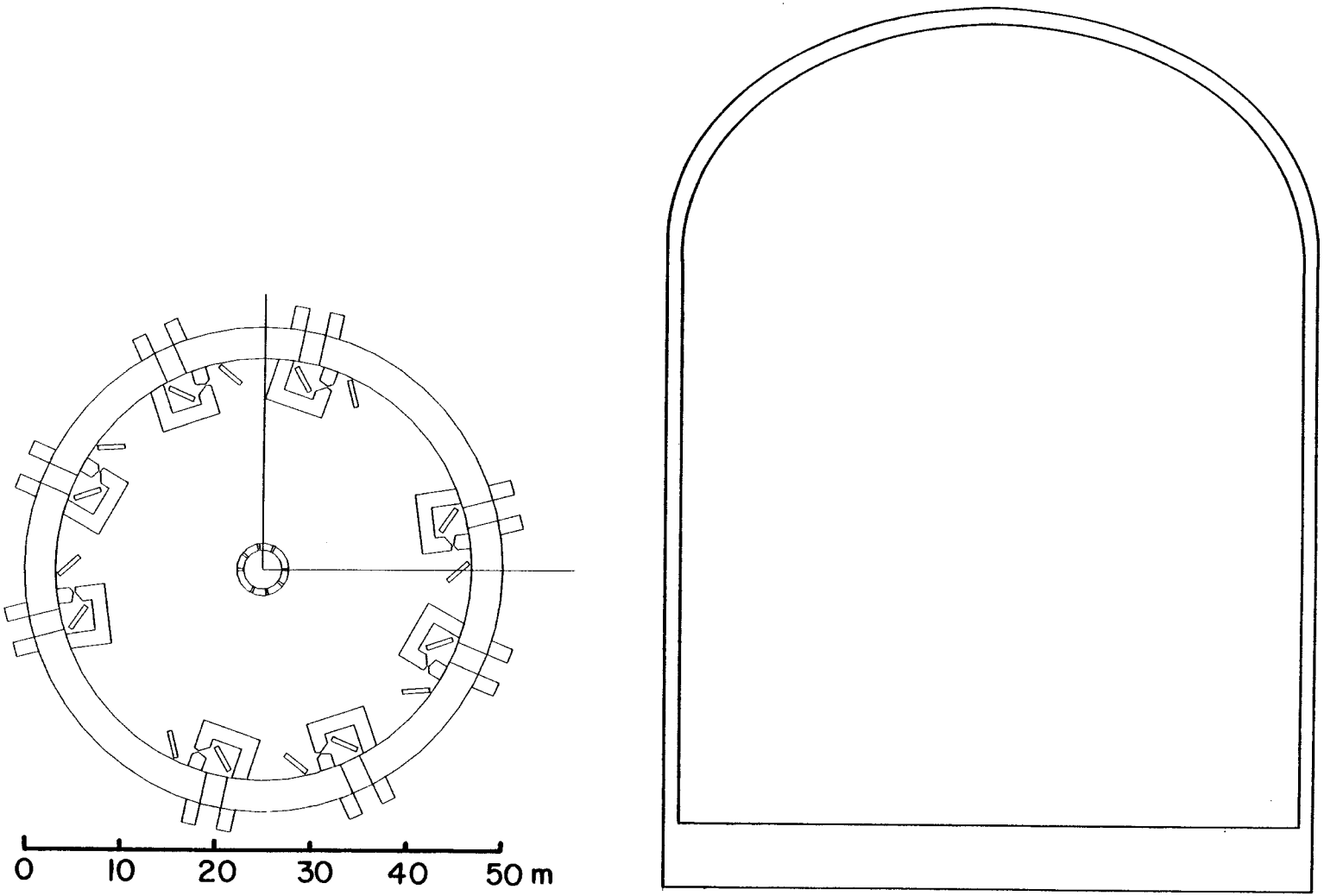

Fig. 5-5. Comparison of the SIRIUS-M reactor building with the existing Super Phenix Breeder reactor building.

cal configuration it dwarfs the SIRIUS-M building. This leads us to believe that the selected parameters for the location of the final optics and the building configuration is reasonable.

5.6 Activation Analysis

We have investigated the activation and the waste disposal rating of SIRIUS-M. Radioactivity calculations have been performed to estimate the radioactivity of the lead reflector, the stainless steel reflector, the final mirror, and the turning mirror after operation time of 5 full power years. The waste disposal ratings of these four components were calculated after one year cooling period.

The layout of the cavity and the mirrors is shown in Fig. 5-2. The compositions of the different zones are listed in Table 5-6. The composition of PCA used in the reflectors is given in Table 5-7, and the composition of Al6061 is given in Table 5-8. Note that the composition of the lead reflector includes also the contributions from the tiles which are assumed to be homogenized in the lead reflector.

We have used the neutron flux calculated by the MCNP code (see Section 5.3), along with radioactivity computer code RACC.[10] RACC uses the Gear's stiffly stable method to solve the system of first order differential equations describing the nuclear decay chain reactions involved in the problem. During this work efforts have been initiated to simplify the input preparation of RACC and to couple it with the neutronic codes ONEDANT and TWODANT.

Table 5-6. Material Composition

Zone		Volume (m^3)	Composition
Pb Reflector		23.9	85% liquid Pb, 11% PCA 2% H_2O, 2% graphite
Steel Reflector		24.1	10% H_2O, 90% PCA
Final Mirror	Front	0.141	75% Al6061, 25% H_2O
	Center	2.83	100% Al honeycomb (ρ = 0.0833 g/cc)
	Back	0.141	75% Al6061, 25% H_2O
Turning Mirror	Back	0.141	75% Al6061, 25% H_2O
	Center	2.83	100% Al honeycomb (ρ = 0.0833 g/cc)
	Front	0.141	75% Al6061, 25% H_2O

Table 5-7. PCA Composition (Density = 8 g/cm^3)

Element	Wt.%	Element	Wt.%
B	0.005	As	0.02
C	0.005	Zr	0.005
N	0.01	Nb	0.03
Al	0.03	Mo	2.
Si	0.5	Ag	0.0001
P	0.01	Cd	0.0002
S	0.005	Sn	0.005
K	0.0003	Sb	0.001
Ti	0.3	Ba	0.001
V	0.1	Tb	0.001
Cr	14.	Ta	0.01
Mn	2.	W	0.05
Fe	balance	Ir	0.001
Co	0.03	Pb	0.001
Ni	16.	Bi	0.001
Cu	0.02		

Table 5-8. Al6061 Composition (Density = 2.7 g/cm^3)

Element	Wt.%	Element	Wt.%
Mg	1.	Mn	0.5
Al	balance	Fe	0.7
Si	0.6	Cu	0.3
Ti	0.15	Zn	0.25
Cr	0.3		

5.6.1 Activation

The buildup of radioactivity in the different zones during operation is shown in Table 5-9 and the decay of this radioactivity (after shutdown) is shown in Table 5-10. The total activity of the turning mirror, after 5 FPY's operation is less than 3 Ci and decays after one hour to 0.1 Ci. The fact that the turning mirror is surrounded by concrete shield reduces the neutron flux considerably. However, this very fact makes the uncertainty in the neutron flux, calculated by MCNP, very large. The neutron group energy fluxes, calculated by MCNP in the three parts of the turning mirror, are all zero except for one low energy group that contains a very small number of neutrons.

With respect to the front mirror, the total activity after 5 FPY's operation (for the three parts of the mirror front/center/back) is 9.1×10^4 Ci. The activity of this mirror has saturated to almost this value after only one full power month of operation. The major contributions to the activity in this mirror come from Na^{24} ($t_{1/2} \sim 15$ hr) and Al^{28} ($t_{1/2} \sim 2.3$ min), both of which are beta emitters. Na^{24} is produced by (n,p) reaction with Mg^{24} and through (n,α) reaction with Al^{27}. Al^{28} is produced primarily by (n,γ) reaction with Al^{27}.

The largest activation in SIRIUS-M comes from the steel reflector and the lead reflectors, with end-of-life activities of 275×10^6 Ci and 174×10^6 Ci, respectively. The primary source of activation in both zones is the PCA alloy. The elements contributing to this activity and their impacts on the waste disposal rating are discussed in the following section.

Table 5-9 Radioactivity Build-up (Ci)

		TIME :	Ø.6ØØØe+Ø2S	Ø.36ØØe+Ø4S	Ø.263Øe+Ø7S	Ø.1578e+Ø8S	Ø.3156e+Ø8S	Ø.6312e+Ø8S	Ø.1578e+Ø9S
Lead Reflector		:	Ø.52Ø887e-Ø7	Ø.263239e+Ø8	Ø.13Ø513e+Ø9	Ø.148575e+Ø9	Ø.155434e+Ø9	Ø.163Ø51e+Ø9	Ø.174844e+Ø9
Steal Reflector		:	Ø.445Ø65e-Ø6	Ø.4666ØØe+Ø8	Ø.221Ø43e+Ø9	Ø.2525ØØe+Ø9	Ø.259183e+Ø9	Ø.265795e+Ø9	Ø.275534e+Ø9
Front Mirror	Front	:	Ø.	Ø.22ØØØ8e+Ø5	Ø.366472e+Ø5	Ø.367664e+Ø5	Ø.369360e+Ø5	Ø.3692Ø2e+Ø5	Ø.37Ø111e+Ø5
	Center	:	Ø.	Ø.161634e+Ø5	Ø.26Ø193e+Ø5	Ø.26Ø99Øe+Ø5	Ø.261462e+Ø5	Ø.262Ø24e+Ø5	Ø.262639e+Ø5
	Back	:	Ø.	Ø.185573e+Ø5	Ø.28Ø215e+Ø5	Ø.281ØØ3e+Ø5	Ø.281455e+Ø5	Ø.282ØØ3e+Ø5	Ø.282539e+Ø5
Turning Mirror	Back	:	Ø.	Ø.763119e+ØØ	Ø.8651Ø3e+ØØ	Ø.865269e+ØØ	Ø.8654Ø2e+ØØ	Ø.865590e+ØØ	Ø.866Ø39e+ØØ
	Center	:	Ø.	Ø.63Ø846e+ØØ	Ø.715153e+ØØ	Ø.71529Øe+ØØ	Ø.7154ØØe+ØØ	Ø.715562e+ØØ	Ø.715927e+ØØ
	Front	:	Ø.	Ø.853456e+ØØ	Ø.967513e+ØØ	Ø.967698e+ØØ	Ø.967847e+ØØ	Ø.968Ø56e+ØØ	Ø.968559e+ØØ
SYSTEM	TOTAL		Ø.498554e-Ø6	Ø.73Ø4Ø7e+Ø8	Ø.352447e+Ø9	Ø.4Ø1166e+Ø9	Ø.4147Ø8e+Ø9	Ø.428937e+Ø9	Ø.45Ø47Øe+Ø9

Table 5-10 Total Radioactivity (Ci) (After Shut Down)

		TIME :	Ø.6ØØØe+Ø2S Ø.1578e+Ø9S	Ø.36ØØe+Ø4S Ø.3156e+Ø9S	Ø.864Øe+Ø5S Ø.6312e+Ø9S	Ø.6Ø48e+Ø6S Ø.9468e+Ø9S	Ø.263Øe+Ø7S Ø.1262e+1ØS	Ø.1578e+Ø8S Ø.1578e+1ØS	Ø.3156e+Ø8S Ø.3156e+1ØS
Lead Reflector		:	Ø.174844e+Ø9 Ø.961Ø64e+Ø7	Ø.148176e+Ø9 Ø.283178e+Ø7	Ø.839365e+Ø8 Ø.474625e+Ø6	Ø.643ØØ9e+Ø8 Ø.259582e+Ø6	Ø.528668e+Ø8 Ø.222747e+Ø6	Ø.362183e+Ø8 Ø.2Ø6462e+Ø6	Ø.296155e+Ø8 Ø.155268e+Ø6
Steal Reflector		:	Ø.275534e+Ø9 Ø.1Ø8741e+Ø8	Ø.229858e+Ø9 Ø.387765e+Ø7	Ø.1Ø1Ø7Øe+Ø9 Ø.145899e+Ø7	Ø.836972e+Ø8 Ø.12Ø377e+Ø7	Ø.63Ø249e+Ø8 Ø.11Ø758e+Ø7	Ø.353Ø72e+Ø8 Ø.1Ø2862e+Ø7	Ø.2963Ø8e+Ø8 Ø.714798e+Ø6
Front Mirror	Front	:	Ø.37Ø111e+Ø5 Ø.365378e+Ø2	Ø.141Ø84e+Ø5 Ø.952780e+Ø1	Ø.49311Øe+Ø4 Ø.12439Øe+Ø1	Ø.414929e+Ø3 Ø.565ØØ4e+ØØ	Ø.364114e+Ø3 Ø.466515e+ØØ	Ø.251836e+Ø3 Ø.4247Ø3e+ØØ	Ø.18753Øe+Ø3 Ø.292481e+ØØ
	Center	:	Ø.262639e+Ø5 Ø.243637e+Ø2	Ø.948496e+Ø4 Ø.635826e+Ø1	Ø.329636e+Ø4 Ø.83Ø831e+ØØ	Ø.281851e+Ø3 Ø.377588e+ØØ	Ø.245955e+Ø3 Ø.31176Øe+ØØ	Ø.168339e+Ø3 Ø.283793e+ØØ	Ø.125188e+Ø3 Ø.195356e+ØØ
	Back	:	Ø.282589e+Ø5 Ø.236327e+Ø2	Ø.9Ø9711e+Ø4 Ø.616752e+Ø1	Ø.313459e+Ø4 Ø.797124e+ØØ	Ø.278529e+Ø3 Ø.358351e+ØØ	Ø.241325e+Ø3 Ø.295317e+ØØ	Ø.162957e+Ø3 Ø.269774e+ØØ	Ø.121Ø82e+Ø3 Ø.185ØØ1e+ØØ
Turning Mirror	Back	:	Ø.866Ø39e+ØØ Ø.247235e-Ø3	Ø.977736e-Ø1 Ø.651Ø62e-Ø4	Ø.465811e-Ø2 Ø.452739e-Ø5	Ø.973Ø59e-Ø3 Ø.314538e-Ø6	Ø.944161e-Ø3 Ø.218524e-Ø7	Ø.823559e-Ø3 Ø.151819e-Ø8	Ø.718629e-Ø3 Ø.75845Øe-14
	Center	:	Ø.715927e+ØØ Ø.2Ø4382e-Ø3	Ø.8Ø8263e-Ø1 Ø.538728e-Ø4	Ø.385Ø71e-Ø2 Ø.374265e-Ø5	Ø.8Ø4397e-Ø3 Ø.26ØØ18e-Ø6	Ø.79Ø5Ø8e-Ø3 Ø.18Ø646e-Ø7	Ø.68Ø81Øe-Ø3 Ø.1255Ø4e-Ø8	Ø.594Ø67e-Ø3 Ø.626980e-14
	Front	:	Ø.968559e+ØØ Ø.2765Ø8e-Ø3	Ø.1Ø9348e+ØØ Ø.728Ø94e-Ø4	Ø.52Ø953e-Ø2 Ø.5Ø6333e-Ø5	Ø.1Ø8825e-Ø2 Ø.351772e-Ø6	Ø.1Ø6593e-Ø2 Ø.244392e-Ø7	Ø.921Ø5Øe-Ø3 Ø.169791e-Ø8	Ø.8Ø3699e-Ø3 Ø.848234e-14
SYSTEM	TOTAL		Ø.45Ø47Øe+Ø9 Ø.2Ø4834e+ØØ	Ø.378Ø59e+Ø9 Ø.67Ø945e+Ø7	Ø.185Ø18e+Ø9 Ø.193362e+Ø7	Ø.147999e+Ø9 Ø.146335e+Ø7	Ø.115892e+Ø9 Ø.133Ø33e+Ø7	Ø.715261e+Ø8 Ø.123ØØ8e+Ø7	Ø.592462e+Ø8 Ø.87ØØ57e+Ø6

5.6.2 Waste Disposal Rating (WDR)

One of the indices of the radiological hazard for radioactive materials is the waste disposal rating. In this index, the hazard is assumed to be exposure to members of the public after proper emplacement of the waste at a disposal site; occupational exposures and accidents are not considered. The waste disposal rating is calculated based on the dose that could be received by an intruder to the waste site after hundreds of years. The dose to this intruder should not exceed the maximum permissible dose (MPD) if he comes in direct or indirect contact with the radioactive waste.[11,12]

The WDR is usually calculated for structural materials only. For this reason activation calculations were done with the exclusion of all the liquid materials (Pb, H_2O) in Table 5-6. We have used the WDR indices provided by Fetter.[13] A summary of the WDRs is given in Table 5-11. From this table the WDR of both reflectors are classified as deep geological burial waste. The numerical value of Index C could be interpreted as a dilution factor that is required for the waste to meet the specifications of the near surface burial Class C waste. If both reflectors are considered as one unit, the dilution factor would be 5.2. If, however, the activity is averaged over the total chamber volume including the inner target cavity (33.5 m^3) a dilution factor of 3 is required.

Only long lived isotopes contribute to the WDR. The contributing isotopes to the rating of both reflectors are given in Table 5-12. It appears from this table that Nb^{94} is the major driver to WDR. Nb^{94} is produced through the (n,γ) reaction of the intrinsic Nb^{93} in PCA ($\sim$ 0.03%, Table 5-7), and through (n,p), (n,d), (n,T) reactions with Mo^{94}, Mo^{95} and Mo^{96} respectively. The main part of Nb^{94} comes from the (n,γ) reaction of Nb^{93}. Thus re-

Table 5-11. Summary of WDR

	Class	Index A	Index C
Pb Reflector	deep	132	4.4
SS Reflector	deep	160	6.0
Front Mirror	C	1.21	0.11
Turning Mirror	A	0.0	0.0

Table 5-12. Major Isotopic Contributions to WDR (%)

Zone	Lead Reflector (10% PCA)		SS Reflector (90% PCA)	
	A-Index	C-Index	A-Index	C-Index
Value	132.23	4.4039	160.25	5.99
Be-10	0.00*	0.00	0.00	0.00
C-14	0.02	0.00	0.07	0.01
Al-26	0.01	0.04	0.00	0.00
Cl-36	0.00	0.00	0.00	0.00
Cl-36	0.00	0.00	0.00	0.00
K-40	0.00	0.00	0.00	0.00
K-40	0.00	0.00	0.00	0.00
Mn-53	0.00	0.00	0.00	0.00
Co-60	2.08	0.00	0.20	0.00
Ni-59	0.00	0.01	0.01	0.03
Ni-63	1.21	0.01	0.01	0.03
Sr-90	0.00	0.00	0.00	0.00
Zr-93	0.00	0.00	0.00	0.00
Nb-92	0.00	0.00	0.00	0.00
Nb-93M	0.00	0.00	0.00	0.00
Nb-94	18.88	56.69	28.21	75.43
Mo-93	1.74	4.63	0.93	2.21
Mo-93	9.87	26.26	5.30	12.55
Tc-99	66.17	12.35	58.59	9.74
Pb-205	0.00	0.00	0.00	0.00

*Small contribution

ducing the percentage of this element will considerably improve the WDR of PCA.

Finally the WDR of the final mirrors is classified as Class C, and is mainly due to Al^{26} ($t_{1/2} \sim 8 \times 10^5$ y). However, if these mirrors are used for only 4.13 FPY the WDR would be Class A. Because of the very low fluxes the turning mirrors are subjected to, the activation of these mirrors is very small and are considered Class A.

References for Chapter 5

1. M. Ragheb, A. Klein and C. Maynard, "Neutronics Shielding Analysis of the Laser Mirror-Beam Duct System for a Laser Fusion Power Reactor," Nucl. Tech./Fusion 1, 99 (1981).

2. B. Logan et al., "MARS: Mirror Advanced Reactor Study Final Report," UCRL-53480, Lawrence Livermore National Laboratory (1984).

3. H. Oomura et al., "Radiation Streaming Analysis for the Beam Ports of the Laser Fusion Reactor, SENRI-I," ILE 8221P, Institute of Laser Engineering, Osaka University, Japan (1982).

4. "MCNP - A General Monte Carlo Code for Neutron and Photon Transport," LA-7396-M, Los Alamos National Laboratory (1981).

5. D. Garber, "ENDF/B-V," BNL-17541 (ENDF-201), National Nuclear Data Center, Brookhaven National Laboratory (Oct. 1975).

6. I. Oh, R. Rothe and G. Tuk, Reference Critical Experiments, RFP-NUREG-2715 (1977).

7. Theodore Rockwell, III, Reactor Shielding Design Manual, D. Van Nostrand Company (1956), p. 189.

8. ANS-6.1.1 Working Group, M. Battat (Chairman), "American National Standard Neutron and Gamma-Ray Flux-to-Dose Rate Factors," ANSI/ANS-6.1.1-1977(N666), American Nuclear Society (1977).

9. R. O'Dell et al., "User's Manual for ONEDANT: A Code Package for One-Dimensional, Diffusion-Accelerated, Neutral-Particle Transport," LA-9184-M, Los Alamos National Laboratory (Feb. 1982).

10. J. Jung, "Theory and Use of the Radioactivity Code RACC," ANL/FPP/TM-122, 1979.

11. U.S. Nuclear Regulatory Commission, "Final Environmental Impact Statement on 10 CFR Part 61, 'Licensing Requirements for Land Disposal of Radioactive Waste'," NUREG-0945 (November 1982).

12. S.A. Fetter, Ph.D. Thesis, University of California, Berkeley (April 1985).

13. S.A. Fetter, private communications.

6. COST ESTIMATE

A detailed description of the cost estimate for SIRIUS-M can be found elsewhere.[1] Only the most important features of this analysis will be highlighted here. After a brief description of the assumptions, we will deal with the capital costs and the annual operating costs.

6.1 Assumptions

6.1.1 Design Assumptions

We have assumed that the facility is built on federal land, therefore no cost for buying of land is incurred. Also, it is assumed that some infrastructure already exists on the site, therefore the cost of site improvements is only half that for a commercial power plant site. When design details were unavailable (e.g., some buildings, laser power supply, liquid lead cooling circuit), data were taken from other fusion reactor designs (SOLASE, TASKA-M, MINIMARS) with necessary modifications. Care was taken to err on the conservative side in that case. The laser is assumed to be 10% efficient, with 10 ns pulse, with the direct cost of $100 M, although other cases were run (3% efficiency, $250 M direct cost). The target factory also exists on the site and is included in the total cost estimate. Its direct cost is assumed to be $100 M. The target factory and the laser are the biggest "bulk" cost items (the reactor and its equipment were not treated as bulk items but were costed in some detail). There is considerable uncertainty in the literature as to the cost of these two items, and the cost varies in relationship to the assumed maturity of technology (i.e., mature power laser technology for ICF applications will produce cheaper lasers than the ones required for "the next step" experiments). Also assumed is that the only fuel cost would be that of tritium (cost of deuterium and other target materials is neglected). The cost

of tritium in the base case is assumed to be that currently charged by the DOE (Canadian tritium was also assumed in another case). It is possible that DOE will not charge another government facility for the tritium sold. Another assumption in our analysis is that SIRIUS-M would be built at a site that incurs an electricity cost of only 3 ¢/kWh in 1986 currency (a case of electricity cost of 6 ¢/kWh is analyzed as an off-base case). Finally, the cost of replacement engineering test modules is neglected as insignificant.

6.1.2 Economic Assumptions

It is assumed that the federal government will own, build and operate this facility. Therefore, there will be no return on investment charge in the annual facility cost. The analysis of capital costs will also be simplified (e.g., no taxes). It is assumed that debt is incurred to raise money through the sale of treasury bonds, with the rate of return of 9%. The inflation and escalation rates are equal to 6% each for projecting future costs. However, for adjusting non-1986 scaling laws to the level of the 1986 dollar, the consumer price index (CPI) for past years is used,[2] which should combine the effects of inflation and escalation for average consumer items. It is recognized that the prices of plant equipment will behave differently from the CPI and will in fact have different inflation/escalation rates among different types of equipment. However, the CPI is the best we have to go on in many cases. It can also be noted that the scaling laws are now probably more accurate than they were in 1979. Even now, there are some discrepancies among various current scaling laws.[1] The procedure for economic analysis has been adopted from several sources.[3-7] The values of economic parameters for economic analysis of ICF plants[6] have also been adopted here, for the most part. It should be noted, however, that SIRIUS-M is not a power plant, but a

one-of-a-kind test facility, but we nevertheless feel that the projected numbers should be close to reality. Table 6-1 lists the values of economic parameters used in the base case analysis.

6.2 Capital Costs

This subsection will present the itemized direct cost of the facility and its overnight and capital costs. The direct cost includes the cost of hardware and the cost of installation of that hardware, assuming the installation were to happen instantaneously and everything's paid off immediately and on a cash basis. In other words, the direct cost doesn't include the cost of borrowing the money or the cost of escalation and interest during construction. Neither are indirect costs included (administrative, design and field engineering, cost of ownership and project contingency allowance). The "bare" direct cost (BDC) doesn't include the design and spare allowances. These two allowances are included in the total direct cost (TDC) of the facility. The total overnight cost (TOC) is the sum of the total direct and indirect costs, but still assumes instantaneous (or overnight) construction of (and reimbursement for) the facility. The total capital cost (TCC) is the true bottom line cost, including not only the direct and indirect costs, but also the effects of borrowing money and the effect of non-zero construction time.

The base case driver is a $100 M, 10% efficient laser. Other cases were also considered: $250 M, 10% efficient laser and $100 M, 3% efficient laser. The capital cost was parameterized with respect to construction time and inflation rate. All costs are given in 1986 dollars except for the current dollar estimates (given in the dollars of the first year of operation, i.e. 1990 in the base case of a 4-year construction period).

Table 6-1. Base Case Economic Parameters

Parameter	Value
Facility availability	50%
Operations and maintenance fraction	0.03
Salvage fraction	0.00
General inflation rate	0.06
Average cost escalation rate	0.06
Construction time in years	4
Plant life in years	10
Construction factor, f_{91}	0.15
Home office factor, f_{92}	0.15
Field office factor, f_{93}	0.15
Owner's cost factor, f_{94}	0.05
Project contingency factor, f_{95}	0.10
Interest rate on debt	0.09
Fraction of capital from debt	1.00
All tax/tax credit rates	0.00
Levelized interim replacement cost fraction	0.01
Reference year of cost	1986
Fraction construction complete, year 1-4	0.25

Tables 6-2 and 6-3 present the base case itemized direct costs of SIRIUS-M. Figure 6-1 shows pictorially the major cost drivers within each account. The case of the 3% efficient laser is shown next in Table 6-4.

Table 6-5 presents the total costs of the facility (BDC, TDC, TOC and TCC) for the three driver cases: 10% efficient, $100 M laser; 3% efficient, $100 M laser; 10% efficient, $250 M laser. The first case is the base case. The results are expressed both in the constant dollar mode (1986 dollars), and in the current dollar mode (1990 dollars for the 4-year base case construction time).

Results of parametric studies (TCC vs. construction time and TCC vs. inflation rate) are shown in Figs. 6-2 and 6-3. Also shown in Fig. 6-2 is the effect of accelerated construction. This effect is more pronounced the longer the construction time and represents the savings realized by committing more funds to the early phases of construction and less to the later phases than under the level spending assumption. For instance, the case in Fig. 6-2 assumes, for the 12 year construction period, that 25% of the construction budget will be committed in years 1 and 2 each, while 5% will be committed in each of the remaining 10 years of construction.

A comparison can be made between the total costs of SIRIUS-M and TASKA-M, since these two facilities have a similar purpose (materials testing), but employ two different fusion confinement concepts. If one looks at the TASKA-M direct costs,[8] one notices that the major cost drivers are the magnets ($59 M), neutral beam heating ($57 M), RF heating ($91 M), cryogenic system ($14 M) and the vacuum system ($16 M), besides some of the systems (e.g., buildings, instrumentation and control, etc.) that might be similar to the ones of SIRIUS-M. All costs for TASKA-M given above are in 1983 dollars.

Table 6-2. Itemized Direct Costs of SIRIUS-M Equipment

Equipment	Bare Direct Cost, $M
Land	**0.0**
Land and land rights	0.0
Buildings and Site	**82.9**
Site improvements	10.0
Reactor building	49.0
Tritium treatment building	1.7
Control building	2.3
Maintenance building	1.4
Radwaste building	1.4
Administration building	1.5
Diesel generator building	0.5
Cooling system structures	4.6
Hot cell building	7.1
Laser hall, in "Laser Equipment"	N.A.
Rest of buildings	3.4
Heat Rejection Plant	**6.0**
Heat rejection equipment	6.0
Electrical Plant	**37.8**
Ground and cathodic protection	2.1
Rest, excluding laser power supply	3.9
Laser power supply	31.7
Miscellaneous Plant	**23.2**
Miscellaneous plant equipment	23.2
Laser Equipment	**100.0**
KrF laser, including laser hall	100.0
Target Factory	**100.0**
Target factory equipment	100.0

Table 6-3. Itemized Direct Costs, Continued

Equipment	Bare Direct Cost, $M
Reactor Equipment	**102.0**
First wall	4.1
Lead reflector	1.9
PCA reflector	11.8
Pellet injector	1.5
Last mirror shield	2.1
Reactor vacuum	1.5
Vacuum exhaust duct	0.4
Exhaust circulation	0.3
Fuel cleanup	2.0
Hydrogen isotope separation	0.3
Uranium storage beds	0.1
Xe recycle	3.1
Xe inventory	0.6
Radwaste system	0.4
Fuel storage cryogenics	2.7
Fuel storage tank	0.1
Pb cooling, pumps and motor drives	2.7
Pb cooling, SS piping and insulation	13.8
Pb cooling, heat exchangers	4.2
Pb cooling, cleanup system	3.3
Pb cooling, tanks	0.6
Water cooling, pumps and motor drives	3.6
Water cooling, SS piping and insulation	0.5
Water cooling, heat exchangers	3.3
Water cooling, tanks	0.1
Auxiliary cooling	0.9
Laser power supply cooling	0.4
Instrumentation and control	13.6
Maintenance equipment	22.1

Table 6-4. Impact of Laser Efficiency on Selected Direct Costs, $M

Equipment Affected	ΔC, 3% Laser
Cooling system structures	+1.2
Laser power supply cooling	+1.1
Instrumentation and control	+2.5
Reactor maintenance equipment	+4.1
Heat rejection equipment	+4.9
Laser power supply	+73.8
Miscellaneous plant equipment	+7.1
TOTAL	**+94.7**

Table 6-5. Total Cost of Facility for Various Laser Scenarios, $M

Cost Type	10%, $100 M	3%, $100 M	10%, $250 M
BDC	452.	547.	602.
TDC	519.	629.	692.
TOC	855.	1040.	1144.
TCC, $ constant	1016.	1235.	1361.
TCC, $ current	1281.	1559.	1716.

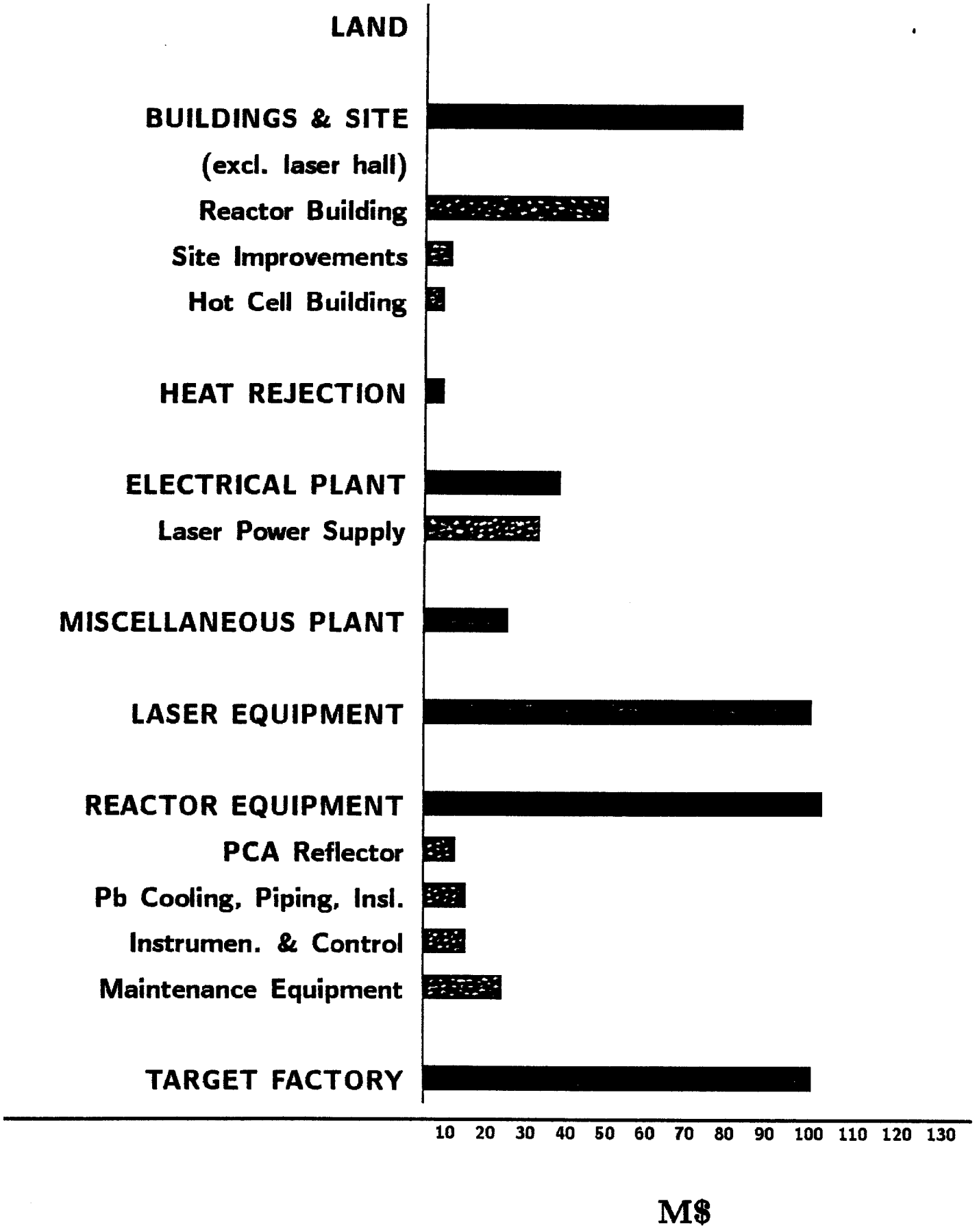

Fig. 6-1. Major accounts and cost drivers within accounts for SIRIUS-M.

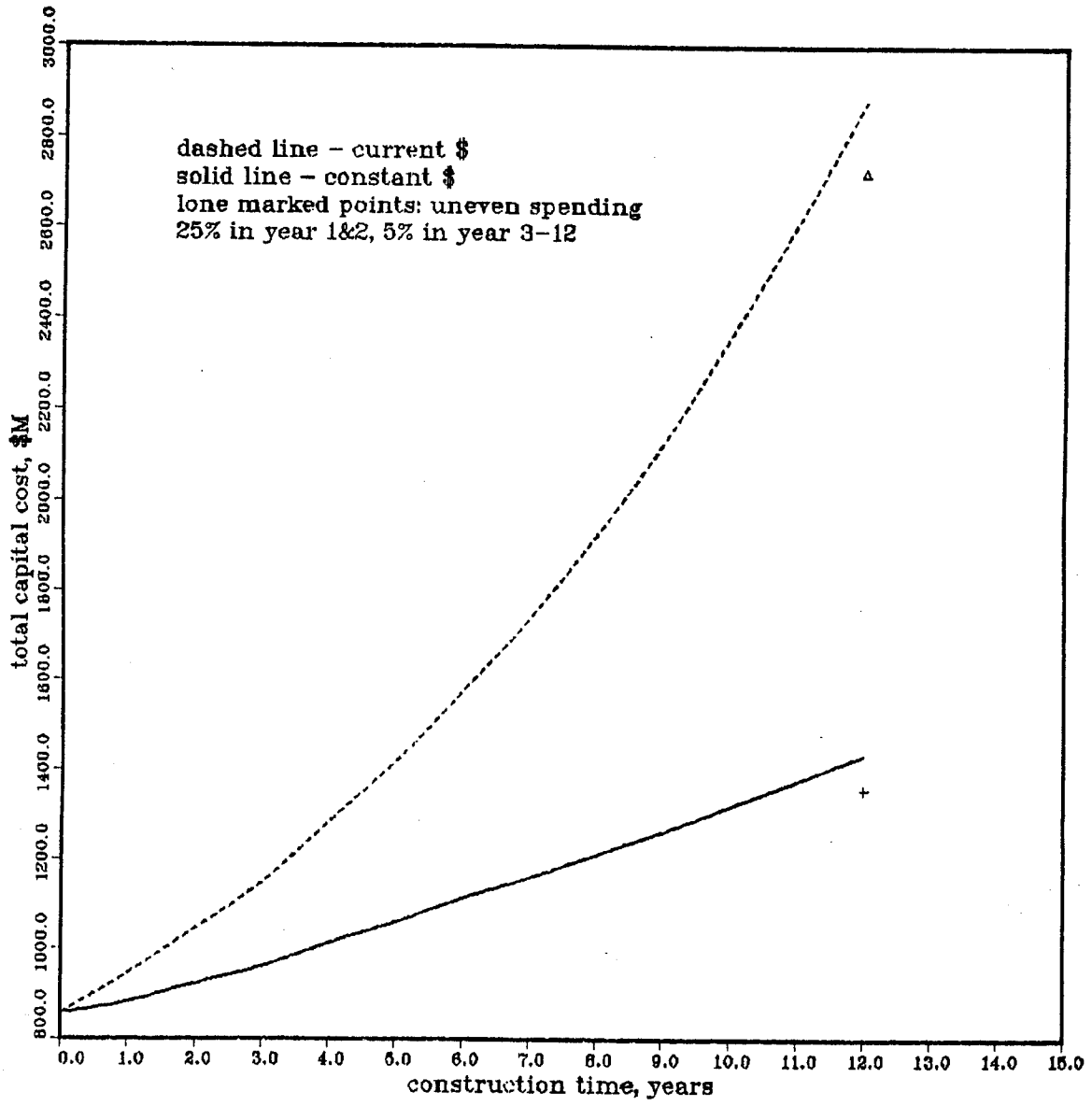

Fig. 6-2. Capital cost as a function of construction time.

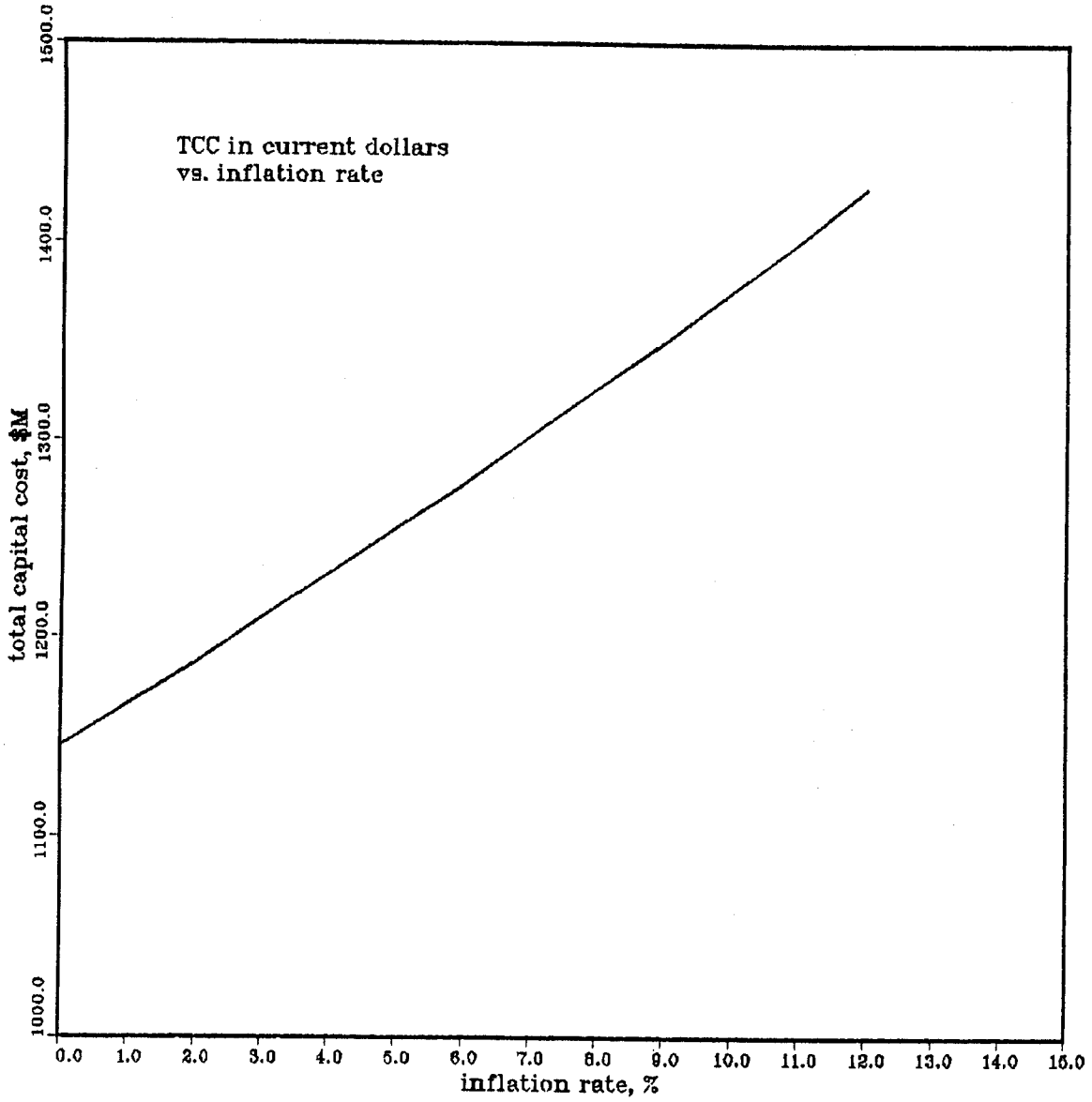

Fig. 6-3. Capital cost as a function of inflation in current dollars.

Figures 6-4 and 6-5 compare the cost impact of major cost drivers between the SIRIUS-M and the TASKA-M facilities. The total direct costs are compared in Fig. 6-6 which is taken from the TASKA-M report,[8] with the SIRIUS-M and TIBER figures added in, after adjustment to the 1983 dollar levels. It can be seen that the direct cost of SIRIUS-M is only slightly greater than that of TASKA-M, but the fusion power is substantially greater.

It should be noted that it is possible to reduce all the costs by proper siting of the facility. Some areas of the country will have construction costs that are substantially lower than the average. For instance, for nuclear power plant construction, the Chicago area is close to the U.S. average, while in the Atlanta area construction costs are 9.1% lower.[9] The construction costs can be further minimized by siting in a low earthquake zone. Low electricity costs are important because of the huge power requirements of the driver.

6.3 Annual Operating Costs

The annual cost of the facility will have several components. Since the government would build and own the facility, the annual cost of paying off the investment would not be charged. The remaining annual costs will include the cost of fuel, electricity and regular operation and maintenance (O&M) costs. The cost of replacement test modules has been neglected, as argued before.

6.3.1 Fuel Cost

The annual fuel cost will consist only of the cost of tritium (the O&M cost of the target factory is included in the O&M cost of the whole facility). The cost of deuterium and of other target materials is assumed to be negligible in comparison.

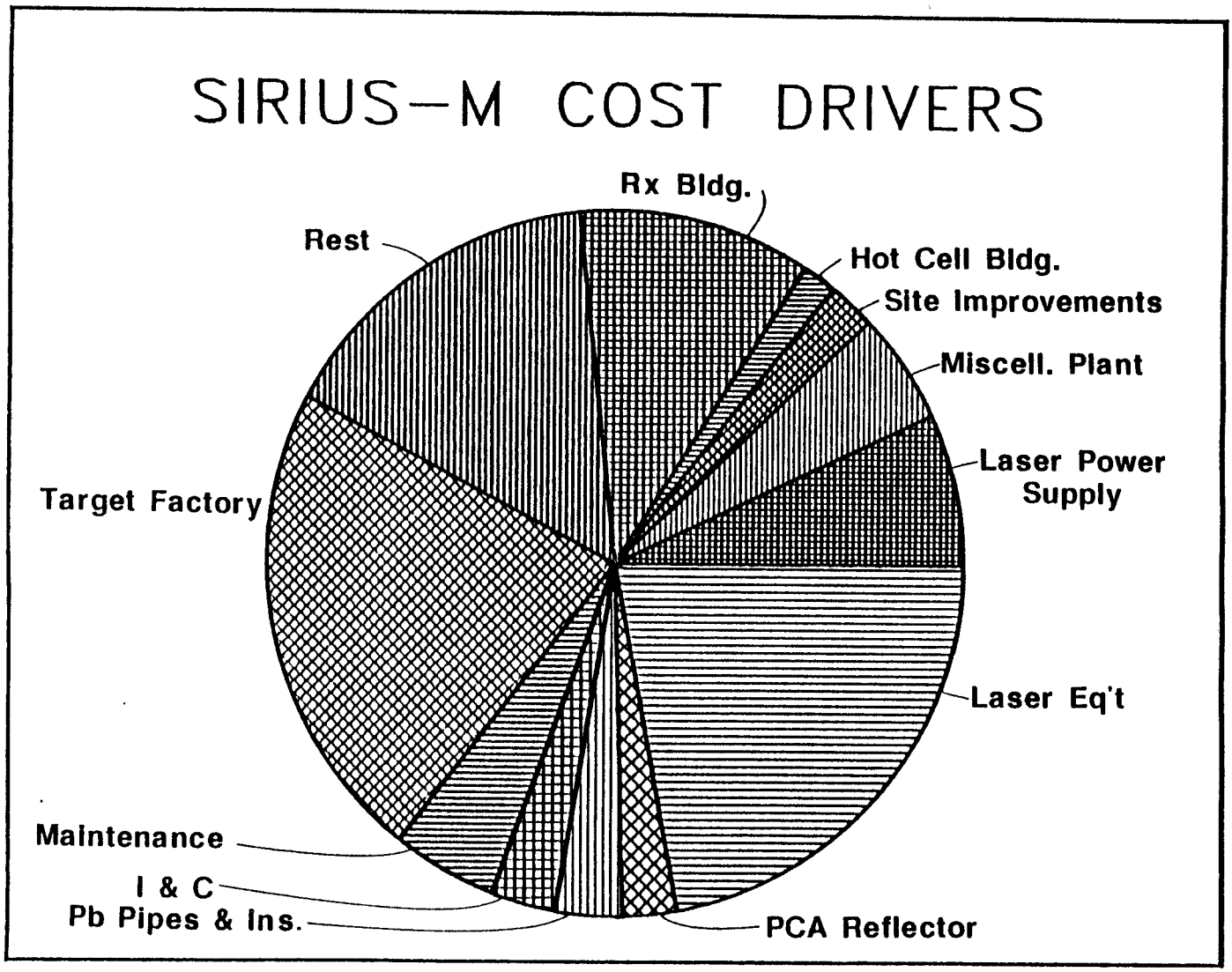

Fig. 6-4. SIRIUS-M major cost drivers as fractions of total direct cost.

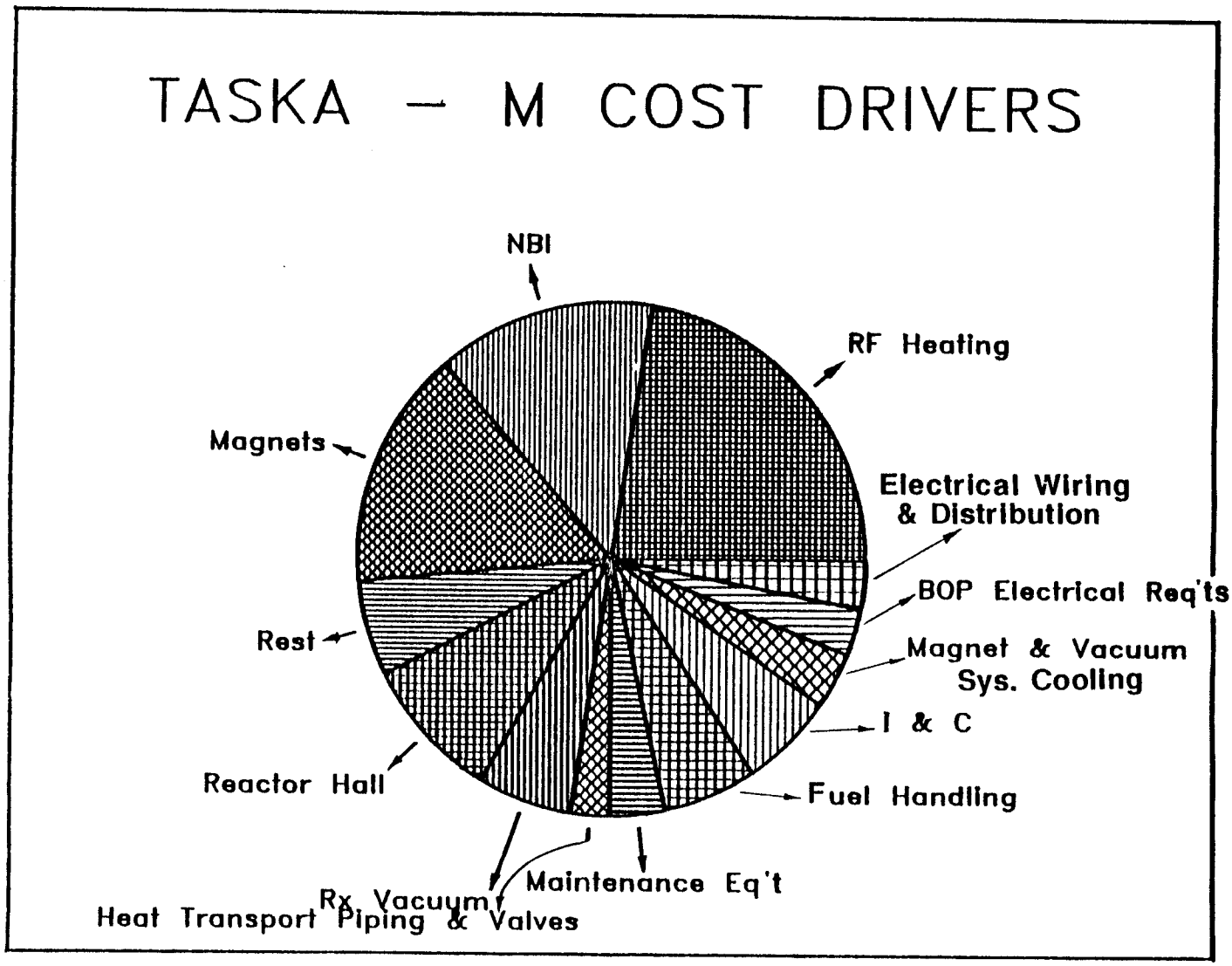

Fig. 6-5. TASKA-M major cost drivers as fractions of total direct cost.

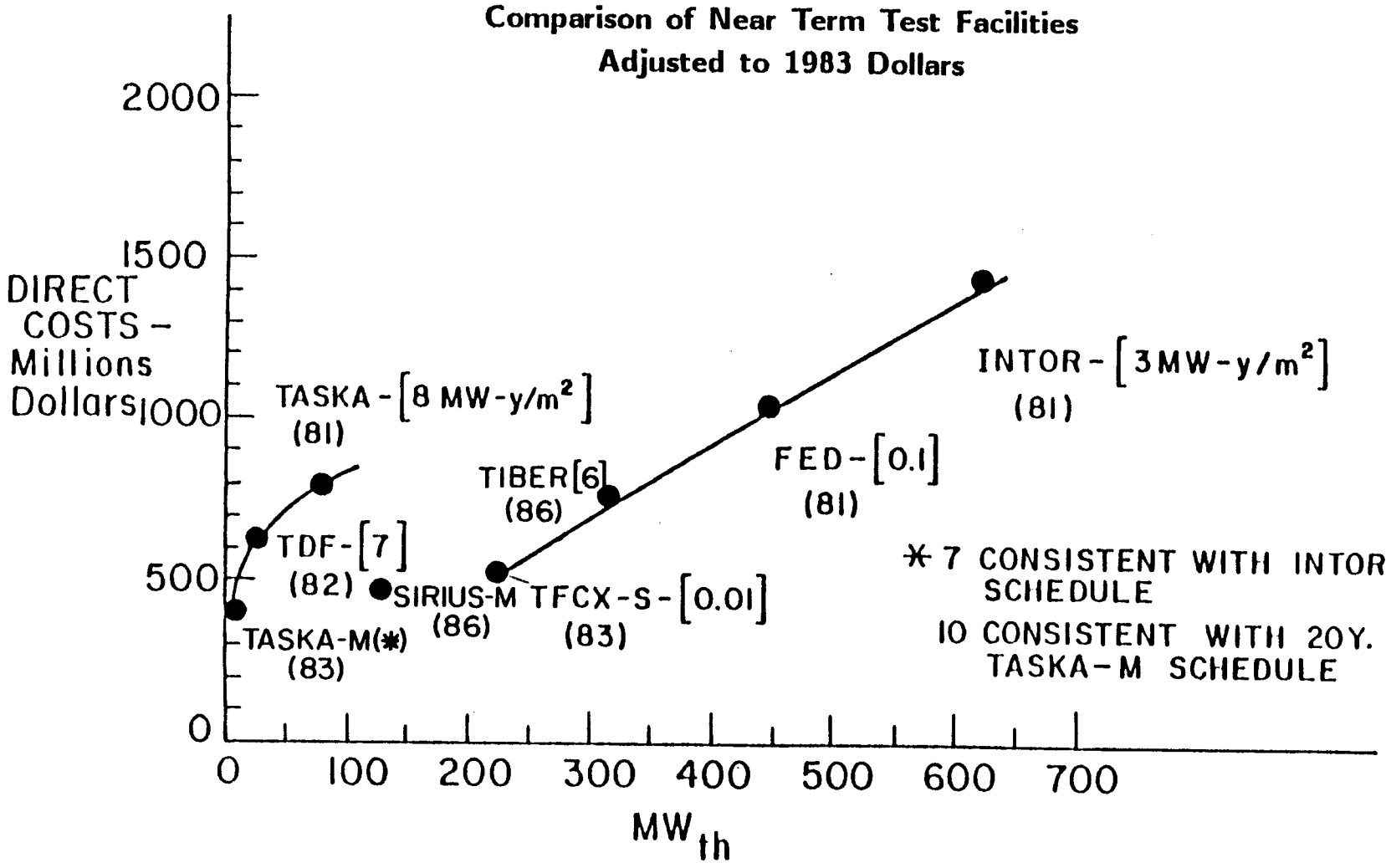

Fig. 6-6. Comparison of near term test facilities.[8]

Estimates for the price of tritium vary, depending on the source of information and the source of tritium. The most widely quoted price for the tritium from DOE production facilities is $1.1/Ci (our target will have 0.85 Ci of tritium, of which about 25% will be consumed). That is about $10,600/g. For the tritium extracted from the heavy water of the Canadian CANDU reactors, the preliminary price quotation is CAN $1.0/Ci, or about US $7,100/g. A full scale tritium extraction plant is ready to go on line at about this time in Canada. The tritium production rate of all the Canadian CANDUs (operating and under construction) is about 2.9 kg/y, which is a little short of our requirement of 3.4 kg/y. A more detailed description of sources of tritium and data can be found elsewhere.[1]

Table 6-6 shows the tritium cost per target for the two sources of tritium described above, while Table 6-7 gives the total annual fuel cost of SIRIUS-M (assuming the baseline availability of 50%). In this scenario, we assume that only the burnt tritium is charged (unburnt tritium receives credit equal to its purchasing price, and there is no wastage).

6.3.2 Cost of Electricity

In this study, a cost of electricity of 3 ¢/kWh is assumed.[10] This low cost might exist in the Pacific Northwest and perhaps some other areas. In Madison, WI, the rate is about 6 ¢/kWh. Tables 6-8 and 6-9 show the annual cost of purchased electricity for the cases of 3 ¢/kWh and 6 ¢/kWh electricity, and for the cases of a 10% efficient and 3% efficient laser. The electricity consumption takes into account only the laser power requirements, excluding auxiliaries such as pumps, instrumentation, etc. (power requirements negligible compared to those of the laser) and excluding the power require-

Table 6-6. Tritium Cost Per Target for DOE and CANDU Tritium

	DOE Tritium	CANDU Tritium
Cost per target, ¢ constant	23.	16.
Cost per target, ¢ current	37.	26.

Table 6-7. Total Annual Fuel Cost of SIRIUS-M

	Source of Tritium	
	U.S. DOE	CANDU
Fuel cost, $M constant	36.3	25.2
Fuel cost, $M current	58.4	41.0

Table 6-8. Annual Cost of Electricity at 3 ¢/kWh

Cost Type	10% Laser	3% Laser
Electricity cost, $M constant	13.2	43.9
Electricity cost, $M current	22.2	74.1

Table 6-9. Annual Cost of Electricity at 6 ¢/kWh

Cost Type	10% Laser	3% Laser
Electricity cost, $M constant	26.3	87.7
Electricity cost, $M current	44.5	148.2

ments of the target factory which are unknown and assumed comparatively negligible.

6.3.3 O&M Costs

The O&M costs include the traditional costs of running a plant, including the cost of personnel on site. The usual procedure is to compute the annual O&M costs as a fraction of TOC (see Table 6-1 for the default value). The fraction that we used is representative of a power plant, and therefore might not be entirely applicable in this case. Table 6-10 shows the annual O&M costs for the three laser scenarios used in Table 6-5.

6.3.4 Total Facility Annual Costs

This subsection will present the total annual cost of operating SIRIUS-M, by assuming a few scenarios. The worst case assumes a 3% efficient, $100 M laser driver for our facility. The targets will be made with DOE tritium. The cost of electricity is 6 ¢/kWh. The base case is for a 10% efficient, $100 M laser driver, burning DOE tritium and the electricity is bought at 3 ¢/kWh. The best case has the same parameters as the base case, except that CANDU tritium is used. One can also imagine the case ("base case without fuel") in which no charge is imposed for the DOE tritium (a plausible argument). Table 6-11 gives the total annual costs for these four cases.

Table 6-10. Annual O&M Cost of SIRIUS-M for Various Driver Cases, $M

Cost Type	10%, $100 M	3%, $100 M	10%, $250 M
Constant $	25.5	31.2	34.3
Current $	43.1	52.8	58.0

Table 6-11. Total Yearly Cost of Running SIRIUS-M

Type Cost	Best Case	Worst Case	Base Case	Base Case w/o Fuel
O&M + fuel + electricity, $M constant	63.9	155.2	75.	38.7
O&M + fuel + electricity, $M current	106.3	259.4	123.7	65.3

References for Chapter 6

1. Zoran Musicki, "The Economic Analysis of SIRIUS-M," University of Wisconsin Fusion Technology Institute Report UWFDM-708, Sept. 1986.

2. "Business Conditions Digest," Bureau of Economic Analysis, U.S. Department of Commerce.

3. "TAG™, Technical Assessment Guide," EPRI-P-2410-SR, Special Report, Electric Power Research Institute, May 1982.

4. J. Sheffield, R.A. Dory, S.M. Cohn, J.G. Delene, L. Parsly, D.E.T.F. Ashby, W.T. Reiersen, "Cost Assessment of a Generic Magnetic Fusion Reactor," Nuclear Technology 9, No. 2 (March 1986).

5. Wayne Meier, "Standard Cost Accounts and Methodology for Inertial Confinement Fusion Reactor Studies, Progress Report," presented at the Second ICF Colloquium, University of Wisconsin, October 2-3, 1985.

6. Wayne R. Meier, "A Standard Method for Economic Analyses of Inertial Confinement Fusion Power Plants," presented at the Seventh Topical Meeting on the Technology of Fusion Energy, Reno, NV, June 15-19, 1986.

7. Zoran Musicki, "A Menu Driven, IBM-PC Based Computer Program for Economic Analyses of ICF Facilities," University of Wisconsin Fusion Technology Institute Report, to be published October 1986.

8. B. Badger et al., "TASKA-M, A Low Cost Near Term Tandem Mirror Device for Fusion Technology Testing," FPA-83-7, KfK-3680, UWFDM-600, Dec. 1983.

9. "Nuclear Energy Cost Data Base," DOE/NE-0044, U.S. Department of Energy (1982 and 1983 update).

10. W.R. Meier, T.J. McCarville, D.H. Berwald, J.D. Gordon and W.G. Steele, "An ICF Tritium Production Reactor," Fusion Technology 8, No. 1, Pt. 2, (July 1985), Proceedings of the Sixth Topical Meeting on the Technology of Fusion Energy, San Francisco, CA, March 3-7, 1985.

7. TARGET DESIGN CONSIDERATIONS

The materials test facility SIRIUS-M[1] was designed around wall-loading estimates from target implosion simulations that used the currently accepted model for heat transport in laser fusion plasmas. More recent experiments[2] and theoretical modeling[3] suggest that the heat transport is more efficient than previously thought. The significance for direct-drive targets is two-fold: higher implosion efficiency and higher laser absorption. In particular, for the SIRIUS-M design the gain is found to increase from 13.5 to 110, and the reflected laser light to decrease from 100 kJ to 70 kJ. Reflected laser light had been found to be the predominant source of damage to the first wall of the reactor. In Section 7.1, the improved modeling of heat transport is used to obtain the new scaling of target performance with laser energy. These results were obtained using the University of Rochester, one-dimensional hydrodynamics code LILAC. Calculations were also begun to examine two-shell target designs in search of improved performance; however, this was abandoned when it came to be concentrated on variations of the original one-shell SIRIUS target.

The results in Section 7.1 assume uniform laser irradiation. Of course some nonuniformities will always be present. Previously, we have calculated and characterized the amount of nonuniformity that should be produced from different sources, e.g., energy imbalance among the beams, beam mispointing, and beam intensity imperfections.[1,4,5] The responses of the target to some of these nonuniformities are discussed in Section 7.2 using simulations from the University of Rochester, two-dimensional hydrodynamics code ORCHID. The results begin to establish tolerances for the quality of irradiation required in a direct-drive facility.

7.1 Target Performance

Improved target performance, compared to the previous SIRIUS design, has been obtained using the higher flux limiter presently supported by both theory and experiment. Heat transport in laser-produced plasmas is typically modeled by flux-limited diffusion. In order to model experiments, it has been necessary to limit the classical Spitzer-Härm heat flux q_s to some fraction f of the electron free-streaming limit $T(T/m)^{1/2}$. The resulting heat flux is of the form:

$$q = \min\left(q_s, f n_e T \sqrt{T/m}\right) .$$

Previously, flux limiters f on the order of ~ 0.04 were required to model experiments with infrared (1 μm) laser irradiation, on planar targets. The small flux limiter could have resulted from a large number of factors, among them: magnetic fields from nonspherical irradiation and nonlocal effects from long mean-free-path electrons in the "tail" of the distribution function.[3] Recent experiments[2] at the University of Rochester, with the 24-beam spherical irradiation system OMEGA operating at short wavelength (0.35 μm), have been successfully modeled[6] with a much higher flux limiter, f = 0.1. Also, numerical simulation with a Fokker-Planck electron transport code[3] has shown that the nonlocal effects are negligible for short wavelength irradiation (due to the high collisionality at the relatively high critical density), and that a flux-limited diffusion model with f = 0.1-0.2 adequately characterizes the heat flow. With this support for a higher flux limiter for short wavelength spherical irradiation, the SIRIUS target designs were reexamined using f = 0.1 instead of 0.04 previously used.

Figure 7-1 shows how the target gain (fusion energy/incident laser energy) changes as the laser energy is varied for f = 0.1 and 0.04. The effect of the higher flux limiter is to provide ~ 20% more target gain with ~ 10% less laser energy. This gain is now about 7 times higher than is required to produce an adequate neutron wall loading. Wall damage from target debris and x-rays might be too large. Of course the target gain can be degraded by modifying the target or laser parameters. The ideal situation would be to reduce the laser energy and to use correspondingly smaller targets. However, smaller targets have smaller plasma scale lengths, resulting in less laser absorption. As targets become smaller, it is increasingly difficult to drive them without reaching very high intensities (that can initiate detrimental plasma processes) and without exceeding an upper limit of ~ 70 on the in-flight aspect ratio (shell radius divided by shell thickness) required to prevent severe performance degradation due to hydrodynamic instabilities. Figure 7-1 shows the sharp decline in target gain as the laser energy decreases. The decline is due mainly to the constraint on aspect ratio and the increase in laser refraction. One possibility for obtaining high gain at lower laser energies would be to develop a "zoom-focus" capability. The present calculations assume current technology whereby each beam is initially focused to completely illuminate a target hemisphere (for optimal uniformity), and the beam size in the target plane does not change during the implosion. As the target decreases in size the outer parts of the beam will miss the target. If the technology can be developed to change the focus during the implosion to minimize refractive losses, a much more efficient laser drive would be possible.

An important point identified in last year's study[1] was that the reflected laser light is the dominant source of damage to the first wall of the

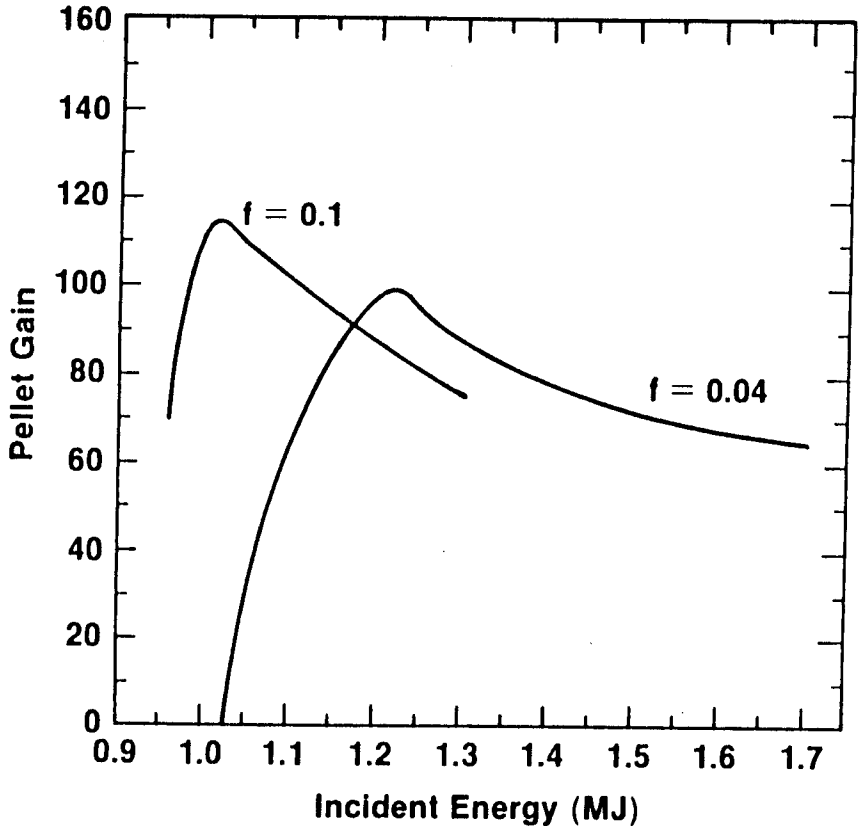

Fig. 7-1. Redesign of single-shell "1.6 MJ" KrF pellet design.

SIRIUS-M design. At that time it was estimated that there would be 100 kJ of reflected light for a 1 MJ laser system. The tolerance of the first wall to the reflected 100 kJ was only marginal. The new target calculations with the higher flux limiter show a higher laser absorption, resulting in a 30% reduction in reflected light. The amount of reflected-light-energy vs. incident-laser-energy is shown in Fig. 7-2. For 1 MJ incident, only 70 kJ are reflected. An additional margin of safety can be added by moving the chamber walls further out to reduce the intensity of reflected light on the walls; the neutron flux would still be more than adequate because of the high target gain. However, for a larger chamber, it will be necessary to burn more tritium than previously considered for the same neutron wall loading, and it might require the breeding of some tritium in the facility.

7.2 Tolerance to Irradiation Nonuniformity

The response of targets to irradiation nonuniformity depends on the spatial wavelength of the nonuniformity in addition to its magnitude. Short wavelength nonuniformities will grow the most rapidly by the Rayleigh-Taylor instability; but they also are most easily smoothed by thermal conduction before they can reach the ablation surface where growth occurs. The spatial wavelength λ of a nonuniformity has been characterized by spherical harmonic modes; the mode ℓ is related to λ by:

$$\ell = 2\pi R/\lambda$$

where R is the target radius. Typically, the relation between irradiation conditions and the mode structure is the following:[1,4,5]

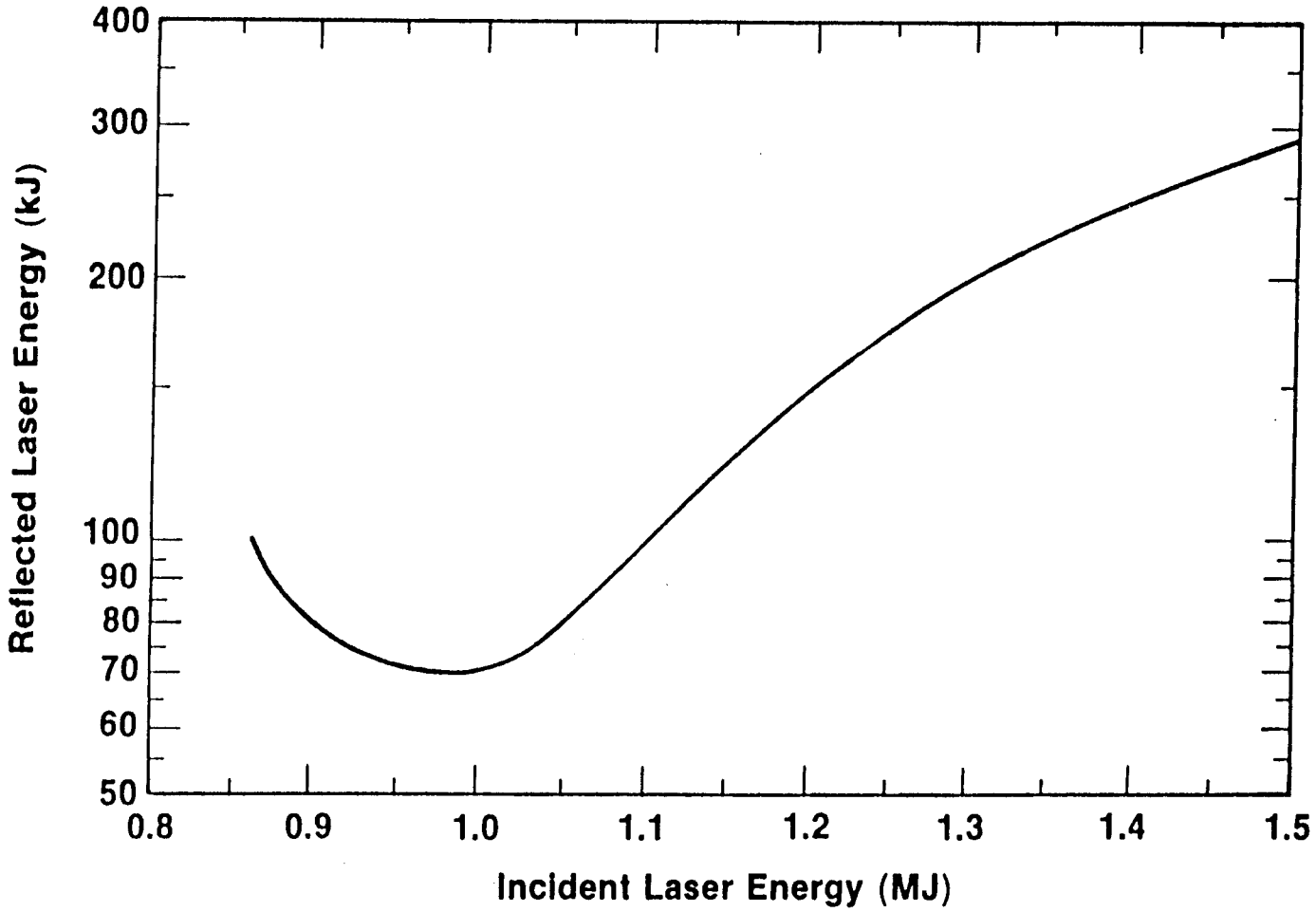

Fig. 7-2. Reflected versus incident laser energy ~ 1 MJ KrF designs.

1. Low-order modes ℓ = 1-3 are produced by energy imbalance among the beams and beam mispointing.
2. Odd-order modes are produced when opposing beams are not identical.
3. For perfect beams, the dominant mode of nonuniformity is roughly $\ell \sim 2\sqrt{N}$ where N is the number of beams (ℓ = 10 is characteristic of the 32 beam geometry used for SIRIUS).
4. Beam imperfections create modes across the entire spectrum.

In the previous SIRIUS-M report[1] the response of the target to the low-order modes ℓ = 2 and 4 was discussed using the two-dimensional hydrocode ORCHID. It was found that the target was able to tolerate these modes to the levels anticipated in a direct-drive facility. The 2-D calculations of the target response have been extended[7,8] to examine higher modes: ℓ = 8 and 16. The target was much less tolerant of these modes. There was evidence of substantial exponential growth of the modes by the Rayleigh-Taylor instability. These nonuniformities would imprint themselves on the target surface early in time before a large enough plasma atmosphere was established to smooth the variations in energy deposition; the initial shell distortions continued to grow during the implosion.

The calculations indicate that the level of nonuniformity in the modes ℓ = 8 and 16 should not exceed about 2% peak to valley. This is at the limit presently considered achievable with a 32 beam system, and it suggests that illumination with a larger number of beams may be required. Figure 7-3 shows the improvement in the σ_{rms} nonuniformity as the number of beams increases. The x-axis is a measure of the beam size relative to the instantaneous size of the target during the implosion: a focus parameter of 1 corresponds to tan-

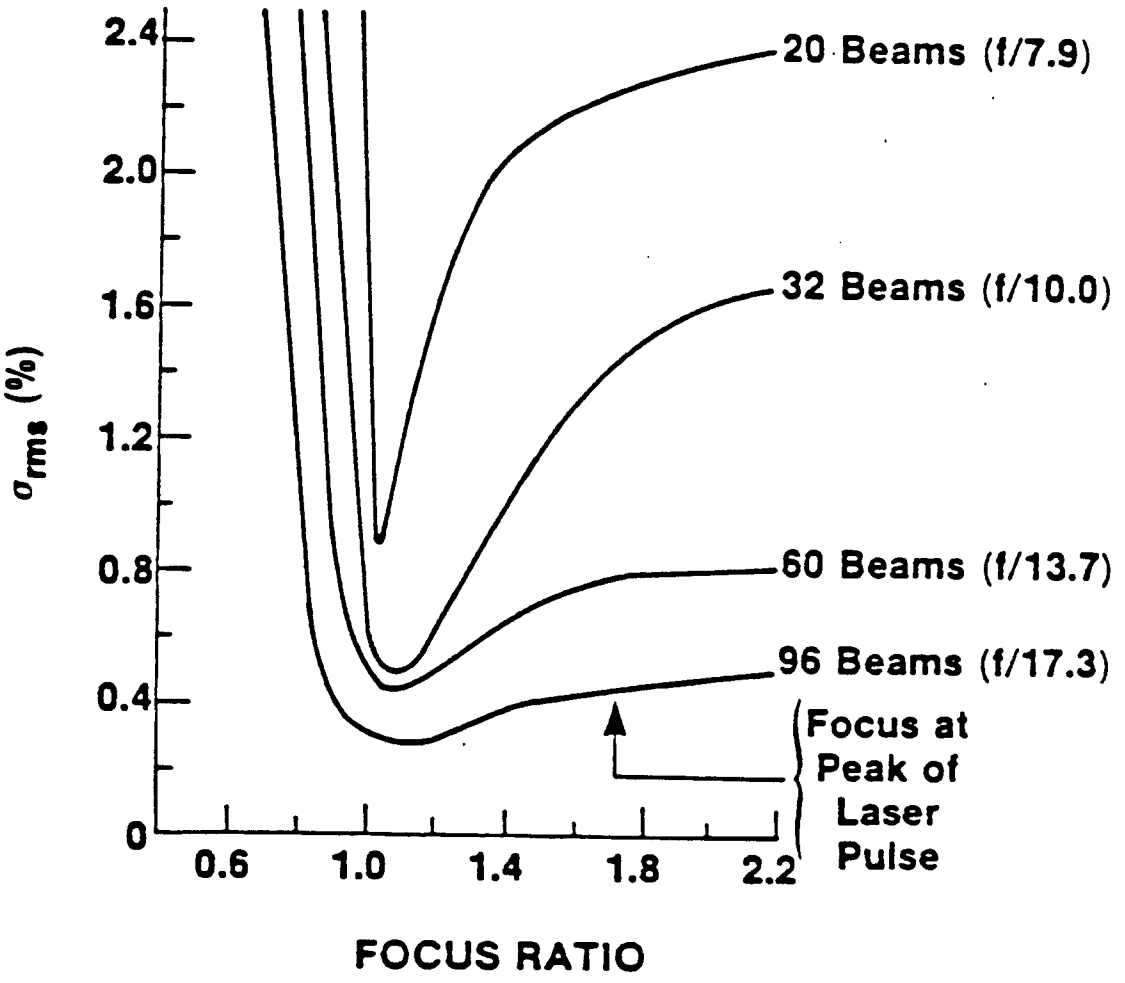

Fig. 7-3. Nonuniformity of laser energy deposition for 2% solid angle fraction.

gential illumination for which each beam irradiates a complete target hemisphere.

These irradiation uniformity calculations were also performed for smaller targets to determine if their response to nonuniformity was any different. The case considered was for 30 kJ incident irradiation, using a scaled-down version of the SIRIUS target. This target had a gain of 0.55 for uniform irradiation. The in-flight aspect ratio was ~ 70 and the convergence ratio (initial radius/compressed core radius) was 24; both are characteristic of the SIRIUS target implosion. An ℓ = 10 irradiation nonuniformity was applied with an initial peak-to-valley variation of 1.2%, characteristic of a 32-beam system. The nonuniformity was allowed to increase as the target imploded; the nonuniformity reached ~ 4% when the shell had imploded to half its initial radius (Fig. 7-4). Substantial degradation of the target performance was observed. The target gain dropped from 0.55 to 0.15. The resultant deviation from sphericity is shown in Fig. 7-5 for the density and temperature contours. This degradation in target performance is characteristic of the degradation in the much larger SIRIUS target with the same imposed nonuniformity. It suggests that to a large extent the response of a target to irradiation nonuniformities is relatively independent of target size for similar drive conditions, and the amount of distortion is determined by the convergence ratio.

7.3 Summary

Using the higher flux limit for heat transport presently supported by theory and experiment, it was found that the SIRIUS-M target can have a gain of about 7 times higher than previously estimated; and the amount of reflected laser light, which previously had been only marginally acceptable, has been reduced by 30% which is now acceptable. The tolerance of this target to ir-

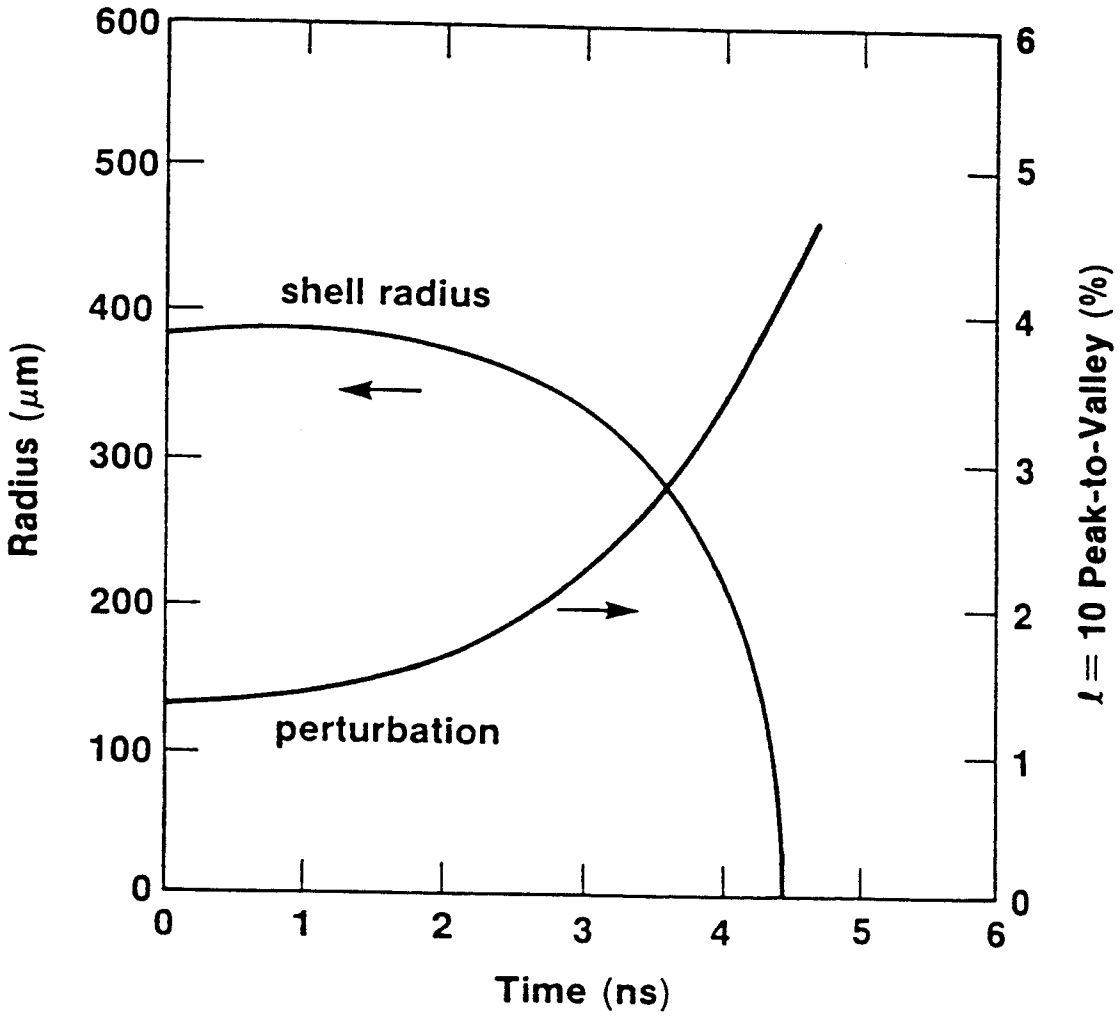

Fig. 7-4. Time-dependent ℓ = 10 irradiation nonuniformity for the 30 kJ target.

radiation nonuniformities corresponding to spherical harmonic modes ℓ = 8 and 16 was found to be marginal for 32-beam irradiation; a larger number of beams may be required.

References for Chapter 7

1. "SIRIUS-M: A Symmetric Illumination Inertially Confined Direct Drive Materials Test Facility," University of Wisconsin Fusion Technology Institute Report UWFDM-651 (Sept. 1985).

2. Yaakobi et al., Phys. Fluids 27, 516 (1984).

3. P. Holstein, J. Delettrez, S. Skupsky and J. Matte, to be published in J. Appl. Phys. (Sept. 1986) and references therein.

4. "Preliminary Conceptual Design of SIRIUS, A Symmetric Illumination, Direct Drive Laser Fusion Reactor," University of Wisconsin Fusion Technology Institute Report UWFDM-568 (March 1984).

5. S. Skupsky and K. Lee, J. Appl. Phys. 54, 3662 (1983).

6. J. Delettrez et al., manuscript in preparation.

7. Work supported in part by Los Alamos Contract 9-X54-H8413-1.

8. Laboratory for Laser Energetics, Quarterly Report 23, 125 (1985), University of Rochester.

8. CONCLUSIONS AND RECOMMENDATIONS

Based on the results presented in this report, the following conclusions can be drawn:

1. An ICF materials test facility, such as SIRIUS-M, which uses symmetrically-illuminated targets can provide the necessary critical data and technology base for an ICF demonstration facility for modest capital and operating costs. The estimated total direct cost for SIRIUS-M is \$519 M (1986 dollars); the total capital cost is \$1016 M while the annual operating cost is \$75 M/yr.
2. The major items contributing to the direct cost of SIRIUS-M are the laser and associated power supply (\$132 M), the target factory (\$100 M) and the reactor building (\$49 M). Hence, in order to minimize the total capital cost and pinpoint it with reasonable accuracy, one should strive to minimize the costs of these "drivers" and learn more about their true costs.
3. The most important parameters affecting the annual operating costs are the laser efficiency, the cost of electricity at the site and the cost of purchased tritium (which might conceivably be zero in case of DOE-supplied tritium). Since the conventional operations and maintenance cost depends on the overnight cost, limiting the facility's direct cost will also help in reducing the annual operating cost. Site selection can also help in lowering both the annual operating cost (via the cost of electricity) and the total capital cost (via lower equipment installation cost, site preparation cost, and lower probability and magnitude of earthquakes and other hazards).
4. Cavity design optimization for SIRIUS-M indicates that the maximum neutron loading (2 MW/m^2) will likely be limited by the amount of re-

flected laser light from the target. If the amount of reflected light can be reduced to the point where cavity size would be limited by the re-radiated x-ray and ionic debris energy, the neutron wall loading could be increased by nearly 80% (3.6 MW/m^2). The economic impact of such a change in target performance is significant. Compared to the reference design, the total lifetime cost can be reduced by ~ 21% if the fusion power and cumulative performance are to be kept the same. The cost per dpa-ℓ can be reduced by nearly 44% without significant change in the total lifetime cost if the fusion power and operational time are to be kept the same.

5. A detailed materials test matrix has been developed for two SIRIUS-M test modules each with 217 capsules. The data to be obtained during the five full-power years of operation should meet the development needs of an ICF demonstration reactor in a timely fashion. Structural material testing is divided into two categories: scoping and qualification studies. The scoping studies are applied to the top four structural candidates selected by the materials community. The qualification tests will concentrate on the two alloys (a primary and a backup) which appear to be the leaders at the beginning of the scoping studies. These tests would concentrate on a finer temperature mesh and include larger test specimens. Nonstructural materials testing can also be performed in SIRIUS-M. This includes accelerated testing (to a few dpa) of laser mirror coatings, mirror support alloys and shielding materials. Long term tests (up to 120 dpa) would include neutron multipliers, solid breeder materials and tiles.

6. A scoping study conducted to identify the unique ICF blanket testing requirements has shown that, with the exception of two, these requirements can be met within the materials test modules. The two unique problems are stress and corrosion effects due to isochoric heating of liquid metals. In the first problem, analysis has shown that under uniform impulsive pressure due to isochoric heating, the maximum dynamic circumferential normal stress is independent of the chamber radius. For a shell thickness of 1 cm, the maximum dynamic stress will be less than 30 MPa, a value well below the endurance limit for structural steels. Experimental verification of these results will be performed in an instrument zone of the Pb reflector in SIRIUS-M.

7. The effect of isochoric heating on corrosion will be tested in a blanket test module to be placed in SIRIUS-M. Such a module has been designed and a testing schedule for qualifying a combination of materials has been developed. It is estimated that one calendar year of operation at 50% availability will be needed to qualify a liquid metal/structural material combination.

8. Eight different shield and building design options were considered for SIRIUS-M. The geometrical configurations differed in these options depending on the location of the building wall and the way the last mirrors are enclosed. We found that the design goal of a biological dose $\tilde{<}$ 2.5 mrem/hr outside the building wall during operating can be achieved with the least amount of shield if a 3.2 m thick concrete building wall is used behind the final mirrors.

9. The base design option for SIRIUS-M requires beam point crossover optics that allow surrounding the turning mirror by a 1.5 m thick concrete

shield with a 0.1 m diameter orifice. This was found to reduce the streaming to the laser building and damage to the final optical windows by about three orders of magnitude. Negligible density changes and very little optical degradation are expected in the optical windows. Preliminary data for ion irradiated coatings indicate that the final focusing mirror will have to be replaced once or twice during a calendar year while the turning mirror should last the entire SIRIUS-M lifetime.

10. Hands-on maintenance for the reactor chamber and final mirrors is not feasible due to the high dose levels resulting from activation of the reactor components. Dose rates greater than 100 rem/hr one day after shutdown will exist inside the reactor building.

11. Activation analysis for the reactor chamber and last mirrors indicated that the chamber components need to be diluted by a factor of ~ 5 to qualify as a class C waste for near surface burial. On the other hand, the final focusing mirror will be a class C waste while the turning mirror is rated as class A segregated waste that needs less stringent packaging and burial requirements. If the final focusing mirror has to be replaced during the reactor life, it will be a class A waste.

12. Single-shell target design calculations using the higher flux limit for heat transport (presently supported by theory and experiment) indicate that the SIRIUS-M targets can have a gain of about 7 times higher than previously estimated. The amount of reflected light from these targets has also been reduced by about 30%. The tolerance of the target to irradiation nonuniformities corresponding to spherical harmonic modes $\ell = 8$ and 16 was found to be marginal for 32-beam irradiation; a larger number

of beams may be required. Such changes in target performance can have a significant impact on the design and cost of the facility.

ACKNOWLEDGEMENTS

Financial support by the U.S. Department of Energy through Contract No. DE-AS08-86DP10529 is acknowledged. Computing time has been provided by the San Diego Supercomputing Center. The comments and suggestions provided by Dr. Steve Bodner of the Naval Research Laboratory during the course of this study are appreciated.